Serum Response Factor and Actin Treadmilling Influence Neuronal Mitochondrial Dynamics

Dissertation

zur Erlangung des Grades eines
Doktors der Naturwissenschaften

der Mathematisch-Naturwissenschaftlichen Fakultät
und
der Medizinischen Fakultät
der Eberhard-Karls-Universität Tübingen

vorgelegt
von

Henning Beck
aus Darmstadt, Deutschland

Juli, 2012

Tag der mündlichen Prüfung:	12.09.2012
Dekan der Math.-Nat. Fakultät:	Prof. Dr. W. Rosenstiel
Dekan der Medizinischen Fakultät:	Prof. Dr. I. B. Autenrieth
1. Berichterstatter:	Prof. Dr. Bernd Knöll
2. Berichterstatter:	Dr. Simone Di Giovanni
Prüfungskommission:	Prof. Dr. Bernd Knöll
	Dr. Simone Di Giovanni
	Prof. Dr. Mathias Jucker
	PD Dr. Andrea Wizenmann

I hereby declare that I have produced the work entitled:
“Serum Response Factor and Actin Treadmilling Influence Neuronal Mitochondrial Dynamics”,
submitted for the award of a doctorate, on my own (without external help), have used only the sources and aids indicated and have marked passages included from other works, whether verbatim or in content, as such. I swear upon oath that these statements are true and that I have not concealed anything. I am aware that making a false declaration under oath is punishable by a term of imprisonment of up to three years or by a fine.

Tübingen, _____ _____

Date Signature

Can’t stop the spirits when they need you.

Anthony Kiedis

Table of Content

1. Introduction 1

1.1 The Transcription Factor SRF 1

1.1.1 Structure and Characterization of SRF 1

1.1.2 Regulation of SRF 3

1.1.2.1 TCF-dependent Regulation of Immediate Early Genes 4

1.1.2.2 MRTF-dependent Regulation of Cytoskeletal Genes 5

1.1.3 Connection between TCF- and MRTF-dependent SRF regulation 6

1.1.4 Neuronal Functions of SRF 7

1.2 The Actin Cytoskeleton 10

1.2.1 Structure of Actin 10

1.2.2 Actin Dynamics 11

1.2.3 Cofilin 14

1.3 Mitochondria 18

1.3.1 Structure and Function 18

1.3.2 Transport and Trafficking 20

1.3.3 Fusion and Fission 24

1.3.4 Mitochondria and the Actin Cytoskeleton 25

1.3.5 Mitochondria in Neurodegenerative Diseases 28

1.4 Aim of this work 32

2. Material and Methods 33

2.1 Technical Devices 33

2.2 Chemicals 34

2.3 Antibodies 36

2.3.1 Primary Antibodies 36

2.3.2 Secondary Antibodies 37
2.4 Plasmids 38
2.5 Oligonucleotides for genotyping 39
2.6 Mouse Lines 39
2.7 Technical Equipment and Reagents 40
2.7.1 Technical Equipment and Reagents for Cell Biological Experiments 40
2.7.1.1 Neuronal Cell Culture 40
2.7.1.2 Stimulation of primary neurons with ephrin-A5 or BDNF 42
2.7.1.3 Stimulation of primary neurons with FCCP 42
2.7.1.4 Immunocytochemistry 42
2.7.1.5 Immunohistochemistry 43
2.7.1.6 HEK293 and PC12 Cell Culture 43
2.7.2 Technical Equipment and Reagents for Microscopy 44
2.7.3 Technical Equipment and Reagents for Molecular Biological Experiments 44
2.7.3.1 Purification of plasmids 44
2.7.3.2 Genotyping 45
2.7.4 Technical Equipment and Reagents for Biochemical Experiments 46
2.7.4.1 Generation of Proteinlysates 46
2.7.4.2 SDS-Polyacrylamid Gel Electrophoresis 47
2.7.4.3 Western Blotting 48
2.7.4.4 Purification of Mitochondria and ATP Production 49
2.8 Experimental Procedures 49
2.8.1 Procedures of Cell Biological Experiments 49
2.8.1.1 Neuronal Cell Culture 49
2.8.1.2 Stimulation of primary neurons with ephrin-A5, BDNF or latrunculin 52
2.8.1.3 Stimulation of primary neurons with FCCP 52

2.8.1.4 Immunocytochemistry 53
2.8.1.5 Immunohistochemistry 53
2.8.1.6 HEK293 and PC12 Cell Culture 54
2.8.2 Microscopy 56
2.8.2.1 Live Cell Microscopy 56
2.8.2.2 Electron Microscopy 56
2.8.3 Procedures of Molecular Biological Experiments 57
2.8.3.1 Purification of plasmids 57
2.8.3.2 Genotyping 58
2.8.4 Procedure of Biochemical Experiments 60
2.8.4.1 Generation of Proteinlysates 60
2.8.4.2 SDS-Polyacrylamid Gel Electrophoresis 61
2.8.4.3 Western Blotting 61
2.8.4.4 ATP production assay 62
2.8.5 Analysis and Statistics 64
2.8.5.1 Analysis of Mitochondrial Size and Occupancy 64
2.8.5.2 Determination of Cofilin and Phospho-Cofilin Intensity 65
2.8.5.3 Analysis of Time Lapse Experiments 65
2.8.5.4 Determination of Neurite Length 66
3. Results 67
3.1 Impact of Serum Response Factor on Mitochondrial Dynamics 67
3.1.1 SRF deficiency impairs mitochondrial structure and distribution *in vivo* 67
3.1.1.1 Mitochondrial ultrastructure is disheveled in *Srf* mutant tissue 67
3.1.1.2 Mitochondrial distribution but not amount is impaired in *Srf* mutant brain 69
3.1.1.3 SRF deficiency decreases ATP content and ATP production rate of tissue extracts 71

3.1.2 *In vitro* Effects of SRF on Mitochondria 73

3.1.2.1 SRF deficiency impairs mitochondrial size, occupancy and ultrastructure *in vitro* 73

3.1.2.2 SRF-deficiency impairs mitochondrial trafficking 76

3.1.2.3 SRF-mediated effects on distribution are mitochondria specific 78

3.1.2.4 Constitutively active SRF-VP16 restores normal mitochondrial size and occupancy in an SRF-deficient background *in vitro* 80

3.1.2.5 SRF-VP16 rescues mitochondrial trafficking in *Srf* mutant neurons..... 83

3.2 Impact of the Actin Cytoskeleton on Mitochondrial Dynamics 85

3.2.1 Mitochondrial size is dependent on the G/F-actin ratio in the cell 87

3.2.2 Actin dynamics modulate mitochondrial dynamics in growth cones 91

3.3 Cofilin Activity and its Influence on Mitochondrial Size and Distribution 95

3.3.1 Phospho-cofilin levels are increased in SRF-deficient cells 97

3.3.2 Non-phosphorylatable cofilin-S3A rescues mitochondrial size and occupancy in *Srf* mutant neurons 99

3.3.3 Cofilin-S3E decreases mitochondrial size and occupancy and circumvents SRF-VP16 mediated effects on mitochondria..... 101

3.3.4 Active Slingshot phosphatase restores phospho-cofilin levels and mitochondrial shape in *Srf* mutant neurons 103

3.4 Neuroprotective Implications of SRF's Function on Mitochondria 106

3.4.1 Constitutively active SRF-VP16 alleviates mutant huntingtin effects on mitochondria *in vitro* 107

3.4.2 SRF expression is impaired in an *in vivo* Huntington model 110

3.4.3 SRF-VP16 protects mitochondria against depolarizing agents 112

4. Discussion 114

4.1 Impact of SRF on mitochondrial dynamics 114

4.1.1 SRF influences mitochondrial (ultra)structure and size 114

4.1.2 SRF affects mitochondrial distribution and trafficking 117
4.2 Influence of actin dynamics on mitochondria 118
4.3 Regulation of cofilin activity and its relevance for mitochondrial dynamics 123
4.4 Neuropathological implications of SRF mediated regulation of mitochondrial function 127
5. Summary 129
6. Abbreviations 130
7. Literature 135

1. Introduction

This work deals with the impact of the serum response factor (SRF) on actin dynamics and its implication on neuronal mitochondria. For this reason, this introduction shall give an overview about SRF, the actin treadmilling process and actin binding proteins (ABPs) involved. Additionally, focus will be directed on neuronal mitochondrial dynamics in due consideration of mitochondrial size, localization and transport in non-pathological and neurodegenerative circumstances.

1.1 The Transcription Factor SRF

1.1.1 Structure and Characterization of SRF

The serum response factor (SRF) is a MADS box transcription factor, primarily described by Treisman and colleagues (Treisman, 1986; Norman et al., 1988). All members of the MADS box transcription factor family share the same conserved domain, the MADS box, named after the four originally identified members of this family: MCM-1 in yeast (Shore and Sharrocks, 1995), AG und DEFA in Drosophila (Sommer et al., 1990) and SRF in mammals. The human *Srf* gene consists of seven exons (Chai and Tarnawski, 2002) and alternative splicing gives rise to four different isoforms of SRF, which are expressed tissue-specifically (Kemp and Metcalfe, 2000).

The SRF protein most frequently found in tissue, especially in the brain, consists of 508 amino acids (aa) that lead to a mass of 67 kilodalton (kDa). Different domains are relevant for the biological function of SRF: a DNA binding domain (the MADS box), a transactivation domain (containing different sites of phosphorylation) and a nuclear localization sequence (NLS) (see Figure 1.1). The MADS box (aa 133-222) mediates dimerization of two SRF proteins and binding of this SRF homodimer to a “serum response element” (SRE). This SRE contains conserved CArG box [$CC(AT)_6GG$] DNA sequences (Minty and Kedes, 1986; Sun et al., 2006) and adjacent *cis*-elements which can be recognized by SRF’s binding partner proteins, e.g. transcription factors of the TCF family (Buchwalter et al., 2004).

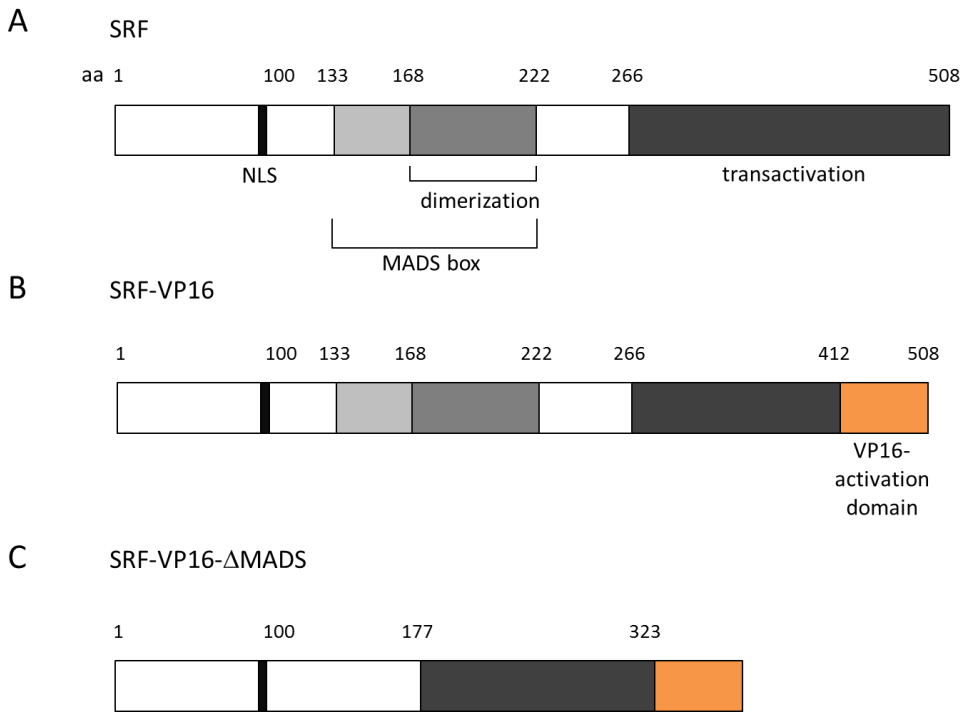

Figure 1.1 Structure of the SRF protein
Fig. 1.1A shows the main domains of the SRF protein (Johansen and Prywes, 1993). The NLS domain enables nuclear localization of SRF, the MADS box is important for DNA binding and dimerization of two SRF proteins. Phosphorylation of serine residues in the transactivation domain regulates SRF's transcriptional function. Figs. 1.1B and 1.1C display two SRF mutant proteins used in this study: SRF-VP16 (B) is constitutively active because parts of the SRF transactivation domain are replaced by the *Herpes simplex* virus VP16 transactivation domain. In contrast, SRF-ΔMADS-VP16 (C) is inactive due to lacking parts of the MADS box (Schratt et al., 2002). aa = amino acid.

The best characterized partner proteins are the ternary complex factors (TCFs) (Buchwalter et al., 2004), which connect mitogen-activated protein kinase (MAPK) signaling to transcriptional activation (see chapter 1.1.2.1), and members of the myocardin related transcription factor family (MRTFs) (Pipes et al., 2006), e.g. MRTF-A/MAL or MRTF-B (Posern and Treisman, 2006).

Besides binding of partner proteins, phosphorylation is another way of regulating SRF's transcriptional activity. Serine/threonine kinases (e.g. casein kinase II or $p44^{MAPK}$) can phosphorylate serine residues in the C-terminal part of the transactivation domain (Marais et al., 1992; Janknecht et al., 1993), the N-terminus of SRF (Manak and Prywes, 1991; Heidenreich et al., 1999) or directly in the MADS box (Iyer et al., 2006). The latter phosphorylation at serine-162 by protein kinase C-α seems to be important to regulate SRF's DNA binding ability.

Figure 1.1 shows the schematic structure of SRF. Furthermore, figures 1B, and 1C display two different SRF mutant proteins used in this study. By partial replacement of the SRF transactivation domain with the VP16 transactivation domain of the *Herpes simplex* virus (Wysocka and Herr, 2003), a constitutively active SRF-VP16 mutant is created. The proper control construct contains an SRF-VP16 protein lacking parts of the MADS box, thereby SRF-ΔMADS-VP16 is incapable of binding to DNA. In doing so, SRF-ΔMADS-VP16 controls for possible VP16 off-target effects (Schratt et al., 2002).

1.1.2 Regulation of SRF

The activity of SRF can be regulated by a variety of external stimuli. In neuronal cells synaptic activity, e.g. triggered by glutamate (Xia et al., 1996) or kainate (Herdegen et al., 1997), as well as KCl activation of voltage sensitive calcium channels (VSCCs) (Misra et al., 1994), leads to an intracellular increase of Ca^{2+} that functions as a second messenger. By activating MAP and Ca^{2+}/calmodulin-dependent (CaM) kinases, Ca^{2+} leads to direct SRF activation (Xia et al., 1996) or indirect stimulation of SRF cofactors (Johnson et al., 1997). Beyond that, SRF activity can be controlled by stimulation with neurotrophic factors like BDNF (Kalita et al., 2006; Meier et al., 2011) or NGF (Wickramasinghe et al., 2008). Furthermore, SRF activity can be stimulated in non-neuronal cells by lysophosphatidic acid (LPA), tumor necrosis factor β (TNFβ) or antioxidant agents (Chai and Tarnawski, 2002).

Control of SRF activity is mediated by different signaling cascades. On the one hand, MAP kinase cascade leads to direct or indirect activation of SRF or TCFs, on the other hand, the Rho-actin pathway activates MRTFs, thereby controlling a different set of SRF target genes (Gineitis and Treisman, 2001).

SRF mediated gene regulation is well described for two different types of genes. Upon engaging TCFs by activation of the MAPK cascade, SRF binds to SREs in the promotor region of immediate early genes (IEGs), thereby driving the expression of IEGs such as *c-fos* or *Egr1* (Schratt et al., 2001). In contrast to that, SRF can be recruited to gene regulatory elements of cytoskeletal genes by binding to MRTFs. This leads to the expression of actin genes (e.g. *Actb*, *Actg*) or actin-related genes (e.g. *Gsn* or *Vcl*), a process that is fine-tuned by the functional actin treadmilling in the cytoplasm (Sotiropoulos et al., 1999) (see Figure 1.2).

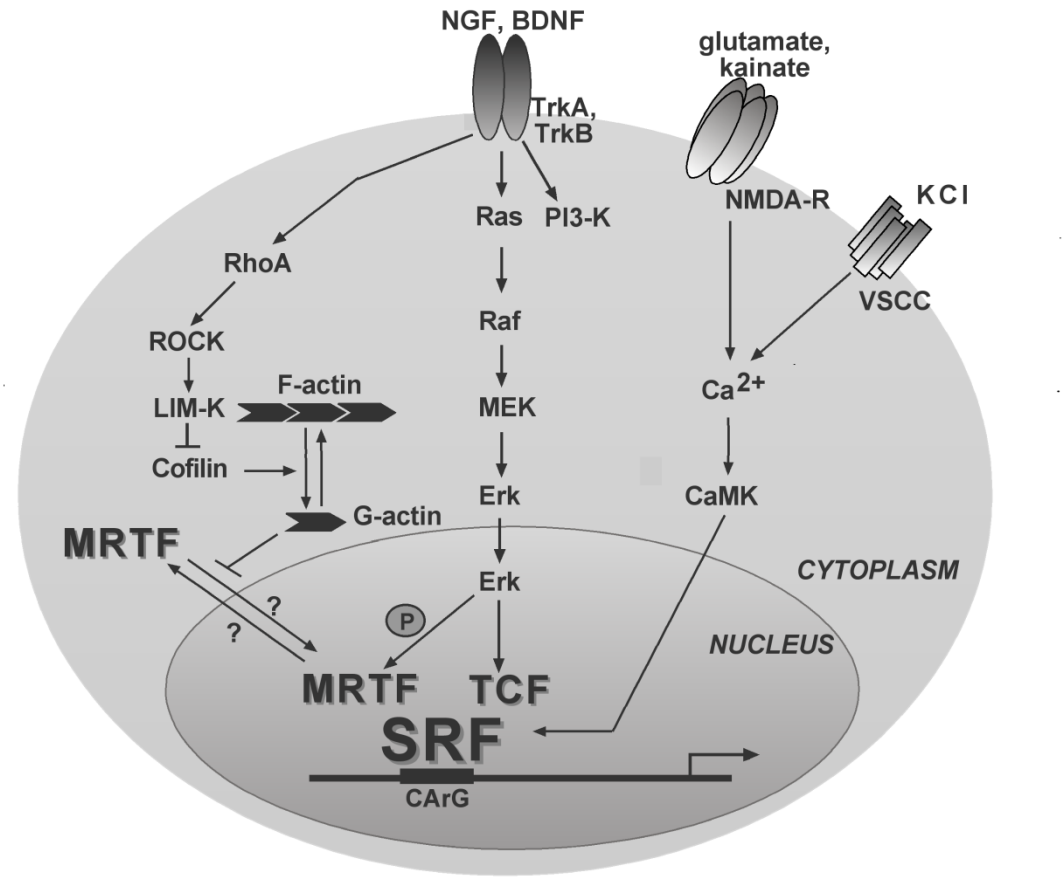

Figure 1.2 Regulation of SRF's transcriptional activity

SRF is regulated by different pathways. On the left side, the Rho-actin-MRTF pathway is depicted, leading to the expression of cytoskeletal genes. In the middle, MAP kinase pathway activates TCFs – that leads to the transcription of IEGs. Additionally, SRF is activated by CaM kinases that are stimulated by increasing levels of intracellular calcium. (Knöll and Nordheim, 2009)

1.1.2.1 TCF-dependent Regulation of Immediate Early Genes

As aforementioned, SRF controls the transcription of immediate early genes (IEGs). This is accomplished by recruitment of SRF partner proteins belonging to the TCF (ternary complex factor) family. Initially, external stimulation activates specific receptors, which in turn stimulate the activity of the small GTPase Ras. Ras itself activates Raf (rapidly accelerated fibrosarcoma), that leads to the initiation of a phosphorylation cascade that goes via MEK (MAP/ERK kinase) and ERK (extracellular signal regulated kinase), finally leading to the phosphorylation of TCFs in the nucleus (Johansen and Prywes, 1993; Hipskind et al., 1994).

TCFs like ELK-1, SAP-1 and NET belong to the family of ETS (E-twenty six) proteins (Yordy and Muise-Helmericks, 2000; Besnard et al., 2011). ETS proteins contain a conserved domain (the ETS domain) in the N-terminal region, which can bind to special regions on the DNA (the ETS motifs). Additionally, ETS proteins contain a B-box, which enables direct interaction with SRF (Hassler and Richmond, 2001) and C-terminal phosphorylation sites, that are targeted by the MAP kinases. Upon activation via phosphorylation by ERK (Zinck et al., 1993), TCF-SRF complex formation gets induced as well as binding of TCFs to the ETS-motifs (Giovane et al., 1994; Hipskind et al., 1994; Whitmarsh et al., 1995).

Of note, not only TCFs, but also SRF itself can be a direct target for phosphorylation. For example, the ribosomal S6-kinase $pp90^{rsk}$, a direct target of the MAP kinase cascade, phosphorylates SRF, thereby enhancing SRF's DNA binding affinity (Rivera et al., 1993). On the other hand, phosphorylation of serine residues in the C-terminus of SRF reduce the expression of IEGs (Janknecht et al., 1993). Thus, SRF's activity can get regulated by direct phosphorylation in different directions.

Recruitment of TCFs enables SRF to drive the expression of IEGs, e.g. *c-fos* or *Egr-1*. Indeed, SRF's participation in gene transcription was shown for the first time for the regulation of *c-fos* (Norman et al., 1988), whose expression increases transiently after serum stimulation (Greenberg and Ziff, 1984). The fast ("immediate early") expression of c-Fos elicits a second gene expression wave ("delayed gene expression") by forming a transcription complex together with c-Jun that leads to the expression of a further set of genes (Turjanski et al., 2007).

1.1.2.2 MRTF-dependent Regulation of Cytoskeletal Genes

Besides regulating IEGs, SRF controls the expression of genes that are cytoskeletal related (e.g. *Actb*, *Actg*, *Gsn* or *Vcl*). This transcriptional activity of SRF is regulated by actin treadmilling and binding of MRTFs (myocardin related transcription factors) to monomeric G-actin (Olson and Nordheim, 2010).

In this context, SRF recruits MRTFs that function as "actin sensing" molecules, thereby integrating the polymerization status of cytoplasmic actin into the control of gene expression. This actin-MRTF-SRF gene expression axis was firstly discovered in non-neuronal cells (Miralles et al., 2003) and relies on MRTF's ability to bind monomeric G-actin thereby modulating nuclear shuttling of MRTFs (Mouilleron et al., 2008). Members of the MRTF

family (e.g. MRTF-A or MRTF-B (Wang et al., 2002)) are able to bind monomeric G-actin through their N-terminal RPEL domains (Miralles et al., 2003). Thus, at high cytoplasmic G-actin concentrations MRTFs form a reversible complex with G-actin and are held back in the cytoplasm in an inactive state (Posern et al., 2002). Furthermore, even nuclear G-actin influences the activity of MRTFs by increasing their nuclear export and interfering with the MRTF-SRF complex formation (Vartiainen et al., 2007).

Upon cell stimulation Rho-GTPases (e.g. Rac, RhoA, Cdc42) become activated (Posern and Treisman, 2006), which finally leads to a shift of the G/F-actin ratio towards filametous F-actin thereupon decreasing the pool of monomeric G-actin. This releases e.g. MRTF-A from G-actin and leads to nuclear entry (Miralles et al., 2003) allowing for MRTF-SRF-complex formation and subsequent expression of cytoskeletal related target genes (Schratt et al., 2002). As actin isoforms (e.g. β-actin) are direct target genes of SRF, an auto-regulatory feedback loop emerges from this signaling cascade: External stimulation leads to Rho activation, decreasing the G-actin pool by forming F-actin, which liberates MRTF-A and increases the expression of new actin proteins that restore the cytoplasmic G-actin pool, causing a decrease of the MRTF mediated SRF activation.

Nuclear shuttling of MRTF molecules has been described for non-neuronal cells. Of note, in neurons different ways of MRTF regulation are likely to exist, as transient nuclear entry of MRTF has been described as well as permanent nuclear localization of this SRF partner protein (Tabuchi et al., 2005; Kalita et al., 2006; Stern et al., 2009).

1.1.3 Connection between TCF- and MRTF-dependent SRF regulation

As TCF- and MRTF-recruitment regulate different sets of genes, it is tempting to assume that these signaling cascades are mutually exclusive. This is supported by the fact that TCFs and MRTFs compete for the same binding domain in the SRF protein (Wang et al., 2004). Furthermore, MRTF-A phosphorylation by ERK1/2 leads to its nuclear export. Thereby MRTF activity is decreased during MAP kinase cascade stimulation (Kalita et al., 2006; Muehlich et al., 2008). Additionally, MRTF can interfere with the MAP kinase signaling by inducing the expression of mitogen-inducible gene 6 (Mig6) or dual specificity phosphatase (DUSP5), both alleviating the activity of MAP kinase signaling (Descot et al., 2009).

1.1.4 Neuronal Functions of SRF

SRF is a ubiquitously expressed transcription factor and exerts its function in many tissues. As this work deals with neuron specific effects of SRF, neuronal functions of SRF shall be described at this point (see Figure 1.3).

SRF is expressed throughout most brain regions, including striatum, cortex and hippocampus and to a less extent in the thalamus (Herdegen et al., 1997; Stringer et al., 2002; Knöll et al., 2006). Outside the brain, SRF is expressed during embryonic development in dorsal root ganglia (DRG) (Wickramasinghe et al., 2008).

Analysis of murine adult brain revealed SRF's influence on neuronal plasticity. SRF is activated upon intracellular increase of Ca^{2+}, as it occurs after strong depolarization processes that lead to opening of NMDA-receptors (Platenik et al., 2000). Thus, it is reasonable that *Srf* depletion has an impact on long term potentiation (LTP) processes, which are important for functional **learning and memory**. In agreement, it was shown that conditional *Srf* depletion in adult brains leads to deficits in learning behavior (Etkin et al., 2006; Johnson et al., 2011). Furthermore, the expression of SRF target genes that are influenced by synaptic activity (e.g. *c-fos*) is reduced as well. Of note, neuronal survival was not impaired during *Srf* depletion in adult brain (Ramanan et al., 2005). However, recent

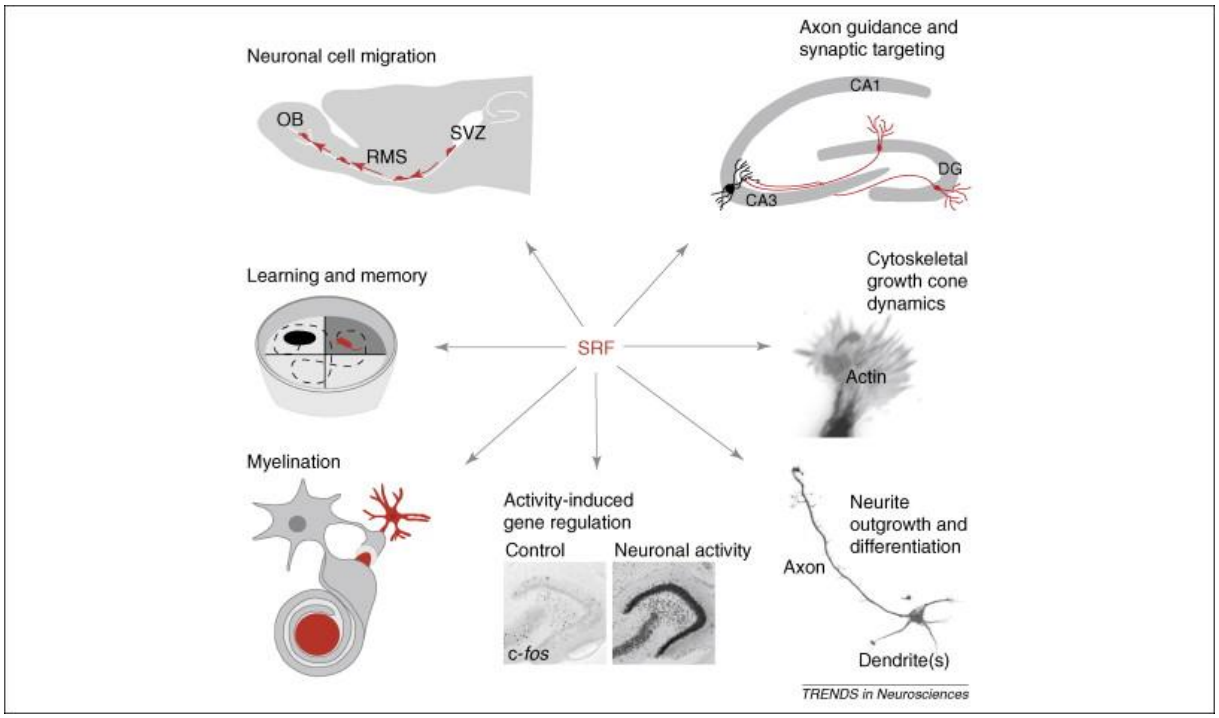

Figure 1.3 Neuronal functions of SRF

Details see text. (Knöll and Nordheim, 2009)

research showed that constitutively active SRF-VP16 is able to improve neuronal survival in a facial nerve injury model (Stern et al., 2012).

In addition, SRF plays a substantial role during development of the central nervous system (CNS). As embryonic knockout of *Srf* is lethal (Arsenian et al., 1998), murine forebrain specific SRF conditional knockout animals have been generated (Wiebel et al., 2002) to address SRF's function in CNS development. In these *Srf* mutant mice, the *Srf* gene is flanked by loxP sites that are recognized by the Cre enzyme (cyclization / recombination). Cre is expressed under the control of the CamKIIα promotor, which is only active in neurons in the hippocampus, cortex and, less prominent, in striatum, thalamus and hypothalamus (Casanova et al., 2001). Upon forebrain specific expression of Cre, *Srf* gets removed in neurons in late embryonic stages allowing for investigation of SRF's impact on neuronal development. These *Srf* knockout mice display a severe phenotype including locomotor and balance impairments, reduced body weight and size and die around three weeks of age (Alberti et al., 2005).

In this context it was found that SRF impairs **neuronal cell migration** from the subventricular zone (SVZ) along the rostral migratory stream (RMS) to the olfactory bulb (Alberti et al., 2005). Furthermore, *Srf* depletion leads to defects in **axonal guidance and synaptic targeting** during hippocampal development (Knöll et al., 2006) and impairs axonal pathfinding and branching in dorsal root ganglia (DRGs) (Wickramasinghe et al., 2008). Recent research revealed SRF's role in development of hippocampal architecture as hippocampal lamination is disturbed in an *Srf* deficient background (Stritt and Knöll, 2010). In line, it was shown that SRF regulates the formation of major axonal tracts in the murine forebrain as *Srf* deletion in neuronal progenitor cells leads to impairments in axonal fiber tract formation (Lu and Ramanan, 2011)

Furthermore, *Srf* deletion has an impact on oligodendrocytes via a paracrine mechanism involving secretion of connective tissue growth factor (CTGF). In this regard, *Srf* deletion leads to impaired oligodendrocyte development and less **myelination** *in vivo* (Stritt et al., 2009).

As neuronal motility is dependent on functional cytoskeletal rearrangements, it is reasonable that at least some of the aforementioned neuronal deficits *in vivo* rely on SRF's ability to influence the actin cytoskeleton. This is supported by the finding that cytoskeletal genes (e.g. *Actb* or *Gsn*) are downregulated *in vivo* and the amount of inactive phospho-

cofilin (an actin severing protein, introduced in more detail in chapter 1.2.3) is increased in an *Srf* mutant brains (Alberti et al., 2005). Furthermore, deletion of the SRF partner proteins that sense the actin polymerization status of the cell, the MRTFs, leads to *in vivo* phenotypes similar to those of SRF deficient animals (Mokalled et al., 2010). *In vitro* studies expanded the view of SRF's role in **microfilament dynamics** in neurons. Cultivated neurons lacking *Srf* display misshaped growth cones that are rounded, lack finger like filopodia and do not respond to guidance cues (e.g. ephrin-A5), indicating non-functional actin motility in this particular neuronal structure (Knöll et al., 2006; Stern et al., 2009). Such *Srf* mutant neurons show a bipolar morphology and reduced **neurite length**, a phenotype that can be reversed by overexpression of constitutively active SRF-VP16 (mentioned in chapter 1.1.1) (Knöll et al., 2006).

To sum it up, SRF loss-of-function (LOF) decreases neurite outgrowth *in vivo* and *in vitro*, impairs axonal pathfinding and response to guidance cues, dishevels hippocampal lamination and reduces myelination. Of note, it was not investigated in detail so far, whether these effects are due to reduced expression of actin related genes in general or whether these effects can be ascribed to changes in the activation status of cofilin, which is highly phosphorylated upon SRF depletion (Alberti et al., 2005; Mokalled et al., 2010). The latter will be addressed in this work.

1.2 The Actin Cytoskeleton

1.2.1 Structure of Actin

Actin is the most abundant protein in eukaryotic cells and is involved in more protein-protein interaction than any other known protein (Dominguez and Holmes, 2011). Actin comes in three main isoforms: α-actin (consisting of three isoforms, expressed in skeletal, cardiac and smooth muscle, respectively), β- and γ-actin, which are expressed in non-muscle (β-actin) and muscle cells (γ-actin) (Tondeleir et al., 2009). The 42 kDa monomeric G-(globular) actin folds into two major domains called α and β. However, a traditional four-subdomain nomenclature is used to describe the particular regions of the molecule (Kabsch et al., 1990). Whereas subdomains 1 and 3 are structurally related, subdomains 2 and 4 can be seen as insertions into subdomains 1 and 3 (see Figure 1.4). The two major domains α and β face only little contact as the polypeptide chain passes twice between these domains forming a hinge region in the middle of the molecule. Thus, two clefts are formed, the upper one between domains 2 and 4 forming a nucleotide binding side, the lower one between domains 1 and 3 mediating longitudinal interactions in the F-(filamentous) actin and between actin and small actin binding proteins (ABPs) (Oda et al., 2009; Fujii et al., 2010). Located in the nucleotide cleft, Ser14 and His73 loops are required to sense the state of the

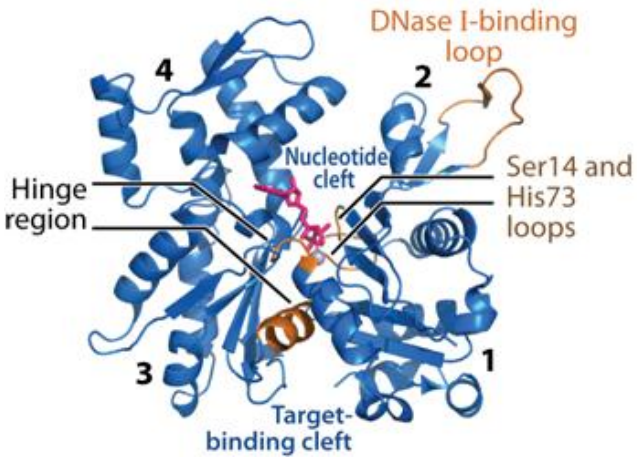

Figure 1.4 Structure of monomeric actin

Monomeric G-actin forms four subunits. Thereby, subdomains 1 and 3 form a hydrophobic target binding cleft and subdomains 2 and 4 create a nucleotide cleft. The DNase I-binding loop is required for alongside interactions in F-actin polymers (Dominguez and Holmes, 2011).

bound nucleotide thereby mediating the structural changes involved during hydrolysis of bound ATP (Graceffa and Dominguez, 2003). Outside the subdomain 2 a sensor loop called DNase I-binding loop is found, which mediates interactions with neighboring actin filaments in the F-actin polymer.

1.2.2 Actin Dynamics

Formation of filamentous actin and the depolymerization of F-actin to monomeric G-actin are important processes underlying cellular motile processes, e.g. growth cone dynamics in neurons (Pak et al., 2008). In this context, assembly and disassembly of F-actin must be highly organized to secure functional cellular motility.

When forming a filamentous actin structure, monomeric G-actin molecules are added to the so called barbed (+) end of a filament. G-actin is associated with ATP, which is hydrolyzed upon binding of actin to the barbed end. This hydrolysis and subsequent P_i release alters actin conformation (Moraczewska et al., 1999) thereby weakening the subunit interactions and facilitating the release of ADP-actin. Of note, ATP hydrolysis comes within seconds after

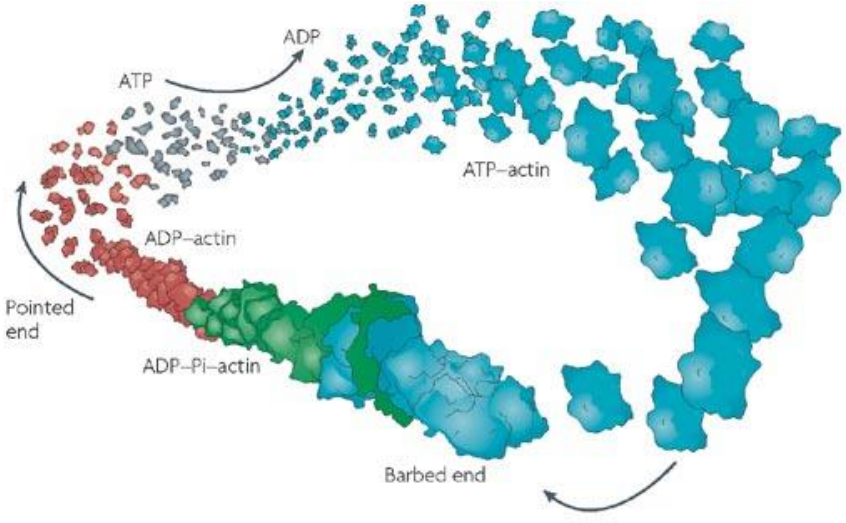

Figure 1.5 Actin dynamics and treadmilling

Monomeric ATP-bound actin assembles at the barbed end. Subsequent hydrolysis and P_i-release result in conformational changes of actin favoring disassembly at the pointed end. At steady-state, assembly and disassembly occur at the same time, a process called treadmilling (Pak et al., 2008).

ATP-actin binding to the barbed end, whereas release of Pi occurs on average 600 seconds after hydrolysis (Pak et al., 2008). Thus, an actin filament can consist of three different types of actin-nucleotide complexes: ATP-actin, ADP-P_i-actin and ADP-actin (see Figure 1.5) whereupon ADP-actin gets released from the F-actin at the pointed (-) end. Finally, ATP/ADP-exchange restores the active ATP-G-actin complex that can assemble at the barbed end again. Notably, the two different ends of an F-actin structure maintain different monomeric G-actin concentrations for assembly, referred as "critical concentrations". Thus, when the concentration of G-actin lies between these two critical concentrations, actin assembly at the barbed end and disassembly at the pointed end occur at the same filament simultaneously. This steady-state process is called actin treadmilling. Interestingly, actin treadmilling is highly energy consumptive and is supposed to account for almost 50% of ATP turnover in cultivated neurons (Bernstein and Bamburg, 2003).

Actin treadmilling has been known for a long time by *in vitro* studies (Wegner, 1976). However, in a cellular environment actin dynamics is much more complex including F-actin bundling, crosslinking and meshwork formation (Pollard and Borisy, 2003). In this context, many actin binding proteins (ABPs) are involved in organization of the actin cytoskeleton.

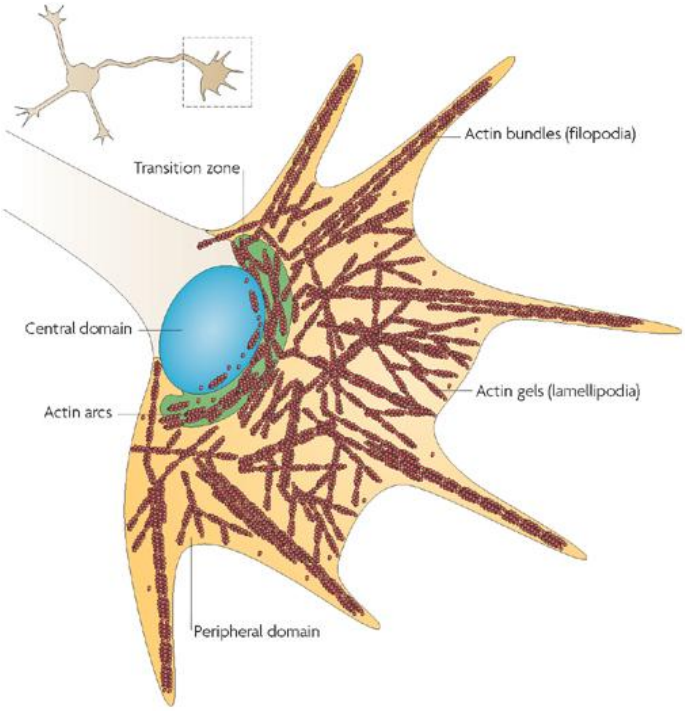

Figure 1.6 Actin superstructures in a growth cone

Actin forms different structures in this model growth cone. Small transverse actin bundles (arcs) are present in the transition zone, whereas the peripheral zone comprises actin meshwork and long bundles (filopodia) (Pak et al., 2008).

Especially neurons show highly organized cellular structures that are dependent on functional actin dynamics, e.g. the growth cone (see Figure 1.6). This substructure is exemplary for the complexity of actin structures in neurons. In a growth cone different types of actin superstructures can be found: The central domain is predominantly free of actin and surrounded by a transition zone comprised of bundled actin (the actin arcs (Gallo and Letourneau, 2004)), followed by mesh-like actin in the peripheral domain, the latter also containing filopodia consisting of long actin bundles. Of note, in neurons formation of F-actin structures is likely to be a local process e.g. in the cell body or the growth cone. In contrast, microtubules can be found throughout the cell body and the neurite but are restricted from the growth cone.

As mentioned above, many ABPs facilitate the formation of these actin superstructures. In neurons, new filaments are nucleated by assistance of formins (Faix and Grosse, 2006), Spir proteins (Kerkhoff, 2006), cofilin (Andrianantoandro and Pollard, 2006) or the Arp2/3 complex (Goldberg et al., 2000), the latter also mediating side branching of F-actin in an angle of 70° (Robinson et al., 2001). F-actin gets anchored at membranes supported by e.g. cortactin (Weaver et al., 2003) or vinculin (Steketee and Tosney, 2002). Finally, F-actin disassembly involves ABPs like gelsolin (Lu et al., 1997) or cofilin (Meberg and Bamburg, 2000).

These ABPs are not only required to maintain the growth cone structure but also to respond to guidance cues (Kalil and Dent, 2005). One distinguishes guidance cues that attract axonal growth (e.g. BDNF) or repulse it (which is regulated e.g. by ephrins). These guidance cues act primarily on growth cone motility as this cellular substructure can easily change its shape by influencing local actin dynamics. Thereby, stimulation with BDNF increases F-actin based filiopodia formation, whereas ephrin-A5 stimulation leads to a growth cone collapse by F-actin depolymerization (Meier et al., 2011).

1.2.3 Cofilin

F-actin disassembly and reorganization is regulated by several ABPs, including those of the ADF (actin depolymerizing factor)/cofilin family. In mammals, three different isoforms of ADF/cofilin are expressed: ADF, non-muscle cofilin (cofilin-1) and muscle cofilin (cofilin-2) (Vartiainen et al., 2002).

Cofilins regulate actin turnover by cleaving F-actin into oligomers, a process called **severing** (see Figure 1.7). Cofilins bind co-operatively to F-actin (Hayden et al., 1993) with highest affinity for ADP-actin (Maciver and Weeds, 1994). Cofilin binding to F-actin induces a twist in the filament (McGough et al., 1997; Galkin et al., 2001) thereby initiating actin subunit loss from the pointed end (Carlier et al., 1997). This cofilin mediated off-rate enhancement of F-actin can lead to further cleavage of the actin oligomers or creates new barbed ends that can function as new seeds for further F-actin polymerization. Thus, whether F-actin severing leads to ultimate disassembly of the actin filament or increases F-actin formation depends on the physiological circumstances (Condeelis, 2001). Furthermore, *in vitro* studies have shown that filament assembly or disassembly also depends on the cofilin/actin ratio (Van Troys et al., 2008). At low cofilin concentrations relative to actin, single cofilin molecules bind to F-actin and induce severing as described above (Andrianantoandro and Pollard,

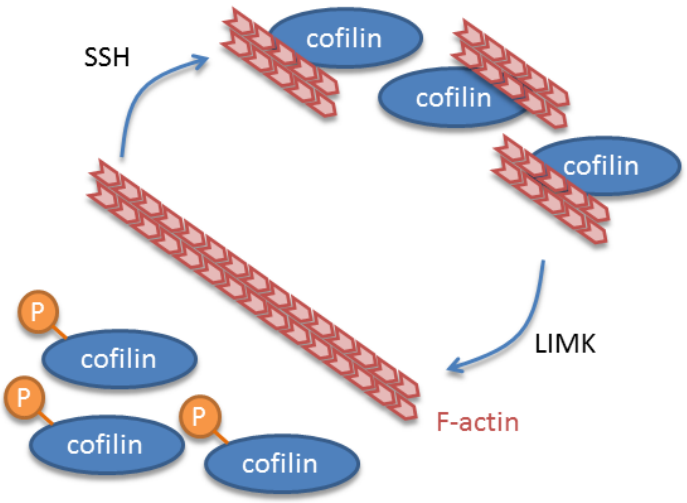

Figure 1.7 Regulation and activity of cofilin

The actin severing protein cofilin is inactive and cannot bind to F-actin if it is phosphorylated. Upon slingshot (Ssh) mediated dephosphorylartion, cofilin regains its binding ability for F-actin and cleaves F-actin into oligomeric parts. LIM kinase (LIMK) inactivates cofilin by phosphorylation at Ser3 (modified after (Huang et al., 2006)).

2006). At higher cofilin/actin ratios, cofilin stabilizes F-actin in a twisted conformation (Chan et al., 2009). When the cofilin/actin ratio is further increased *in vitro*, cofilin can even function as an F-actin nucleator leading to *de novo* synthesis of F-actin (Andrianantoandro and Pollard, 2006). Nevertheless, it remains to be elucidated whether this cofilin/actin ratio-dependence of cofilin's activity has any physiological implication on e.g. growth cone dynamics or whether this is just an *in vitro* observation.

Of note, another cofilin concentration dependent process has been observed recently: If cofilin is overexpressed or cells are oxidatively stressed, the formation of cofilin-actin bundles, called "rods", is induced (Bamburg et al., 2010). These cofilin-actin-rods seem to play a role in neurodegenerative diseases as it was reported that rods impair axonal trafficking and induce synaptic loss in hippocampus (Cichon et al., 2011) and are found in Alzheimer's brains (Minamide et al., 2000) as well as in huntingtin aggregates (Munsie et al., 2011).

As changes in actin dynamics might contribute to neurite growth, it was investigated whether cofilin impacts neurite elongation. It was shown, that activation of LIMK (and subsequent inactivation of cofilin) results in decreased neurite outgrowth (Birkenfeld et al., 2001). In line, knockdown of cofilin or its activating phosphatase slingshot leads to impaired neurite outgrowth, too (Endo et al., 2007). Additionally, overexpression of a constitutively active cofilin construct resulted in an increase of very long neurites *in vitro* (Garvalov et al., 2007). Recent research revealed that cofilin is involved in mediating neurite outgrowth in response to the growth promoting cell adhesion molecule L1 (Figge et al., 2012). This favors a model of active cofilin being required for neurite extension. Therefore, this study addresses whether increased phospho-cofilin levels in *Srf* mutant neurons account for the observed impairments in neurite elongation in case of SRF depletion.

Besides its main function as an F-actin severing protein, cofilin can act in different contexts in the cell. Interestingly, cofilin seems to be involved in nuclear shuttling of monomeric actin. As cofilin has a nuclear localization sequence (Iida et al., 1992) and actin does not, cofilin is assumed to form a piggybag-protein mediating nuclear entry of G-actin (Pendleton et al., 2003; Vartiainen, 2008).

Furthermore, cofilin is supposed to play a role in mitochondria-dependent apoptosis as it was shown that cofilin translocates to mitochondria upon stauroporine stimulation or oxidative stress and induces cytochrome c release (Chua et al., 2003; Klamt et al., 2009). This

cofilin function is independent from actin binding, nevertheless in this context mitochondria dynamics seems to be somehow intertwined with actin dynamics (Rehklau et al., 2011).

How is cofilin regulated?

There are several possibilities to modulate cofilin's function including tyrosine 68 phosphorylation and subsequent ubiquitinylation (Yoo et al., 2009), pH-dependent inhibition (Bernstein et al., 2000; Pavlov et al., 2006) or oxidation (Klemke et al., 2008). However, the most important regulation goes via phosphorylation at serine 3. Phosphorylated cofilin is inhibited from binding to F-actin and thereby incapable of fulfilling its severing activity. Cofilin is phosphorylated by LIM kinases or TES kinases (Van Troys et al., 2008). LIM kinases are targets of the RhoGTPase pathway and become activated e.g. by ROCK1 or ROCK2 (Bernard, 2007). This plays an important role in the Rho signaling pathway mentioned in chapter 1.1.2.2. In this context, activation of LIM kinase leads to inactivation of cofilin and a subsequent shift in the G/F-actin ration thereby inhibiting MRTF-A from entering the nucleus and forming an SRF-MRTF-complex (see Figure 1.2). On the other hand, cofilin can be reactivated upon dephosphorylation via slingshot (Ssh) phosphatase or chronophin (Huang et al., 2006). Research has been focused on the upstream regulation of these kinases and

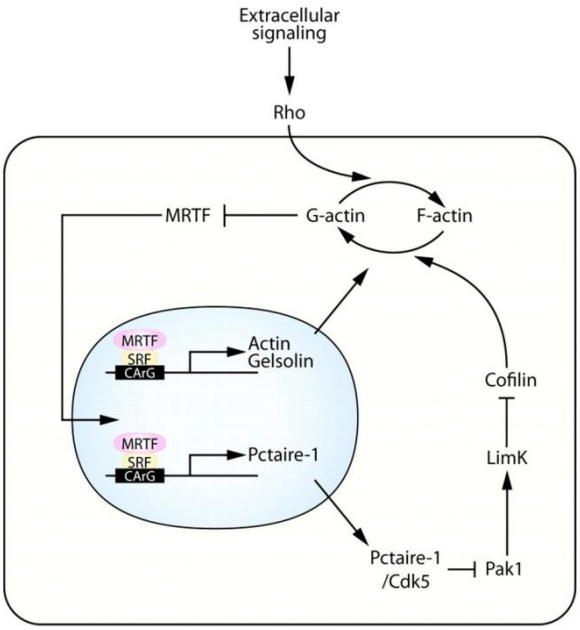

Figure 1.8 Regulation of Cofilin-Activity by MRTF-SRF transcriptional activity
MRTF-SRF mediated gene transcription leads to inactivation of LIMK, thereby decreasing phospho-cofilin-levels. Details see text. (Mokalled et al., 2010)

phosphatases and many signaling pathways seem to be engaged in this context (Bamburg, 1999; Bamburg and Bernstein, 2008). At this point, focus shall be directed on the regulatory loop that emerges from SRF activity (see Figure 1.8).

Cofilin phosphorylation is a hallmark of SRF deficiency in neurons (Alberti et al., 2005). Mokalled and colleges claim, that under basal conditions SRF inhibits cofilin phosphorylation by inhibiting LIM kinase activity (Mokalled et al., 2010). In detail, the MRTF-SRF-transcription complex drives the expression of Pctaire-1, which together with Cdk5 inhibits PAK1, an upstream kinase of LIM kinase. Thereby, PAK1 mediated LIM kinase activation is reduced leading to low levels of phosphorylated cofilin (see Figure 1.8). Thus, active cofilin is present to disassemble F-actin, which can lead to an increase of G-actin and inactivation of MRTF. In that way, a negative regulatory feedback loop is formed, as more G-actin shuts off the MRTF-SRF transcriptional activity. In contrast, SRF depletion leads to hyperphosphorylated cofilin due to permanent activation of LIM kinase and reduces neuronal motility due to impaired actin turnover.

It is worth mentioning that it was unclear so far whether impaired cofilin function underlies the observed phenotypes in *Srf* mutant neurons (Knöll et al., 2006) and could be reversed by restoring cofilin activity. This important question was addressed during this project. It was investigated whether overexpression of an active Ssh phosphatase on an *Srf* mutant background could rescue neurite outgrowth. Furthermore, a constitutively active non-phosphorylatable cofilinS3A mutant was applied to rescue neurite outgrowth in *Srf* mutant neurons. In doing so, this project offers new insights into the role of cofilin in maintaining neuronal motility.

1.3 Mitochondria

Mitochondria are remarkably complex organelles that fulfill many functions in cells. They constantly undergo reorganization in size and shape whereupon the integrity of their highly organized substructure is always maintained. Mitochondria are the main ATP producers in the cell but additionally are involved in e.g. Ca^{2+} buffering and mediating apoptosis.

At this point, focus shall be addressed to mitochondrial function in neurons as this special cell type particularly relies on functional mitochondrial biology. Interestingly, the brain is one of the major consumers of O_2 and glucose, which feed the oxidative phosphorylation and production of ATP: Although the brain represents less than 2% of the whole body weight, it requires more than 20% of the consumed oxygen and glucose (Bolanos et al., 2009). Of note, the metabolism of neurons and their neighboring astrocytes seems to be interconnected as astrocytes are the prime consumers of glucose and they release most of their metabolized glucose as lactate (Bolanos et al., 1994), which then gets metabolized aerobically by neurons (Kasischke et al., 2004). In contrast to astrocytes and other cell types, neurons are totally reliant on functional mitochondria as they cannot switch to glycolytic metabolism if mitochondrial activity is inhibited (Almeida et al., 2001). This is due to the fact that neurons lack 6-phosphofructo-2-kinase/fructose-2,6-bisphosphatase 3 (PFKBP3), an enzyme that stimulates glycolysis. Thereby, neurons are much more sensitive towards mitochondrial stress than other cells as it is reflected by many neurodegenerative diseases that are caused by malfunctioning mitochondria (see chapter 1.3.5).

1.3.1 Structure and Function

Mitochondrial functionality is relying on a defined ultrastructural organization. Mitochondria display a double-membrane architecture, which was initially observed in the 1950s (Palade, 1953). In this regard, the outer mitochondrial membrane (OMM) is permeable to uncharged molecules up to a size of 5 000 kDa due to insertion of voltage dependent anion channels (VDACs) into the outer membrane (Mannella, 1992). In contrast, the inner mitochondrial membrane (IMM) is impermeable and forms many loops and invaginations (called cristae) into the innermost area of the mitochondrion, the mitochondrial matrix (see Figure 1.9). Of note, one should not consider mitochondrial objects as static organelles with a persistent

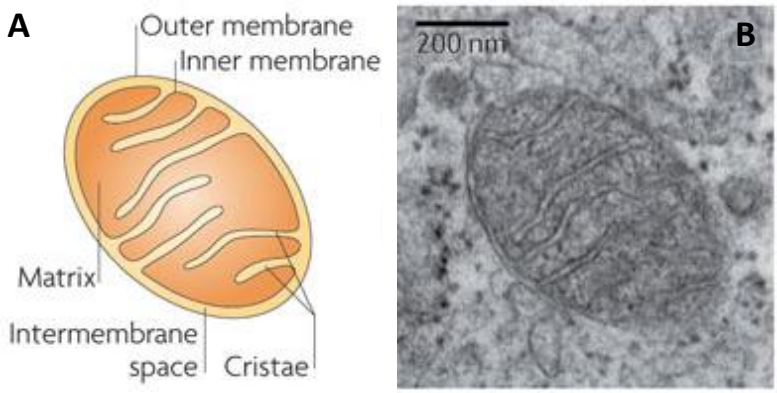

Figure 1.9 : Structure of a single mitochondrion

A: Scheme of the mitochondrial ultrastructure. Mitochondria have an outer and an inner membrane, the latter folding cristae into the matrix.
B: Electron microscopic picture of a mitochondrion.
(Westermann, 2010)

morphology, because mitochondria constantly undergo structural rearrangements in size and shape and form large network like structures as initially observed by live cell microscopy in the 1980s (Bereiter-Hahn, 1990). Recent research revealed that even cristae formation should not be seen as static parallel invaginations as depicted in textbooks (or in Figure 1.9), because electron microscopic based visualization revealed complex cristae tubules and lamellae (Frank et al., 2002; Riva et al., 2010).

Structure and function of mitochondria are closely interconnected. Mitochondria are the main producers of ATP in cells, which is generated at the IMM in a process called oxidative phosphorylation. This involves the transfer of electrons from NADH or $FADH_2$, generated in the degradation of glucose, pyruvate, amino acids or fatty acids, to the electron transport chain consisting of complex I, II, III and IV sitting at the IMM. Electron transport along these complexes leads to a transport of protons across the IMM into the intermembrane space, creating a negative membrane potential of mitochondria compared to the cytosol ($\Delta\Psi$ between -150mV and -180mV) (Duchen, 2004). When protons move back into the matrix through the F_O-F_1-ATPase, this electrochemical gradient is used to create new ATP molecules (Nakanishi-Matsui et al., 2010).

Additionally, the negative membrane potential is used for another function of mitochondria i.e. buffering of cytosolic calcium (Szabadkai and Duchen, 2008). In this context, a Ca^{2+} uniporter transports Ca^{2+} into the matrix and subsequently Ca^{2+} can be stored as an insoluble phosphate-salt by reaction with PO_4^{3-}. This ability to regulate calcium homeostasis is

important for signaling processes as Ca^{2+} serves as a second messenger within many signaling pathways (Berridge et al., 2000).

Of note, mitochondria play an important role in controlling apoptosis (Danial and Korsmeyer, 2004). Cellular stress can lead to a cyctochrome c release from the mitochondrial matrix (Goldstein et al., 2000). Normally, cytochrome c is needed to transport electrons from complex III to complex IV in the electron transport chain, but upon mitochondrial release cytochrome c binds to cytoplasmic APAF-1 (apoptotic protease activating factor), which finally leads to activation of effector caspases such as caspase-3 that perform the ultimate cell death (Li et al., 1997). Interestingly, it was shown that the ABP cofilin is able to translocate to mitochondria after apoptosis induction and lead to cytochrome c release (Chua et al., 2003; Klamt et al., 2009). Thus, additionally to the well described apoptotic pathways known so far, there seems to be an interconnection of apoptosis-related mitochondrial function and the actin cytoskeleton.

1.3.2 Transport and Trafficking

Many neuron specific processes are highly ATP-consumptive, especially reversing the ion influx after membrane depolarization in case of action potentials or synaptic transmission. Furthermore, neurons are polarized cells and distinct cellular regions can be a long way away from each other (one imagines motor neurons that project their axons more than 1 meter along the spinal cord). As ATP cannot diffuse to the areas of its consumption (Hubley et al., 1996), mitochondria must be transported to their final destinations to fulfill the energy needs at different regions in the cell (as depicted in Figure 1.10) (MacAskill and Kittler, 2009; Sheng and Cai, 2012).

When mitochondria are visualized during time-lapse imaging microscopy, it becomes obvious that transport of mitochondria is not following a permanent, one-directional trafficking pattern. It is rather a dynamic movement behavior showing phases of transport alternating with phases of stopping, changing the direction or immobilization (Hollenbeck and Saxton, 2005; Misgeld et al., 2007; Kang et al., 2008). This is due to the fact that mitochondria associate with different motor proteins, which mediate mitochondrial transport. In this context, long range transport processes are accomplished by motor

proteins travelling along microtubules. Microtubules are composed of α- and β-tubulin forming a tube-like structure that is arranged in a polarized manner with plus and minus ends. In axons, microtubules are oriented with their minus end towards the cell body and the plus end directed distally (Heidemann et al., 1981), thereby defining the general elongated shape of an axon (Baas, 2002). Transport of mitochondria along microtubules is

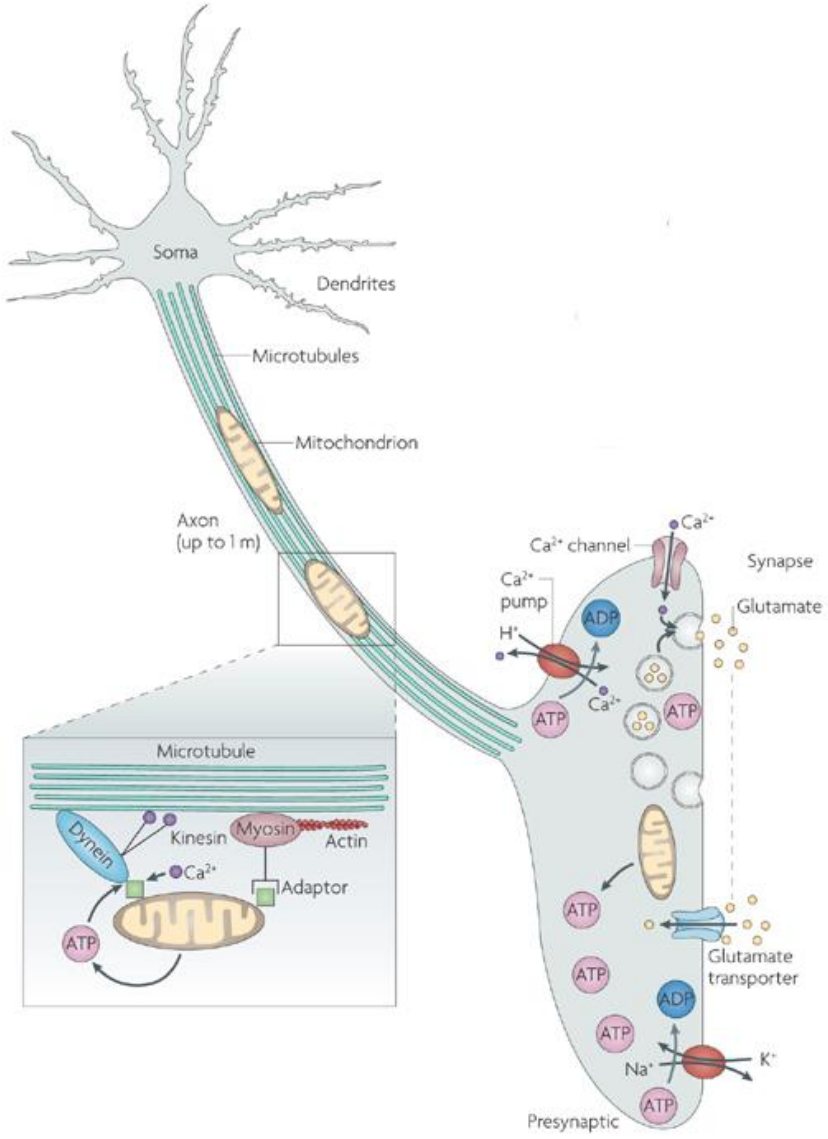

Figure 1.10 Mitochondria involved in neuronal function

Mitochondria are important to supply ATP for energy demanding processes in a neuron, which are mainly linked to maintaining the ion homeostasis across the plasma membrane. Fast axonal transport of mitochondria goes via microtubule associated transport molecules. Kinesins mediate anterograde transport, dyneins transport mitochondria retrogradely. Myosins are supposed to mediate short range movement along actin filaments. Transport molecules bind to mitochondria via certain adaptor molecules. (Knott et al., 2008)

performed by kinesin superfamily proteins (KIFs) and dynein (Hirokawa et al., 2010). Most of the kinesins move towards the plus end of microtubules, whereas dyneins move the opposite direction. In doing so, kinesins mediate anterograde movement (i.e. towards distal parts, e.g. the growth cone or synapse) and dyneins are engaged in retrograde transport towards the cell body (Martin et al., 1999).

In case of KIFs, at least 45 different genes, which are classified into 14 families, have been described (Hirokawa et al., 2010). Most important for neuronal mitochondrial transport are members of the kinesin-1 family (known as KIF5) (Tanaka et al., 1998; Pilling et al., 2006). The motor domain is located in the N-terminus of a KIF5 heavy chain, whereas the C-terminus contains interaction domains for kinesin light chains, cargoes or cargo adaptors (MacAskill and Kittler, 2009). KIF5 interacts indirectly with mitochondria via the Milton adaptor protein or the mammalian Milton orthologues TRAK1 and TRAK2 (Brickley et al., 2005), respectively. Milton itself mediates bridging of KIF5 and Miro (Mitochondrial rho), a RhoGTPase located in the OMM (Fransson et al., 2006). For this, Milton binds to the C-terminal cargo-binding domain of the kinesin heavy chain (Glater et al., 2006). Thereby, Milton, Miro and KIF5 form an anterograde transport complex, which is specific for mitochondria. Additionally, another adaptor protein has been identified that mediates the contact of KIF5 and mitochondria: syntabulin (Cai et al., 2005). Syntabulin attaches directly to the OMM and the cargo-binding domain of KIF5.

In contrast to KIF5, dynein motors are much larger and display a more complex assembly of two heavy and several light chains and facilitate retrograde mitochondrial transport (Karki and Holzbaur, 1999; Pilling et al., 2006). Whereas dynein heavy chains function as motors, dynein light and intermediate chains, together with other polypeptides, are involved in mediating the interaction with mitochondria. However, these interaction processes are poorly understood so far. Several anchoring mechanisms for dynein motors have been proposed, including interaction with mitochondrial outer membrane protein voltage-dependent anion-selective channel 1 (VDAC1) (Schwarzer et al., 2002) or Miro (Russo et al., 2009). Furthermore, it is unclear whether additional adaptor molecules are required for mitochondrial interaction, e.g. dynactin (King and Schroer, 2000), a molecule that enhances the processivity of the dynein motor and is believed to link dynein to microtubules and mitochondria.

How is mitochondrial transport regulated?

As mitochondria move bidirectionally, it is likely that kinesin and dynein motor proteins are simultaneously associated with a mitochondrion. Indeed, dynein has been colocalized with mitochondria moving anterogradely and retrogradely (Hirokawa et al., 1990). However, impairing kinesin-driven transport does not automatically lead to dynein-mediated retrograde mitochondrial movement (MacAskill et al., 2009; Wang and Schwarz, 2009). Hence, kinesin and dynein motors together seem to coordinate mitochondrial transport rather than simply act antagonistically in a "tug of war" fashion (Ligon et al., 2004; Welte, 2004). It is more likely that bidirectional mitochondrial transport is controlled by different processivities of the motor proteins which is accomplished by diverse adaptor molecules linking kinesin or dynein to a mitochondrion (Sheng and Cai, 2012).

Mitochondria must be stopped at regions where their ATP production is needed. For this, docking mechanisms require proteins that immobilize mitochondria at microtubules. This particular mechanism has been shown for syntaphilin, which forms a "static anchor" for mitochondria at microtubules (Kang et al., 2008), thereby disrupting both, kinesin- and dynein-driven mitochondrial transport. Interestingly, the dynein light chain LC8 has been identified to stabilize the syntaphilin-microtubule interaction (Chen et al., 2009). This argues for a model of dynamic interactions between docking molecules, transport proteins and cytoskeletal compartments.

Mitochondrial transport is regulated by neuronal metabolism and electrophysiological activity. In this regard, mitochondria are stopped at regions of low ADP (Mironov, 2007) as well at high concentrations of Ca^{2+} (MacAskill et al., 2009). Calcium levels are a key regulator of mitochondrial transport as recent research revealed that the Miro protein is the essential calcium sensor leading to the arrest of mitochondria at levels of high Ca^{2+} (Saotome et al., 2008; MacAskill et al., 2009; Wang and Schwarz, 2009). For this, Miro's EF hand domains bind Ca^{2+} leading to conformational changes of the whole protein that disrupt kinesin mediated transport. However, the exact mechanism of Miro-kinesin interaction is still a matter of controversy.

1.3.3 Fusion and Fission

Mitochondria constantly undergo rearrangements in structure and size during processes called fission and fusion (see Figure 1.11) (Detmer and Chan, 2007). These mechanisms allow for the control of the number and size of mitochondria and additionally regulate the mixing of metabolites of different mitochondrial particles.

Mitochondrial fission is performed, at least in part, by two evolutionary conserved proteins, Drp1 and hFis1 (Knott et al., 2008). While hFis1 is present at the OMM (Mozdy et al., 2000), Drp1 is suggested to form 8-12 unit oligomers during a self-nucleating process (Ingerman et

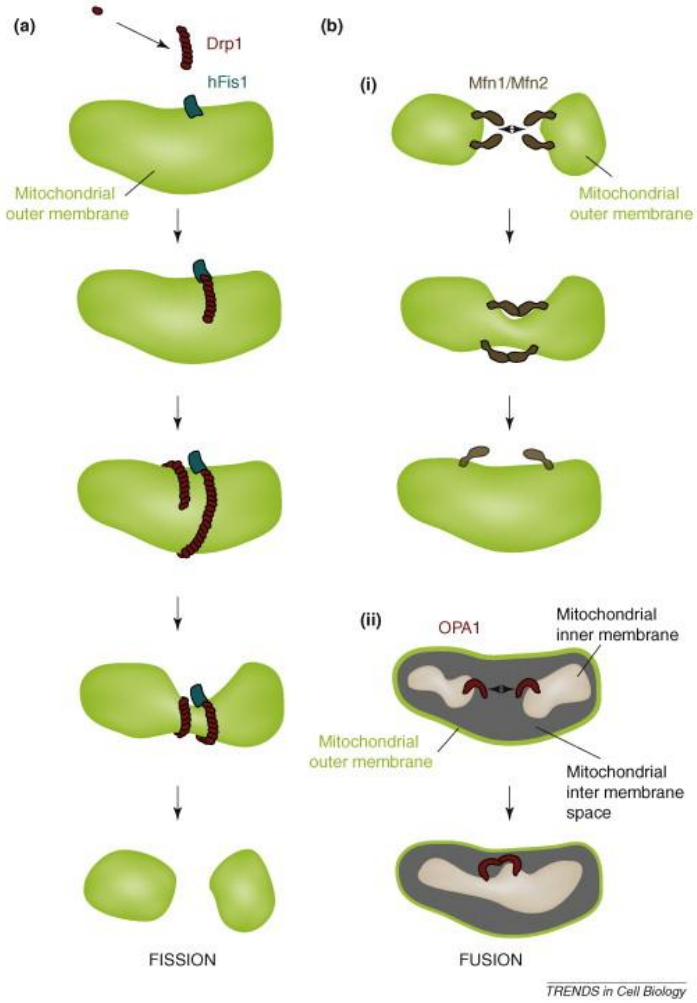

Figure 1.11 Mitochondrial fission and fusion

(a) Drp1 primarily oligomerizes and is recruited to the outer membrane by hFis1. Susbequently formed Drp1 spiral chains constrict upon GTPase activity of Drp1 that leads to fission of the mitochondrion.

(b) (i) Fusion of the outer membrane is mediated by *trans*-dimerization of mitofusins and following GTPase activity that tethers the outer membranes.
(ii) Inner membrane fusion occurs in a similar manner upon dimerization of OPA1.

(MacAskill and Kittler, 2009)

al., 2005). Drp1 itself belongs to the family of dynamin GTPases with an N-terminal GTPase domain and a C-terminal GED interaction domain (Smirnova et al., 1998). Recruitment of Drp1 to the OMM by hFis1 leads to fully Drp1 oligomerization and formation of a spiral chain around the mitochondrion. Afterwards, hydrolysis of Drp1 bound GTP leads to conformational changes in the Drp1 ring like structure (Ingerman et al., 2005) leading to a reduction of the mitochondrial diameter from 0.5 µm to 0.1 µm, which finally results in mitochondrial fission.

On the other hand, mitochondrial fusion is a two-step process requiring fusion of the outer and the inner membrane. In mammals, OMM fusion is mediated by mitofusin 1 (MFN1) and mitofusin 2 (MFN2) that are sitting in the OMM and exhibit a C-terminal hydrophobic coiled-coil structure that facilitate *trans* hetero- or homodimerization between MFN1 and MFN2 (Chen et al., 2003). Subsequently, GTPase activities of the MFN proteins induce conformational changes leading to convergence of the outer membranes of two fusing mitochondria (Koshiba et al., 2004). Inner membrane fusion is performed by the GTPase OPA1 that is located at the IMM. Similar to mitofusins, OPA1 seems to interact with itself in *trans* to tether mitochondrial inner membranes (Meeusen et al., 2006).

Mitochondrial fusion and fission is controlled by several signaling processes. For instance, synaptic activity increases mitochondrial fission (Rintoul et al., 2003; Li et al., 2004) as do increasing levels of nitric oxide (Zanelli et al., 2006). In this context, Drp1 seems to be the main regulated protein and can be phosphorylated (Chang and Blackstone, 2007), sumoylated (Harder et al., 2004) or ubiquitinylated (Karbowski et al., 2007). Thus, the fusion-fission balance can be fine-tuned by multiple signaling cascades (Knott et al., 2008).

1.3.4 Mitochondria and the Actin Cytoskeleton

So far, mitochondrial dynamics in neurons has been described mainly in the context of microtubule associated proteins. Of course, long distance fast axonal transport is mediated via microtubules, but additionally the actin cytoskeleton plays a poorly understood role in short range movement, anchoring of mitochondria and recruiting of adaptor molecules. In this context, one should remember that microtubules are distributed throughout the neurite whereas F-actin is mainly found in the cell body, the growth cone and side branches of a

neurite. For this reason, the actin cytoskeleton *per se* cannot function as a platform for long-range movement; nevertheless it could influence local positioning of mitochondria.

Actin based movement has been described in detail for yeast where most of the mitochondrial transport is mediated along F-actin (Frederick and Shaw, 2007). But also in neurons actin microfilaments are important cytoskeletal compartments in the cell body or growth cones. Additionally, it has been shown that even in the axon mitochondria are transported along F-actin (Morris and Hollenbeck, 1995; Ligon and Steward, 2000) but it is generally believed that microfilaments rather assist short-range mitochondrial movement in contrast to long-distance microtubule based transport. Movement processes along F-actin require the action of myosin motor proteins (Foth et al., 2006) that are slower than kinesin or dynein motors. Recent research revealed that myosin XIX might be one possible myosin motor involved in mitochondrial transport (Quintero et al., 2009). Furthermore, myosin V can form hetero-motor complexes with dynein light chain; thereupon a "dual motor complex" comprising dynein and myosin could coordinate mitochondrial transport (Naisbitt et al., 2000). This leads to the question, how such different transport processes can be regulated.

Up to now, research data indicates a rather antagonistic function of microtubule- and actin-based mitochondrial transport: Disrupting F-actin leads to an increase in mitochondrial movement (Morris and Hollenbeck, 1995) and F-actin is required for mitochondrial docking in axons (Chada and Hollenbeck, 2004). Recently it has been shown that silencing of

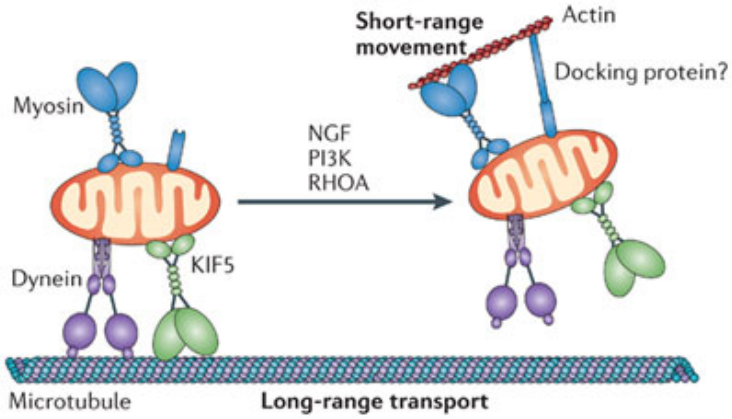

Figure 1.12 Mitochondrial Transport along Microtubules and Actin Filaments

Long-range transport is mediated by microtubule associated dyneins and kinesins (in case of axonal transport: KIF5). Upon NGF signaling or RhoA activation, mitochondria get detached and transferred to actin based short-range movements performed by myosins. It is unclear whether docking proteins are involved in arresting mitochondria at microfilaments (Sheng and Cai, 2012).

myosin V or myosin VI increased mitochondrial transport (Pathak et al., 2010). This favors a model in which myosins distract mitochondria from microtubules and lead to fine-tuned and slower mitochondrial transport in areas that are F-actin rich and rather microtubule free (e.g. growth cones, see Figure 1.12). This would also explain the saltatory movement pattern observed during mitochondrial transport consisting of pausing, restarting, slowing down and accelerating as well as directional changes.

If this is the case, F-actin enrichment leads to mitochondrial arrest and thereby regulates mitochondrial mobility. Indeed, it has been shown that nerve growth factor (NGF) mediated signaling leads to docking of mitochondria at F-actin rich structures (e.g. the growth cone) (Chada and Hollenbeck, 2004). Nevertheless, it is not known whether this NGF mediated stopping of mitochondrial transport is mediated by a direct mitochondrion-actin interaction or by an unidentified docking molecule. However, independently from NGF mediated docking of mitochondria, mitochondrial tethering in dendritic spines can be facilitated by WAVE1 (Sung et al., 2008). Normally, WAVE1 (together with Arp2/3) functions as an actin filament nucleator (Pollitt and Insall, 2009) but here WAVE1 seems to serve as an actin-mitochondria linking molecule. Additionally, it has been shown that stimulation of RhoA cascade by lysophosphatidic acid (LPA) can lead to an inhibition of fast mitochondrial transport, indicating that actin-based arresting of mitochondria seems to be important to regulate signal-dependent mitochondrial stopping (Minin et al., 2006).

Little attention has been directed to actin's contribution to modeling mitochondrial size and shape. Up to now, it is assumed that mitochondria require stationary phases to assemble their fission machinery (Pathak et al., 2010). Consequently, increasing mitochondrial transport would decrease fission and lead to larger mitochondria. This is supported by experiments showing larger mitochondria upon expression of an arresting-incompetent Miro protein (Saotome et al., 2008). Furthermore, mitochondrial size is decreased upon Miro null-mutations (Russo et al., 2009) speaking in favor of a fission machinery requiring stationary mitochondria. Interestingly, F-actin needs to be present in an endothelial cell line to recruit Drp1 to mitochondria (De Vos et al., 2005).

To sum it up, actin's contribution to functional mitochondrial dynamics is poorly understood so far. It is supposed that actin mediates short-range movement at slower velocities as observed during long-range transport. Little focus has been addressed on alterations in mitochondrial size and shape according to the F-actin status in a neuron. It is believed that

immobilization of mitochondria at F-actin is required to recruit the fission machinery, although experimental data is meager. Furthermore, it is not known if a shift in the G/F-actin ratio influences mitochondrial dynamics with regard to size and structure. This study shall address these novel points and tries to discover actin's contribution to mitochondrial size, shape and trafficking.

1.3.5 Mitochondria in Neurodegenerative Diseases

As aforementioned, neurons are highly reliant on functional mitochondria and are much more sensitive to mitochondrial dysfunction than other cell types. Therefore, many neurodegenerative diseases are linked to malfunctioning mitochondria and have been extensively reviewed (DiMauro and Schon, 2008).

Ascribing neurodegenerative diseases to mitochondrial malfunction is always somewhat controversial as it is often unclear whether a disease is caused by mitochondrial failure or whether the latter is a secondary effect arising from progression of the neurodegeneration. Of course, some neurodegenerative diseases have been directly linked to dysfunctional mitochondrial proteins. In this context, miscellaneous parts of mitochondrial function can be impaired, e.g. complex I or II activity in the respiratory chain (entailing Leigh syndrome (Tatuch et al., 1992)), protein transport across the IMM (leading to Mohr-Tranebjaerg syndrome (Roesch et al., 2002)), KIF5-mediated mitochondrial transport (causing hereditary spastic paraplegia (Fichera et al., 2004)), OPA1-assisted IMM-fusion (resulting in autosomal dominant optic atrophy (Alexander et al., 2000)) or outer membrane fusion by mitofusins (inducing Charcot-Marie-Tooth disease (Zuchner et al., 2004)). Early onset and acute clinical problems are common to all of these classical mitochondrial diseases. But there is emerging evidence that mitochondrial dysfunction is a general problem underlying also neurodegenerative diseases with late-age onset.

In case of **Parkinson's disease** this link to mitochondrial impairment is well described (Burbulla and Kruger, 2011). During this sporadic age-related disease, neuronal death in the substantia nigra leads to motor impairments. Research revealed functional disturbances of different proteins in Parkinson's disease: Parkin is associated with the OMM, serves as a E3 ubiquitin ligase and has a protective role against mitochondrial swelling during apoptosis

(Darios et al., 2003). PINK1 is a mitochondrial kinase that also protects against apoptosis (Petit et al., 2005). Furthermore Omi/HTRA2, DJ-1, α-synuclein and mortalin are involved in mitochondrial mediated apoptosis. Malfunctions in any of these proteins play a role in Parkinson's disease (Polymeropoulos et al., 1997; Strauss et al., 2005; Zhang et al., 2005; Burbulla et al., 2010).

Amyotrophic lateral sclerosis is another late-onset sporadic or familial neurodegenerative disease whereupon motor neurons in the cortex as well as in the spinal cord are affected. It is believed that impaired function of the Cu,Zn-superoxid dismutase 1 (SOD1) serves as the molecular basis of this disease. SOD1 can be found partly in the intermembrane space of mitochondria (Sturtz et al., 2001) and functions as a protection enzyme against O_2^--superoxide radicals . Abnormalities of SOD1 function lead to accumulation of SOD1 in mitochondria (Liu et al., 2004) and opening of mitochondrial transition pores, resulting in mitochondrial swelling (see Figure 1.13) (Martin et al., 2009).

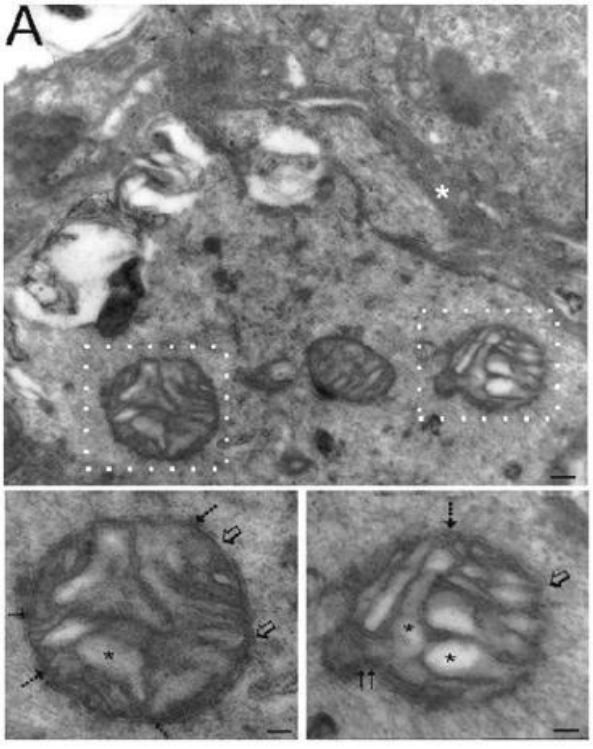

Figure 1.13 Mitochondrial swelling in an ALS disease model

Electron microscopic pictures of mitochondria in spinal cord ventral horn dendrites of a mutant SOD1 model mice show ultrastructural changes. Mitochondria display IMM and OMM contacts (hatched arrows), openings of the OMM (open arrow) and vesicularization (asterisks). Scale bars = 0.63 µm (A); 0.3 µm (A, insets).
(Martin et al., 2009)

Alzheimer's disease is a neurodegenerative disorder of late onset and long course (Mattson, 2004). This dementing disease is characterized by neuronal loss especially in cortex and hippocampus. Whereas the main histopathological hallmarks are clear (accumulation of extracellular β-amyloid plaques and neurofibrillary tangles comprising hyperphosphorylated microtubule associated protein tau (Jucker and Walker, 2011)), the molecular basis for this disease remains enigmatic. This is particularly true for the role of mitochondria in this regard. It has been reported long ago that mitochondrial activity seems to be impaired in Alzheimer's disease (Azari et al., 1993; Mastrogiacomo et al., 1993). Later research showed that also axonal transport is affected (Pigino et al., 2003; Stokin et al., 2005), which might contribute to mitochondrial mislocalization. However, it is still controversial whether mitochondrial impairments are causative for the onset of Alzheimer's or just a subsequent secondary effect. Interestingly, occurrence of so called cofilin-actin rods (see chapter 1.2.3) has been shown in Alzheimer's disease model brains (Minamide et al., 2000; Fulga et al., 2007). These rods co-localize with hyperphosphorylated tau tangles (Whiteman et al., 2009) as well as β-amyloid plaques (Zhao et al., 2006) and could also be induced *in vitro* by amyloid-beta protein (Davis et al., 2009). Of note, cofilin-actin rod-formation seems to be detrimental for mitochondrial function as rod-formation blocks intracellular trafficking thereby affecting mitochondrial function (Cichon et al., 2011).

In case of **Huntington's disease** (HD) mitochondrial contribution to disease onset and progression is understood in more detail. HD is an autosomal dominant disorder characterized by progressive chorea, rigidity, seizures, dementia and psychical disturbances which result from progressive loss of GABAergic neurons in striatal brain regions as well as in the cortex (Rosas et al., 2002). HD is caused by malfunctioning huntingtin, which is an extremely large protein (approximately 350 kDa) with multiple cellular functions ranging from transcriptional activity (Kegel et al., 2002) or protein trafficking (Strehlow et al., 2007) to vesicle transport (Caviston et al., 2007) and mitochondrial movement (Orr et al., 2008). Huntingtin develops pathological impact upon an N-terminal expansion of glutamate repeats. Normally, less than 35 glutamate repeats do not have a pathological consequence, whereas more than 40 repeats lead to full penetrance of HD (Myers, 2004). It has been assumed for a long time that poly-glutamatergic huntingtin forms neuronal aggregates impairing normal neuronal function (DiFiglia et al., 1997). However, the exact mechanism by which huntingtin exerts its abnormal function remains elusive as even normal huntingtin's

role is complex and not fully understood so far (Cattaneo et al., 2005). Recent research revealed that one main target of dysfunctional huntingtin might be mitochondria and huntingtin's impact on mitochondrial function has been extensively reviewed (Bossy-Wetzel et al., 2008).

In brief, three main hypotheses have been postulated how mutant huntingtin could impair mitochondrial function. Firstly, mutant huntingtin seems to impair transcriptional regulation of several mitochondrial genes. This is accomplished by a huntingtin-mediated transcriptional block of PGC-1α (Cui et al., 2006). PGC-1α is a key transcriptional co-regulator involved in the expression of genes controlling mitochondrial respiration or oxidative stress defense (Puigserver and Spiegelman, 2003). Although it was observed that PGC-1α was reduced in mutant huntingtin mouse R6/2 brains (Cui et al., 2006; Weydt et al., 2006), which decreases PGC-1α mediated neuroprotective effects, it cannot explain all the mitochondrial defects in HD.

Secondly, it is believed that mutant huntingtin interferes with mitochondrial trafficking. Interestingly, normal huntingtin interacts with HAP-1 (huntingtin associated protein 1) that in turn can bind to dyneins or kinesins thereby facilitating mitochondrial transport (Gauthier et al., 2004; McGuire et al., 2006). In this context, phosphorylation of huntingtin regulates the switch from anterograde to retrograde transport (Colin et al., 2008). Mutant huntingtin interacts more tightly with HAP-1 thereby inhibiting mitochondrial transport (Gauthier et al., 2004). Furthermore, it is believed that huntingtin aggregates can form physical roadblocks that hamper mitochondrial trafficking (Chang et al., 2006).

Thirdly, mutant huntingtin is supposed to impair the mitochondrial fusion/fission balance, although this hypothesis has not been studied in detail. Still, some observations indicate that mutant huntingtin leads to mitochondrial fission. For example, mitochondria in HD model systems show distribution patterns similar to DRP1 (Panov et al., 2002), mutant huntingtin effects could be circumvented *in vitro* by overexpression of Mfn2 (Wang et al., 2009) or mutant huntingtin overexpression resulted in activation and mitochondrial localization of DRP1 resulting in fission (Costa et al., 2010).

1.4 Aim of this work

Mitochondrial dynamics has been studied in detail with special regard to microtubule assisted long-range transport (MacAskill and Kittler, 2009). However, little attention has been paid on contribution of other cytoskeletal components to mitochondria.

Especially the role of actin microfilaments in mitochondrial dynamics is poorly understood so far. Although there is some evidence for a possible function of actin in mediating short-range movement (Chada and Hollenbeck, 2003) and recruitment of the fission machinery (Pathak et al., 2010), the general function of actin treadmilling and its impact on mitochondria has not been studied. Furthermore, it is not known whether actin binding proteins participate in controlling mitochondrial dynamics; however, some functions have been shown for cofilin (Klamt et al., 2009; Cichon et al., 2011).

As SRF is a key regulator of actin as well as cofilin dynamics, an SRF based approach was used to investigate actin's and cofilin's contribution to mitochondrial dynamics. This work addresses this issue in the following manner:

At first, the general impact of SRF on mitochondrial dynamics was investigated. For this, *Srf* mutant animals were used in a loss-of-function (LOF) study. Furthermore, in a gain-of-function (GOF) approach constitutively active SRF-VP16 was applied and mitochondrial (ultra)structure as well as trafficking properties (transport and distribution) analyzed.

Second, it was examined whether the observed phenotypes could be explained by altered actin treadmilling. For this purpose, actin mutants as well as BDNF and ephrin-A5 stimulation were applied, allowing for a selective shift in the G/F-actin ratio.

Third, cofilin's contribution towards actin-based mitochondrial dynamics was explored. In this context, again LOF and GOF approaches (using cofilin and slingshot mutant proteins) were applied to recapitulate *Srf* mutant phenotypes or to circumvent the latter.

In doing so, this work reveals the impact of the **SRF-cofilin-actin axis** with regard to mitochondrial dynamics as well as neuronal motility in general.

Additionally, a neuroprotective function of SRF on mitochondria was investigated in case of Huntington's disease. Thereby, a new view on SRF's and actin's contribution to functional mitochondria is delivered that might serve for better understanding of neurodegenerative diseases as well as neuronal mitochondrial dynamics in general.

2. Material and Methods

2.1 Technical Devices

Technical Device	Manufacturer
Analytical balance	BP 210S, Sartorius
Benchtop centrifuges	Heraeus Pico 17, Fresco 17, Thermo Scientific
Centrifuge for cell culture	Megafuge 1.0R, Thermo Scientific
Dry block heating system	QBD2, Grant
Electron microscope	Tecnai G2, FEI
Electroporator	Dr. L. Fischer, Heidelberg
Fluorescence lamp	X-Cite 120, EXFO
Fluorescence microscope	Axiovert 200M, Zeiss
Ice machine	Scotsman
Incubator	HERAcell 150i, Thermo Scientific
Laminar flow	Heraeus
Light microscope	Leica
Live cell incubator	Incubator XI-3, Tempcontrol 37-2, CTI-Controller 3700, Pecon
Luminometer	Lumat LB 9507, Berthold
Magnetic stirrer	Heidolph
NanoDrop	NanoDrop 1000, Thermo Scientific
pH meter	mettler Toledo
Photometer	Genesys 105 UV-Vis, Thermo Scientific
Power supply	EV231, peqlab
Precision balance	PCB, Kern
SDS-PAGE and blotting apparatus	BioRad
Stereomicroscope	Stemi DV4, Zeiss
Vibratome	VT1000S, Leica
Vortex mixer	scientific industries
Waterbath	memmert

2.2 Chemicals

Chemical	Reference
ß-mercaptoethanol	AppliChem
Adenosindiphosphate (ADP)	AppliChem
Adenosintriphosphate (ATP)	Molecular Probes
Agar	AppliChem
Agarose	AppliChem
Ammonium persulfate	Genaxxon
Ampicillin	Roth
B27 supplement	Invitrogen
Borax	AppliChem
Boric acid	Sigma
Bromphenol Blue	AppliChem
Bovine serum albumin fraction V	AppliChem
Calcium chloride ($CaCl_2$)	AppliChem
DAPI (4',6-Diamidino-2-phenylindol)	AppliChem
Dimethyl sulfoxide (DMSO)	AppliChem
Dithiothreitol (DTT)	Molecular Probes
Ethanol	Sigma
Ethylenediaminetetraacetic acid (EDTA)	AppliChem
Ethidium bromide	Roth
Firefly luciferase	Molecular probes
Formaldehyde	Roth
Fetal calf serum (FCS)	AppliChem
Gentamicin	Invitrogen
Glucose	Sigma
Glycerol	AppliChem
Glycine	AppliChem
HBSS	Gibco
Hydrogen chloride (HCl)	Roth
Hydrogen peroxide (H_2O_2)	Fischar
Isopropyl alcohol	Fluka

Kanamycin	Sigma
Laminin	Sigma
Latrunculin B	Sigma
L-Glutamine	Invitrogen
Magnesiumchloride ($MgCl_2$)	Merck
Magnesiumsulfate ($MgSO_4$)	AppliChem
Malic acid	Sigma
Methanol	Sigma
Mowiol	Calbiochem
Nitric acid (HNO_3)	AppliChem
Nonfat dried milk powder	AppliChem
Paraffin	Merck
Paraformaldehyde (PFA)	AppliChem
Penicillin-Streptomycin (Pen/Strep)	Invitrogen
Peptone	AppliChem
Petri dishes (100 x 15 mm)	BD Falcon
Phalloidin-505	Invitrogen
Phalloidin Texas Red-X	Invitrogen
Phenylmethylsulfonyl fluoride (PMSF)	AppliChem
Phosphate buffered saline (PBS)	AppliChem
Polyacrylamide (PAA)	AppliChem
Poly-L-lysine (PLL)	Sigma
Ponceau-S	Sigma
Potassium chloride (KCl)	AppliChem
Propyl gallate	AppliChem
Protease inhibitor (complete, EDTA free)	Roche
Proteinase K	Roche
Sodium chloride (NaCl)	Sigma
Sodium dodecyl sulfate (SDS)	AppliChem
Sodium fluoride (NaF)	AppliChem
Sodium hydrogen carbonate ($NaHCO_3$)	Sigma
Sodium hydrogen phosphate (Na_2HPO_4)	Merck
Sodium dihydrogen phosphate (NaH_2PO_4)	Merck

Sodium hydroxide (NaOH)	Roth
Sodium orthovanadate (Na_3VO_4)	Sigma
Sodium pyruvate	Invitrogen
Sucrose	AppliChem
Tetramethylethylendiamine (TEMED)	Roth
Tris(hydroxymethyl)aminomethane	Sigma
Triton®-X-100	AppliChem
Tryptone	AppliChem
Tween 20	AppliChem
Xylene	VWR

2.3 Antibodies

2.3.1 Primary Antibodies

Antigen	Isotype	Source	Dilution	Application
Acetyl-tubulin	mouse	Sigma	1:2000	Western Blot (WB)
c-Jun	rabbit	Santa Cruz	1:500	Immunohistochemistry (IHC)
Cofilin	rabbit	Bamburg laboratory, Colorado State University, Colorado	1:500	Immunocytochemistry (IC)
Cofilin	mouse	Cell Signaling	1:1000	WB
FLAG	mouse	Sigma	1:300	IC
GFP	rabbit	Molecular Probes	1:1000	WB
GFP	mouse	Roche	1:1000	IC
GM130	rabbit	Abcam	1:1000	IC, WB
His	rabbit	Bethyl	1:10.000	IC
Human IgG (Fc-specific)	goat	Sigma	10 µg / ml	oligomerisation of ephrin-A5
Lamp1	rat	Santa Cruz	1:300	WB
MRTF-A	rabbit	Santa Cruz	1:500	WB
pan-actin	mouse	Linaris	1:500	WB

Phospho-cofilin	rabbit	Bamburg laboratory, Colorado State University, Colorado	1:500	IC
Phospho-cofilin	rabbit	Cell Signaling	1:1000	WB
RelA	rabbit	Santa Cruz	1:500	IHC
SOD2	rabbit	Millipore	1:500	WB
SRF	rat	Nordheim laboratory, University of Tübingen	1:200	WB
Tom20	rabbit	Santa Cruz	1:500	IHC, IC
ubiquitin	mouse	Abd Serotec	1:1000	IHC
VP16	rabbit	Abcam	1:1000	IC
VP16	mouse	Santa Cruz	1:500	IC
β-Tubulin	mouse	Sigma	1:5000	IC, WB
GFP	mouse	Roche	1:1000	WB

2.3.2 Secondary Antibodies

Antigen	Label	Isotype	Source	Dilution	Application
Mouse IgG	Alexa-488	goat	Molecular Probes	1:1500	IC
Mouse IgG	Alexa-660	goat	Molecular Probes	1:1000	IC
Rabbit IgG	Alexa-488	goat	Molecular Probes	1:1500	IC
Rabbit IgG	Alexa-660	goat	Molecular Probes	1:1000	Ic
Rabbit IgG	HRP	goat	Thermo Scientific	1:2000	WB
Mouse IgG	HRP	goat	Thermo Scientific	1:2000	WB
Rat IgG	HRP	goat	Santa Cruz	1:2000	WB

2.4 Plasmids

Plasmid	Function	Source
CofilinS3A-GFP	Non-phosphorylatable cofilin mutant; GFP-tagged	Bradke Laboratory, DZNE Bonn
CofilinS3E-GFP	Phosphomimetic cofilin mutant; GFP-tagged	Bradke Laboratory, DZNE Bonn
CofilinWT-GFP	Wildtype cofilin; GFP-tagged	Bradke Laboratory, DZNE Bonn
G15S-actin	Actin mutant favoring F-actin assembly, low cofilin binding capacity; FLAG-tagged	Posern Laboratory, MPI of Biochemistry, Munich
GFP	Expression of Green Fluorescent Protein (GFP)	Amaxa
HTT130-GFP	Aggregate forming huntingtin mutant construct with 130 glutamine repeats; GFP-tagged	Xiao-Jiang Li Laboratory, University School of Medicine, Atlanta, USA
HTT23-GFP	Non-aggregating huntingtin construct with 23 glutamine repeats; GFP-tagged	Xiao-Jiang Li Laboratory, University School of Medicine, Atlanta, USA
pDSRed2Mito	Expression of an RFP, targeted to mitochondria by a cytochromeC-targeting sequence	Rapaport laboratory, University of Tübingen
R62D-actin	Nonpolymerizable actin mutant; FLAG-tagged	Posern Laboratory, MPI of Biochemistry, Munich
S14C-actin	Actin mutant favoring F-actin assembly; high cofilin binding capacity; FLAG-tagged	Posern Laboratory, MPI of Biochemistry, Munich
SRF-VP16	Constitutively active fusion construct of aa 1-412 of murine SRF and VP16-transactivation domain	Nordheim laboratory, University of Tübingen
SRF-ΔMADS-VP16	Identical to SRF-VP16 plasmid but lacking parts of the DNA binding MADS-box domain	Nordheim laboratory, University of Tübingen
SshL	Active slingshot phosphatase; His/myc-tagged	Bradke Laboratory, DZNE Bonn
SshS	Inactive slingshot phosphatase; His/myc-tagged	Bradke Laboratory, DZNE Bonn
Synaptophsin-RFP	RFP-tagged synaptic vesicle protein synaptophysin	Gundelfinger Laboratory, University of Magdeburg

2.5 Oligonucleotides for genotyping

Genotype	Primer	Primersequence in 5'-3' direction
CamKIIα	CreS	ATG CGG TGG GCT CTA TGG CTT CTG
	CreAS	TGC ACA CCT CCC TCT GCA TGC ACG
	PCR3	AAG AAG GGT CCG GCC CCG AAG ATG CTG GGC
	PCR4	CTG GAT GCC CTC TCC TTC CCC GGA GCC CTG
Srf	AW	AGT TCA TCG ACA ACA AGC TGC GG
	BW	GAG ATT TCC ACA GAA AGC AAC GG
	CW	TGA TAT TGC TGA AGA GCT TGG CGG C

2.6 Mouse Lines

C57/Bl6	AG Prof. Dr. Bernd Knöll, University of Tübingen
CamKIIα-iCre	Prof. Dr. Schütz Laboratory, DKFZ Heidelberg
Srf(flex1neo/flex1neo)	Prof. Dr. Nordheim Laboratory, University of Tübingen
Srf(flex1neo/flex1neo) CamKIIα-iCre	Prof. Dr. Nordheim Laboratory, University of Tübingen
R6/2 huntingtin transgenic	Jackson Laboratories, Bar Harbor, USA

2.7 Technical Equipment and Reagents

2.7.1 Technical Equipment and Reagents for Cell Biological Experiments

2.7.1.1 Neuronal Cell Culture

35 mm / 60 mm dishes	BD Bioscience
4-well plate	Nunc
6-well plate	BD Bioscience
Coverslips	diameter of 12 mm or 20 mm, Menzel
Borate buffer	0.05 M Boric acid 12.5 mM Borax pH 8.5 steril filtration, storage at 4°C
DMEM	Invitrogen
Elastosil® silicone rubber	Wacker
Electroporation cuvettes	Amaxa
Electroporation pipettes (1 ml)	Amaxa
Electroporation solution	Mirus
Forceps	Student Dumont Forceps #5, Fine Science Tools
HBSS	Invitrogen

Horse serum	Invitrogen
NMEM / B27	1x MEM (Invitrogen) 2 % B27 supplement 0.6 % glucose 2 mM L-glutamine 0.22 % $NaHCO_3$ 1 mM Sodium pyruvate steril filtration, storage at 4°C immediately before use: 5 µg / µl gentamicin
Pasteur pipette	Hirschmann
Spring scissor	Fine Science Tools
Sterile filter (0.45 µm)	Millipore
Sterile reaction tubes (15 ml and 50 ml)	BD Bioscience
Sterile syringe	Henke Sass Wolf
Tail lysis buffer	100 mM Tris, pH 8.3 5 mM EDTA 0.2 % SDS 200 mM NaCl immediately before use: 0.2 µg / ml proteinase K
1x Trypsin / EDTA	Invitrogen

2.7.1.2 Stimulation of primary neurons with ephrin-A5 or BDNF

Human recombinant BDNF	PeproTech
Human recombinant ephrin-A5 Fc chimera	R&D Systems

2.7.1.3 Stimulation of primary neurons with FCCP

FCCP (carbonyl cyanide-p-trifluoromethoxyphenylhydrazone)	Sigma

2.7.1.4 Immunocytochemistry

Blocking solution	2 % BSA / PBS or 5 % FCS / 0.05 % Tween / PBS
DAPI	2 µg / ml in PBS
Fixation solution	4 % PFA 5 % Sucrose in PBS, pH 7.3, store at -20°C
Mowiol	25 g mowiol powder in 100 ml PBS stir slowly o/N at room temperature add 50 ml glycerol, stir slowly o/N at room temperature spin down for 15 min at 4000 rpm add spatula tip of n-propyl-gallate to the supernatant and stir until it is dissolved spin down for 15 min at 4000 rpm freeze at -20°C, before use: pre-warm at 37°C

Permeabilization solution	0.1 % or 0.2 % Triton-X-100 in PBS

2.7.1.5 Immunohistochemistry

Fixation solution	4 % PFA / PBS 4 % formaldehyde / PBS (for paraffin embedding)
Embedding solution	4 % agarose / PBS
Blocking solution	5 % normal goat serum (NGS) in PBS 2 % BSA in TBS, pH 7.6 (paraffin sections)
Washing solution	0.01 % Tween / PBS 0.01 % Tween / TBS (paraffin sections)

2.7.1.6 HEK293 and PC12 Cell Culture

1x Trypsin / EDTA	Invitrogen
Cell culture medium	DMEM / Glutamax (Gibco) + 10 % FCS (heat-inactivated, sterile filtered) + 1 % Pen / Strep
75 cm^2 cell culture flask	BD Bioscience
Freezing medium	cell culture medium + 20 % DMSO (sterile filtered)
Screw cup tube	Simport
Opti-MEM	Invitrogen

2.7.2 Technical Equipment and Reagents for Microscopy

Live cell incubator XL-3	Pecon
Heating unit / Tempcontrol 37-2	Pecon
CO_2 cover / CO_2 controller	Pecon
Humidification bottle	Pecon
Immersion oil	Zeiss

2.7.3 Technical Equipment and Reagents for Molecular Biological Experiments

2.7.3.1 Purification of plasmids

LB-medium	0.5 % yeast extract 1 % NaCl 1 % Tryptone in H_2O, pH 7.2-7.5 autoclave, store at 4°C
2x LB-medium	1 % yeast extract 2 % NaCl 2 % Tryptone in H_2O, pH 6.1 sterile filtrate, store at 4°C
PEG 3350	50 % PEG 3350 (w/v) in H_2O

Competency buffer	50 % 2x LB (v/v) 10 % PEG 3350 5 % DMSO 10 mM $MgCl_2$ 10 mM $MgSO_4$ 10 % glycerol
E. coli (DH5α strain)	Nordheim laboratory, Tübingen University
KCM-solution	100 mM KCl 30 mM $CaCl_2$ 50 mM $MgCl_2$
LB agar plate	add 1.5 % agar to LB-medium, autoclave, cool down at approximately 50°C, add according antibiotic (100 µg / ml ampicillin, 30 µg / ml kanamycin), pour into petri dishes, cool down, store at 4°C
QiaFilter Maxi Kit	Qiagen

2.7.3.2 Genotyping

10x PCR buffer	Fermentas
dNTP set	Genaxxon (final contentration 10 mM, pH 7.0)

tail lysis buffer	100 mM Tris pH 8.3 5 mM EDTA 0.2 % SDS 200 mM NaCl 0.2 µg / ml proteinase K
DreamTaq polymerase	Fermentas

2.7.3.2.1 Agarose gel electrophoresis

Agarose gel, 2 % (w/v)	dissolve 3 g agarose in 150 ml 1x TAE by heating in a microwave, cool down to 50°C, add 6 µl ethidium bromide
Ethidium bromide solution	1 % (w/v), 10 mg / ml

2.7.4 Technical Equipment and Reagents for Biochemical Experiments

2.7.4.1 Generation of Proteinlysates

Lysis buffer	50 mM Tris pH 7.4 150 mM NaCl 1 mM EDTA 1 % Triton-x-100 1 mM PMSF 1 mM sodium orthovanadate 1 mM sodium fluoride 1 mM sodium pyrophosphate 1x protease inhibitor

Cell scraper	TPP
Bradford reagent	BioRad
0.7 x 22 gauge syringe	Henke Sass Wolf
6x protein loading buffer	300 mM Tris, pH 6.8 600 mM β-mercaptoethanol 6 % SDS 60 % glycerol 0.1 % bromphenolblue

2.7.4.2 SDS-Polyacrylamid Gel Electrophoresis

2x Stacking gel buffer	0.25 M Tris/HCl, pH 6.8 0.2 % SDS
4x Resolving gel buffer	1.5 M Tris/HCl, pH 8.8 0.4 % SDS in H_2O
1x Running buffer	25 mM Tris/HCl, pH 8.3 192 mM glycine 0.1 % SDS
4 % Stacking gel	4 % PAA 0.1 % SDS 0.1 % TEMED 0.05 % APS in 1x stacking gel buffer

10 % Resolving gel	10 % PAA 0.1 % SDS 0.075 % TEMED 0.05 % APS
Protein molecular weight marker	Fermentas

2.7.4.3 Western Blotting

1x Transfer buffer	25 mM Tris/HCl, pH 8.3 192 mM glycine 20 % (v/v) methanol
1x TBST	50 mM Tris/HCl, pH 8.0 150 mM NaCl 0.1 % (v/v) Tween-20
Ponceau S-staining solution	0.02 % Ponceau S 0.3 % trichlor acidic acid
Blocking solution	5 % milk powder (w/v) in 1x TBST
PVDF transfer membrane	Millipore
Whatman paper	Whatman
ECL-substrate	Pierce
X-ray films	Ceaverken AB
Stripping buffer	62.5 mM Tris / HCl, pH 6.7 2 % SDS 100 mM β-mercaptoethanol

2.7.4.4 Purification of Mitochondria and ATP Production

Isolation buffer	1mM Na_2EDTA 10 mM Tris / HCl, pH 7.4 320 mM Sucrose 1x Complete Proteaseinhibitor
Malic Acid	100 mM in H_2O
Pyruvate	100 mM, Invitrogen
ATP determination kit	Molecular Probes

2.8 Experimental Procedures

2.8.1 Procedures of Cell Biological Experiments

2.8.1.1 Neuronal Cell Culture

2.8.1.1.1 Acid Treatment of Coverslips

Coverslips (Menzel, 12mm) were acid treated for optimal sterilization and better adhesion of the following poly-L-lysin (PLL) coating. For this purpose, coverslips were put into 2 M NaOH for one hour, following three times washing in H_2O and incubation in HNO_3 for at least three days. After that, coverslips were washed in H_2O for three times and incubated in 37 % HCl for at least one hour. In the following 24 hours, coverslips were washed 10 times in H_2O, transferred into 100 % ethanol, washed once in H_2O again and finally stored in 70 % ethanol. Before using them in the experiments, coverslips were air-dried.

2.8.1.1.2 Preparing Live Cell Culture Dishes

Live Cell Culture Dishes were prepared as follows: A hole of 2 cm in diameter was cut centrally into a 60 x 15 mm cell culture dish. On the rear side a 40 mm acid-treated coverslip was glued with Elastosil® silicone rubber that vulcanized o/N at room temperature. On the next day, live cell culture dishes were sterilized by UV-radiation for 30 min.

After using live cell culture dishes for live cell microscopy experiments, these were cleaned by removal of the culture medium, washing off the cells with 70 % ethanol, washing twice with H_2O, air-drying and final sterilization for 30 min by UV-radiation. Live cell culture dishes were reused for 4 times.

2.8.1.1.3 Coating of Coverslips, Live Cell Culture Dishes and 6-well plates

Acid-treated coverslips as well as live cell culture dishes and 6-well plates were coated with PLL and laminin for better adhesion of primary neurons. For that, air-dried coverslips and 6-well plates were sterilized by UV-radiation for 5 min. Live cell culture dishes were sterilized for at least 30 min. Afterwards, coverslips and live cell culture dishes were coated with 100 µg/ml PLL in borate buffer for one hour at 37°C. 6-well plates were coated with 10 µg/ml PLL in borate buffer. This was followed by three times washing with H_2O and coating with 20 µg/ml (coverslips and live cell culture dishes) or 2 µg/ml (6-well dishes) laminin in HBSS for at least 2 hours at 37°C. Finally, coverslips (transferred into 4-well plates), live cell culture dishes or 6-well plates were washed three times with HBSS and kept in NMEM / B27 at 37°C until cells were plated out.

2.8.1.1.4 Preparation of primary neurons

Primary neurons were isolated from hippocampal or cerebellar tissue of newborn mice. In case of hippocampus preparation, mice were maximum 2 days postnatal (P2 = postnatal day 2), cerebellum was prepared until P7.

First of all, newborn mice were decapitated and the head transferred into ice-cold PBS. For genotyping, a piece of tail was cut off and transferred into tail lysis buffer. The head was put into a 3 cm culture dish filled with HBSS. The cranium was opened, the brain dissected and

transferred carefully into HBSS. Afterwards, cerebellum and optical tectum were separated by a coronal section. Meninges were removed from the cerebellum, the residual tissue was cut into three pieces and finally transferred into a new dish with HBSS. Hippocampus preparation involved sagittal sectioning of both hemispheres followed by cutting off the ventral striatum and the bulbus. Hippocampus was dissected from isolated cortices and the banana-like structure transferred into a new dish with HBSS. Hippocampus and cerebellum, respectively, were transferred into a 15 ml Flacon with 3 ml of pre-warmed trypsin solution and trypsinized for 10 min in a water bath at 37°C. Trypsinization was stopped by washing twice with HBSS. Afterwards, HBSS was removed completely and 1 ml of pre-warmed DMEM / 10 % horse serum (HS) added. Each hippocampus and cerebellum was triturated for 1 min with a flame-treated Pasteur pipette (full diameter) and 1 min with a Pasteur pipette with half diameter. This was followed by centrifugation at 600 rpm for 5 min at room temperature. The resulting supernatant was discarded and the cell pellet resuspended in 500 µl NMEM / B27 medium. Cell titer was determined using a Neubauer cell counting chamber and cells plated at the following densities: 30 – 50 x 10^6 cells per coverslip, 50 x 10^6 cells per live cell culture dish, 100 – 150 x 10^6 cells per 6-well. Primary neurons were incubated for one to three days in NMEM / B27 at 37°C and 5 % CO_2.

2.8.1.1.5 Electroporation of primary neurons

Electroporation is an efficient method to bring plasmid DNA into cells. This is achieved by an electric pulse, generated by a fast discharging capacitor, that leads to a transient permeabilization of the cellular membrane enabling external plasmid DNA to enter cytoplasm and the nucleus.

Before electroporation, plasmid DNA was prepared and kept on ice. In case of single-electroporation experiments, involving only one type of plasmid-DNA, 3 µg DNA was put into a 1.5 ml reaction tube. If two different plasmids were co-electroporated, 1.5 µg of each one was used. Triple electroporation experiments involved 1 µg DNA of each plasmid. Only in case of slingshot experiments, slingshot constructs were applied at 3 µg and pDSRed2Mito at 0.3 µg to ensure that every MitoRFP-positive cell was also expressing the slingshot construct.

Preparation of primary neurons was performed as described in chapter 2.8.1.1.4. After counting the cells, these were centrifuged again for 5 min at 600 rpm. The supernatant was

removed completely and the resulting cell pellet resuspended in 200 µl nucleofection solution. 100 µl of this cell suspension was added to the previous prepared DNA, mixed carefully by pipetting up and down once and transferred to an electroporation cuvette. The cuvette was put into the electroporator and electroporation was performed at 210 V (pulse length of 5 ms, capacitance of 1200 µF). Immediately after electroporation, the cells were transferred to 400 µl of pre-warmed NMEM / B27 medium and plated at the densities described in 2.8.1.1.4.

2.8.1.2 Stimulation of primary neurons with ephrin-A5, BDNF or latrunculin

Cultivated primary neurons were stimulated by applying recombinant human BDNF (final concentration of 10 ng / µl) or recombinant ephrin-A5-Fc directly into the culture medium. Ephrin-A5 was pre-clustered with an Fc-specific antibody for 30 min at room temperature and then applied at 1 µg / ml directly to the culture medium, the Fc-specific antibody was used at 10 µg / ml. BDNF stimulation was performed for one hour, ephrin-A5 stimulation was stopped and cells fixed after 10 min in order to induce only a mild growth cone retraction thereby avoiding a full collapse.

To induce actin depolymerization latrunculin A was applied to neurons at a concentration of 2 µM. Neurons were fixed after 20 min of stimulation.

2.8.1.3 Stimulation of primary neurons with FCCP

To induce mitochondrial fragmentation in primary neuronal cell culture, cells were treated with an uncoupler of oxidative phosphorylation in mitochondria. FCCP works as an H^+ ionophore, meaning that the membrane potential of mitochondria is broken down by FCCP administration. FCCP was dissolved in DMSO and directly added to the culture medium to give a final concentration of 0.5 µM. Control cells were stimulated with a similar amount of DMSO. Cells were fixed 150 min after stimulation.

2.8.1.4 Immunocytochemistry

For immunocytochemical staining of cells, culture medium was removed completely and cells washed once with pre-warmed PBS. Cells were fixed for 15 min in 5 % PFA / 4 % Sucrose / PBS, followed by three times washing in H_2O and permeabilization for 10 min in 0.1 % Triton-X-100 / PBS. In case of FLAG-staining 0.2 % Triton-X-100 was used. After three times washing with H_2O, cells were blocked for 30 min in 2 % BSA / PBS and primary antibodies applied at 4°C overnight or 2 h at room temperature at the mentioned dilutions (see chapter 2.3.1). Afterwards, cells were washed three times with PBS and secondary antibodies applied for 1 h at room temperature. Cells were washed three times again in PBS and stained for nuclei with DAPI for 5 min at room temperature. Finally, cells were washed once in PBS and embedded in mowiol. For that, mowiol-reagent was dropped on a microscope slide, the coverslip put on the mowiol drop and air-dried o/N in the dark.

FLAG-staining differed from the above mentioned procedure in using different blocking buffer (5 % FCS / 0.05 % Tween / PBS) and washing solutions (0.05 % Tween / PBS). Washing steps were performed for 5 min each at room temperature.

2.8.1.5 Immunohistochemistry

For *in vivo* investigation of neuronal mitochondrial distribution and size, mouse brains of P14 old animals (wildtype or *Srf*-mutant) were dissected and fixed for 24 h at 4°C in 4 % PFA / PBS. Afterwards, brains were embedded in 4 % agarose / PBS and sliced into 30 µm sections with a vibratome. Slices were collected in ice-cold PBS on a 4-well plate with four slices per well. Slices were washed three times for 5 min in 0.1 % Tween / PBS (PBST) and blocked for 30 min with 5 % normal goat serum (NGS) in PBST. Primary antibodies were applied as mentioned in chapter 2.3.1 in blocking buffer o/N at 4°C. After that, slices were washed three times for 15 min with PBST. Secondary antibodies were applied for 1 h at room temperature in blocking solution. Slices were then washed three times for 15 min in PBST, counterstained with DAPI (2 µg / ml in PBS) for 5 min and washed once in PBST. Finally, slices were embedded in mowiol on a microscope slide with 4 slices per slide.

To check for SRF expression in presence of aggregation competent huntingtin, R6/2 mice brains expressing a mutant huntingtin transgene were dissected as described above. After that, tissue was fixed in 4 % formaldehyde / PBS for one week, dehydrated by a series of

ethanol and xylene (30 %, 70 %, 90 %, 3x 100 % ethanol, 50 % xylene / 50 % ethanol, 2x 100 % xylene, 3 hours each) and embedded in paraffin for 1 hour. Tissue was sliced into 5 µm sections with a microtome and paraffin removed by heating for one hour at 60 °C. After that, slices were further dehydrated by washing them twice in xylene for 5 min and in 100 % ethanol for 5 min, 3 min and finally twice for 2 min. Slices were treated with 2 % H_2O_2 / H_2O for 10 min and washed in H_2O for 2 min. After that, slices were put into cooking 0.01 % Tris / pH 10 for 10 min to unmask the antigens. Slices were washed with H_2O for 10 min and blocked for 10 min with 2 % BSA / TBS. Further staining was performed as described above.

2.8.1.6 HEK293 and PC12 Cell Culture

2.8.1.6.1 Thawing of HEK293 and PC12 cells

Cell culture of HEK293 and PC12 involved similar media and procedures. Cells stored in liquid nitrogen were thawed quickly in a 37°C pre-warmed water bath and transferred into 5 ml of pre-warmed medium. After centrifugation for 5 min at 1000 rpm, the cell pellet was resuspended in 10 ml pre-warmed medium and split 1:2 in 75 cm^2 flasks.

2.8.1.6.2 Cell Culture Routine

Cells were split every 2-3 days according to their confluency. For this, cell culture medium was removed and cells washed once with 10 ml PBS. To detach cells from the flask, 2 ml of pre-warmed trypsin / EDTA solution was added and incubated at 37°C for a few minutes. After adding of 10 ml pre-warmed medium, the whole cell suspension was spun down for 5 min at 1000 rpm and the resulting cell pellet resuspended in 10 ml culture medium. Cells were split 1:3 in a new flask to a final volume of 10 ml.

2.8.1.6.3 Transfection of HEK293 and PC12 cells

HEK293 cells and PC12 cells can be transfected with PromoFectin (HEK) or Lipofectamine (PC12), respectively. On the day before transfection, cells were plated at an adequate density to give 60 % confluency on the following day (300.000 HEK cells or 200.000 PC12 cells per well of a 6-well plate). For each well 3 µg of total DNA and 6 µl PromoFectin or Lipofectamine was used. DNA was diluted in 100 µl serum free Opti-MEM, vortexed shortly and spun down. In a second tube PromoFectin or Lipofectamine were added to 100 µl Opti-MEM, shortly vortexed and spun down. The PromoFectin- or Lipofectamine-solution was added to the DNA solution, carefully mixed by inverting three times, spun down and incubated at room temperature for 20 min. Meanwhile, cell culture medium was replaced with pre-warmed serum-free Optim-MEM. 200 µl of DNA-transfection solution was added dropwise on each well and dispersed by gently swirling the plate. After 8 h incubation of the cells at 37°C and 5 % CO_2, medium was replaced by serum-containing culture medium. Cells were harvested for protein lysates after two further days of incubation. In case of PC12 cells, one day post transfection cells were stimulated with 100 ng / ml nerve growth factor (NGF, Sigma) and harvested one day later.

2.8.1.6.4 Storing HEK293 and PC12 cells in Liquid Nitrogen

Cells were trypsinized (see chapter 2.8.1.6.2) and spun down. The resulting cell pellet was resuspended in 2 ml of 100 % FCS and stored on ice for 5 min. Afterwards, 2 ml of cell culture medium and 20 % DMSO were added, cells stored on ice for additional 5 min and aliquoted in 2 x 2 ml screw cup tubes. Cells were frozen for 2 h at -20°C, then o/N at -80°C and finally in liquid nitrogen.

2.8.2 Microscopy

2.8.2.1 Live Cell Microscopy

To visualize mitochondrial dynamics in living neurons, these were monitored by time lapse microscopy. For that purpose, a live cell culture dish with plated neurons was placed into a heating insert P (Pecon) of an incubator XL-3 (Pecon) at a Zeiss 200M inverted microscope. Thereby cells could be aerated with 5 % CO_2 and warmed at 37°C. Before starting the time lapse microscopy, cells were incubated for 30 min to reduce condensation on the top cover of the cell culture dish. For the time lapse recording of mitochondrial movement, only cells that showed discrete staining of mitochondria were chosen. In case of multiple electroporation experiments (e.g. pDSRed2Mito together with SRF-VP16 or SRF-ΔMADS-VP16), neurons showing RFP2Mito expression were considered to be positive for the second construct as well (which was confirmed by a series of exemplary stainings). Time lapse recording was performed for 5 min, taking a picture every 5 s. UV-radiation was reduced to a minimum to avoid phototoxicity and individual recording of the mitochondrial signal did not exceed 500 ms.

2.8.2.2 Electron Microscopy

For electron microscopy of *in vitro* neuronal cell culture, cells were fixed in 2.5 % glutaraldehyde / 2.5 % PFA / PBS. Brain tissue samples of P14 mice (wildtype or *Srf* mutant) were prepared earlier by the working group of Prof. Dr. Knöll. In brief, animals were perfused with 2.5 % glutaraldehyde / 2.5 % PFA in PBS. Brains were dissected and 500 µm vibratome sections prepared. All the following steps were performed at the laboratory of Dr. Heinz Schwarz, Max Planck Institute for Developmental Biology, Tübingen. Briefly, cell cultures and vibratome sections were post-fixed with 1 % osmium tetroxide in 100 mM phosphate buffer (pH 7.2) for 1 h on ice, afterwards washed with H_2O, treated with 1 % aqueous uranyl acetate for 1 h at 4°C, dehydrated through a graded series of ethanol, washed with propylene oxide, then infiltrated with propylene oxid / resin mixtures and finally embedded in Epon (using glycidether 100). Ultrathin sections were collected on coated slot grids, stained with uranyl acetate and lead citrate and finally viewed on a Tecnai G2 electron microscope.

2.8.3 Procedures of Molecular Biological Experiments

2.8.3.1 Purification of plasmids

2.8.3.1.1 Generation of Competent Bacteria

E. coli (strain DH5α) were grown o/N in 2 ml antibiotic-free LB-medium at 37°C. On the next day 100 µl of the *E. coli* culture were inoculated into 100 ml LB-medium and grown to an OD_{600} of 0.5. The culture was centrifuged at 3500 rpm for 5 min at 4°C and the resulting pellet resuspended in 5 ml freshly prepared ice-cold competency buffer. Bacteria were incubated on ice for 10 min, aliquots frozen on dry-ice first and stored at -80°C.

2.8.3.1.2 Transformation of Competent Bacteria

For transformation of competent bacteria, these were slowly thawed on ice. Meanwhile 0.1 µg of DNA was mixed in 90 µl KCM. The DNA / KCM mixture was added to 90 µl bacteria solution, carefully mixed by inverting 3 times and incubated on ice for 15 min. This was followed by a 2 min heat shock at 42°C in a water bath and putting back on ice for at least 2 min. Afterwards, 1 ml of pre-warmed LB-medium was added and the mixture incubated for 30 min at 37°C. Bacteria were then spun down for 2 min at 1000 rpm and the resulting pellet resuspended in 100 µl LB-medium. 10 µl and 90 µl of the bacteria solution were plated on LB agar plates with the corresponding antibiotics. Incubation was performed in inverted position o/N at 37°C. On the next day, single bacteria clones were picked and inoculated in 2 ml LB-medium (with antibiotics). After 8-10 h growth at 37°C and 250 rpm, 200 µl of this culture were inoculated in 200 ml LB-medium (with antibiotics) and grown o/N at 37°C.

2.8.3.1.3 Plasmidisolation

Plasmids were isolated from 200 ml o/N-culture with the Qiafilter® maxi kit. For this, 200 ml bacteria culture was centrifuged at 4300 rpm for ten minutes, the resulting pellet resuspended in P1 buffer and the following purification procedure performed after the Qiagen instruction protocol. Differing from the manual, the final DNA precipitation involved two centrifugation steps for 1 h at 4500 rpm and 4°C with 100 % isopropanol and 70 %

ethanol, respectively. The final DNA pellet was resuspended in 300 µl elution buffer (PeqLab).

2.8.3.2 Genotyping

To delete *Srf* specifically in murine forebrain, a particular mouse line was used. This *Srf(flex1neo/flex1neo)CamKIIα-iCre* mouse line was generated by crossing of mice which have a floxed *Srf* allele, meaning that the *Srf* locus on the DNA is flanked by two loxP-sequences. These loxP-sites can be recognized by the Cre recombinase, which leads to a removal of the floxed *Srf* allele (reviewed by (Metzger and Feil, 1999)). For this project, Cre recombinase was expressed under control of a calcium/calmodulin dependent protein kinase type IIα (*CamKIIα*) promotor, which is only active in murine forebrain. Crossing of a mouse line expressing *CamKIIα-iCre* with an SRF*(flex1neo/flex1neo)* mouse line generated mice that showed a forebrain-specific knockout for *Srf* (Wiebel et al., 2002).

In case of the loxP sites, one has to distinguish between the two different alleles as only both floxed alleles could give rise to a knockout. A floxed but not recombined *Srf* allele was indicated by a superscript "+", a recombined allele indicated by a superscript "-". For the *Cre* allele no differentiation between the two alleles was necessary. As only Cre expressing cells with both *Srf* alleles floxed can delete *Srf* completely, the corresponding mouse genotype was indicated by *Srf(flex1neo$^{-/-}$)CamKIIα-iCre^{+}* and considered as a knockout. All the other genotypes (even in case of heterozygous floxed *Srf* alleles) were considered as wildtype.

2.8.3.2.1 Preparation of Tissue Samples and PCR Based Genotyping

To determine the mouse genotype, a piece of tail was cut off and incubated o/N at 55°C in tail lysis buffer. On the next day samples were centrifuged at 13000 rpm for 5 min, the supernatant transferred into a new tube and stored at 4°C until genotyping. Each sample was tested separately for the presence of floxed *Srf* alleles as well as Cre recombinase. For that purpose, the following pipetting scheme was used:

Reagent	µl / sample for *Cre* genotyping		µl / sample for *Srf* genotyping	
H_2O		37.5		36.0
10x PCR buffer		5.0		5.0
DMSO		-		2.5
dNTPs [10 mM]		1.2		1.0
Primer	CreS	1.2	AW #5	1.5
	CreAS	1.2	BW #6	1.5
	PCR3	1.2	CW #7	0.5
	PCR4	1.2		-
DNA sample		1.0		1.5
DreamTaq polymerase		0.5		0.5
Total volume		**50.0**		**50.0**

The DreamTaq polymerase was added after denaturation of the samples for 10 min at 98°C. After that, the following PCR protocol was started:

94°C 2 min
94°C 30 s
63°C 30 s
72°C 30 s
} 35 cycles
72°C 7 min
4°C ∞

2.8.3.2.2 Agarose Gel Electrophoresis

To separate the PCR products generated in 2.8.3.2.1, an agarose gel electrophoresis was performed. Samples were loaded on a 2 % agarose gel containing ethidium bromide. Electrophoresis was performed at 120 V, 400 mA for maximal 2 h. Samples were visualized by UV radiation as ethidium bromide intercalates with DNA to give a fluorescent signal if radiated with UV light. The size of the PCR products was determined by a simultaneously

loaded molecular weight standard for DNA electrophoresis (Genaxxon). In case of *Srf* genotyping, a wildtype band was expected at 600 base pairs (bp), *Srf* deleted animals showed a band at 530 bp. Heterozygous animals showed both bands. For *Cre* genotyping an internal control band (resulting from the PCR-protocol) at 500 bp was observed, transgene animals showed a band at 300 bp.

2.8.4 Procedure of Biochemical Experiments

2.8.4.1 Generation of Proteinlysates

2.8.4.1.1 Generation of Proteinlysates from Mouse Brain Tissue

To generate protein extracts from murine forebrain tissue, cortices or hippocampi were dissected in ice-cold PBS and transferred into a 1.5 ml reaction tube, which was transferred immediately into liquid nitrogen. After preparation of all tissue samples, these were lysed by adding 200 µl lysis buffer in each 1.5 ml reaction tube. Tissue was homogenized by applying a 0.7 x 22 gauge syringe for 10 times and the resulting homogenate was incubated on ice for 5 min, vortexed briefly and put on an overhead rotator for 30 min at 4°C. Hereafter, protein lysates were centrifuged for 2 min at 13000 rpm (4°C) and the supernatant transferred into a new ice-cold reaction tube. Protein concentration was determined using Bradford reagent by mixing 5 µl of lysate sample, 795 µl PBS and 200 µl RotiQuant solution, incubating for 5 min at room temperature and measuring the extinction at a wavelength of 595 nm. By comparison with a standard curve, created by using known BSA concentrations, protein amount could be calculated. After that, 6x protein loading buffer was added to protein lysates and boiled for 5 min at 95°C. These protein lysates were frozen at -20°C.

2.8.4.1.2 Generation of Proteinlysates from Cell Culture

HEK293 or PC12 cells, cultivated on 6-well plates, were washed once with ice-cold PBS. PBS was removed completely and 200 µl lysis buffer added per each well. This was followed by 5 min incubation on ice and scraping off the cells using a cell-scraper. Cell lysates were

transferred into a reaction tube on ice and overhead rotated for 30 min at 4°C. Following steps were performed as described in 2.8.4.1.1.

2.8.4.2 SDS-Polyacrylamid Gel Electrophoresis

Proteins can be separated according to their molecular weight by discontinuous polyacrylamide gel electrophoresis (PAGE). 15 µg of SDS denatured protein samples (see 2.8.4.1.1 and 2.8.4.1.2) were loaded on each lane of a 4 % stacking gel. Next to all of the protein samples 5 µl of a prestained protein ladder (Fermentas) was loaded. Gel electrophoresis was performed in a 10 % resolving gel for 10 min at 80 V following 90 min at 150 V.

2.8.4.3 Western Blotting

After SDS-PAGE, resolved proteins were transferred on a PVDF membrane by western blotting. For that purpose, the stacking gel was cut off the resolving gel and the latter equilibrated in transfer buffer for a couple of minutes. Likewise, sponges and whatman paper, used in the western blotting, were equilibrated in transfer buffer. The PVDF membrane was activated by 15 s incubation in pure methanol, 2 min washing in H_2O and 5 min equilibrating in transfer buffer. Western blotting itself was performed as a wet blot and gel and membrane orientated in the following order (starting at the cathode leading to the anode): sponge, whatman paper, gel, PVDF membrane, whatman paper, sponge. This orientation allowed negatively charged proteins to get transferred to the PVDF membrane, which is on the positively charged side of the assembly. Air bubbles were removed from this "sandwich assembly" and the latter transferred into the blotting apparatus. Transfer was performed at 150 V for 1 h cooled at 4°C. To check for successful blotting, the PDVF membrane was stained with Ponceau S-solution and visualized protein lanes cut at their according size. The PVDF membrane was destained by washing in transfer buffer for a couple of minutes and blocked for unspecific antibody binding by incubation for 30 min in 5 % milk powder in TBST. After that, the first antibody was applied o/N at 4°C. On the next day the membrane was washed three times for 15 min in TBST and then incubated with the

secondary antibody for 1 h at room temperature. Afterwards, the membrane was washed twice in TBST, then once for 15 min and finally three times for 5 min in TBST. To detect proteins, the membrane was incubated for 1 min with ECL reagent, which served as a substrate for the horse radish peroxidase, that was coupled to the secondary antibody, to give a chemiluminescent reaction. This chemiluminescence was detected by exposition of the membrane to an X-ray film.

In case of re-probing the membrane, the antibodies were stripped by the following procedure: The membrane was washed three times for 5 min in TBST, then incubated for at least 30 min at 50°C in stripping buffer and finally washed twice in TBST for 10 min. Afterwards, the membrane could be blocked and incubated with a first antibody again.

2.8.4.4 ATP production assay

2.8.4.4.1 Isolation of Mitochondria

Isolation of mitochondria involved dissection of hippocampal tissue, homogenization and subsequent steps of differential centrifugation (see Figure 2.1).

To isolate mitochondria from mouse brain tissue, the hippocampus was dissected in PBS and transferred into 2 ml isolation medium. Hippocampal tissue was cut into smaller pieces and homogenized using a Potter Elvehjem homogenizer with a Teflon coated pestle only applying hand-forced drill for 20 strokes on ice. The homogenate was washed twice at 1500 g for 10 min at 4°C and the resulting supernatant was centrifuged at 14000 g for 15 min at 4°C. The resulting pellet was washed twice and finally resuspended in 200 µl isolation buffer. Supernatants were collected as cytosolic fractions. Protein amount of mitochondrial and cytosolic fractions was determined using Bradford reagent (see 2.8.4.1.1).

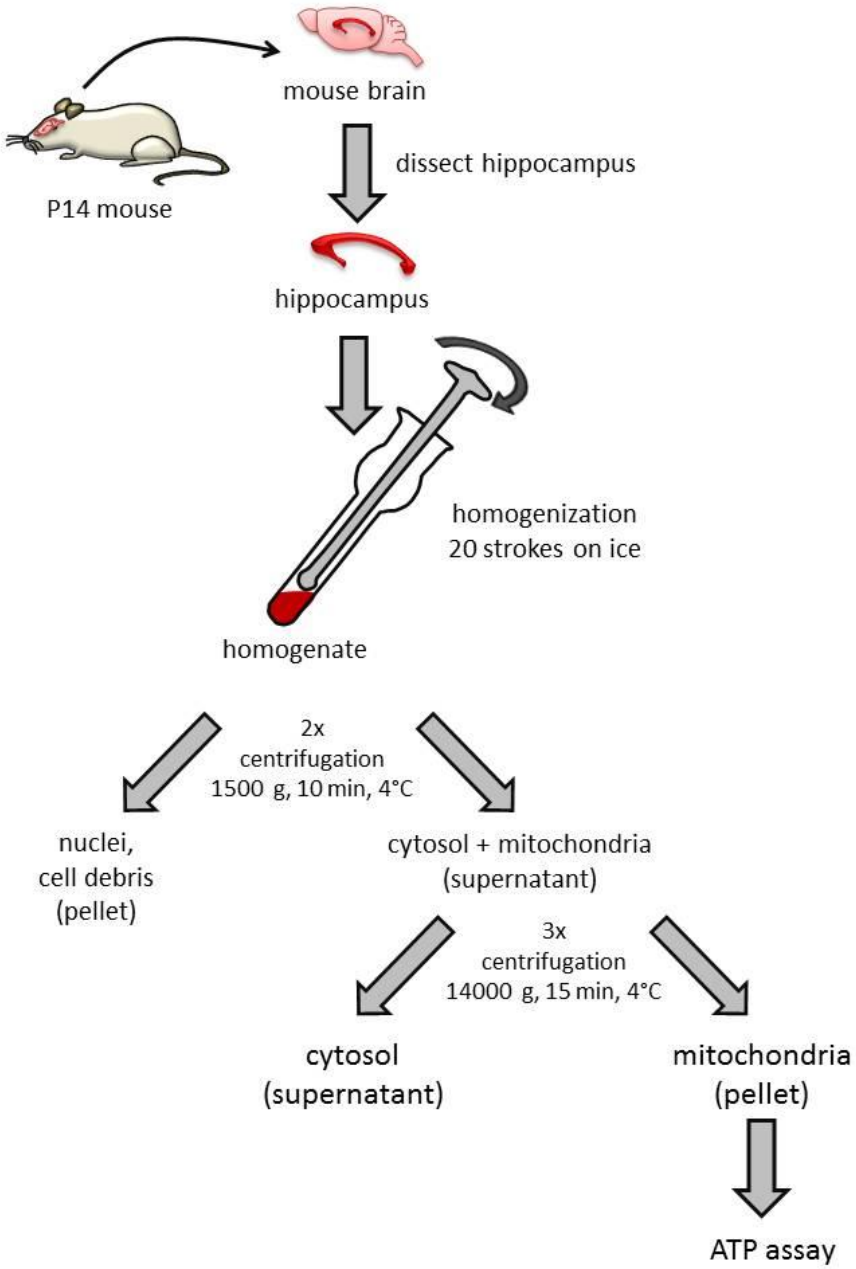

Figure 2.1 Isolation procedure of mitochondria

Mitochondria were isolated from mouse hippocampal tissue by differential centrifugation. Details see text.

2.8.4.4.2 Measurement of ATP production

To measure ATP production of the previously prepared mitochondrial fractions, an ATP determination kit (Molecular Probes) was used. The principle of this approach is based upon the fact that mitochondria are the main producers of ATP. ATP amount can be measured by the light emission generated by the activity of firefly luciferase, an enzyme that catalyzes the ATP-dependent conversion of luciferin to oxyluciferin. Addition of purified mitochondria to a luciferase / luciferin containing medium does not have any effect until an adequate substrate for mitochondria (in this case malate, pyruvate and ADP) is added. This in turn activates mitochondrial ATP production, which can be finally measured by the luciferase generated light emission.

Firstly, 10 µl of the resulting mitochondrial and cytosolic fractions were added to 270 µl of luciferase reaction solution (Molecular Probes). The latter contained D-luciferin and firefly luciferase. Luciferase reaction solution was prepared according to the ATP determination kit manual. To the mitochondrial fraction mixed in the luciferase reaction solution 20 µl of substrate solution (malate and pyruvate, final concentrations 3.3 mM) were added. Reaction was started by adding 2.5 mM ADP (final concentration) and recorded for 5 min with a luminometer. ATP production was determined by calculating the initial slope of the graph with Excel and normalized to protein amount of the mitochondrial or cytosolic fraction.

2.8.5 Analysis and Statistics

2.8.5.1 Analysis of Mitochondrial Size and Occupancy

Mitochondrial size was determined by SlideBook 5 software (Intelligent Imaging Innovation, USA). Pictures taken at the 200M Zeiss Axiovert microscope were imported in SlideBook and the mitochondria specific channel masked by the “Create Mask” tool. Signal intensity threshold was set identical for all experiments performed at the same time. Mitochondrial objects were identified by the “Gate Objects By Size” tool defining a minimum size of 0.01 µm². Finally, the size of all mitochondrial objects in the given mask was calculated by the “Mask Statistics” tool of the SlideBook software. For the following analysis only discrete mitochondrial objects (and no network like syncytial structures) were taken into account. For each experiment mitochondria of 15-20 neurons were analyzed and each experiment

repeated 3 times. The average mitochondrial size was calculated for each experiment and the mitochondrial size averaged for all experiments.

Mitochondrial occupancy measures the neurite distance that is covered by mitochondria in percent. For this, neurite length was measured with the Zeiss Axiovision software. Additionally, the length of all mitochondria in the given neurite were measured, summed up and set into relation of the whole length of the neurite. This was done for 15-20 neurons per experiment and each experiment repeated minimum 3 times.

For statistical analysis a one-way analysis of variance (ANOVA) was performed. Statistical significance was determined by a following Bonferroni posthoc test with *, ** and *** indicating $p \leq 0.05$, 0.01 and 0.001, respectively. In bar charts, calculated with Excel®, error bars show standard deviation.

2.8.5.2 Determination of Cofilin and Phospho-Cofilin Intensity

Intensities of cofilin and phospho-cofilin, respectively, in single cells were determined using SlideBook 5 software. Fluorescence of cofilin- and phospho-cofilin staining was measured with same acquisition parameters. After that, images were imported in SlideBook and equal thresholds applied for all pictures of the same experiment. Sum of all intensities in a single cell was calculated using the "Sum of Intensity" tool. Intensities were averaged for all measured cells of a single experiment (at least 15) and each experiment repeated for 3 times. Statistical analysis involved one-way ANOVA and following Bonferroni posthoc test (see 2.8.5.1).

2.8.5.3 Analysis of Time Lapse Experiments

To calculate the velocity and amount of moved mitochondria, pictures from a time lapse video were imported into the SlideBook 5 software. Mitochondrial objects were identified as described in 2.8.5.1, followed by an analysis of the movement pattern by the "Basic Particle Tracking" tool. Applying the "Mask Statistics" tool for the movement parameters gave the average velocities for all identified mitochondria in the given frame. Mitochondrial objects were considered to be moving if they moved for more than 1.5 µm in three consecutive

frames. This resulted in a saltatory trafficking pattern with phases of moving and stopping mitochondria. Mitochondria without any movement for more than three consecutive frames throughout the whole recording time were counted as stationary. The average velocities of all moving phases of moving mitochondria were measured as well as the percentage of moving mitochondria. For each condition, experiments were repeated three times with recording mitochondrial movement in 10 neurons in every experiment, resulting in analysis of at least 300 mitochondrial objects for each condition. Statistical analysis involved one-way ANOVA and following Bonferroni posthoc test with *, ** and *** showing $p \leq 0.05$, 0.01 and 0.001.

For better visualization, kymographs were generated. For that, Zeiss images were opened in ImageJ, curved neurites, containing mitochondria, selected and mitochondrial movement visualized by the "MultipleKymograph" plugin. Resulting kymographs display the distance on the x axis, whereas recorded time (5 minutes) is shown on the y axis. (Mangiarini et al., 1996)

2.8.5.4 Determination of Neurite Length

Neurite length was measured with the Zeiss Axiovision software applying the "Curved Spline" tool. For each neuron the length of the longest neurite (visualized by β-tubulin staining) from the cell body to its most distant part was measured. For each condition three independent experiments with 15-20 randomly picked neurons were performed. The average length of the neurites in a single experiment was calculated and the overall neurite length averaged for all experiments. Statistical analysis involved one-way ANOVA and following Bonferroni posthoc test with *, ** and *** showing $p \leq 0.05$, 0.01 and 0.001.

3. Results

3.1 Impact of Serum Response Factor on Mitochondrial Dynamics

As described in the introduction, SRF is one of the major gene regulators controlling the function of actin dynamics. To investigate SRF's impact on neuronal cells forebrain-specific *Srf* knockout animals have been generated (Wiebel et al., 2002). These mice display severe phenotypes with regard to hippocampal architecture, neuronal motility, axonal guidance and myelination (Alberti et al., 2005; Knöll et al., 2006). However, little attention has been paid on mitochondrial dynamics in these animals. Consequently, it was initially observed whether SRF-deficiency had any impact on mitochondria *in vivo*, before investigating the mitochondrial phenotypes in more detail *in vitro*.

3.1.1 SRF deficiency impairs mitochondrial structure and distribution *in vivo*

3.1.1.1 Mitochondrial ultrastructure is disheveled in *Srf* mutant tissue

To investigate SRF's influence on mitochondria *in vivo*, corpus callosal cross-sections of P14 *Srf* mutant mice were generated. The corpus callosum is the major nerve fiber tract connecting both brain hemispheres and is rather free of neuronal cell bodies. It consists of axons surrounded by glial cells (in this case oligodendrocytes), thereby cross-sectioning and following electron microscopy allows for axon specific investigation of mitochondrial structure.

Mitochondria in *Srf* mutant tissue displayed severe ultrastructural defects in comparison to wild-type control animals (see Figure 3.1 C vs. D). Mitochondria in control tissue were round in shape and had a clearly defined double membrane allowing for easy identification of mitochondria in these cross sections (arrows in Figure 3.1). Furthermore, the matrix was electron-dense and rather granular. However, mitochondria in *Srf* mutant brains appeared

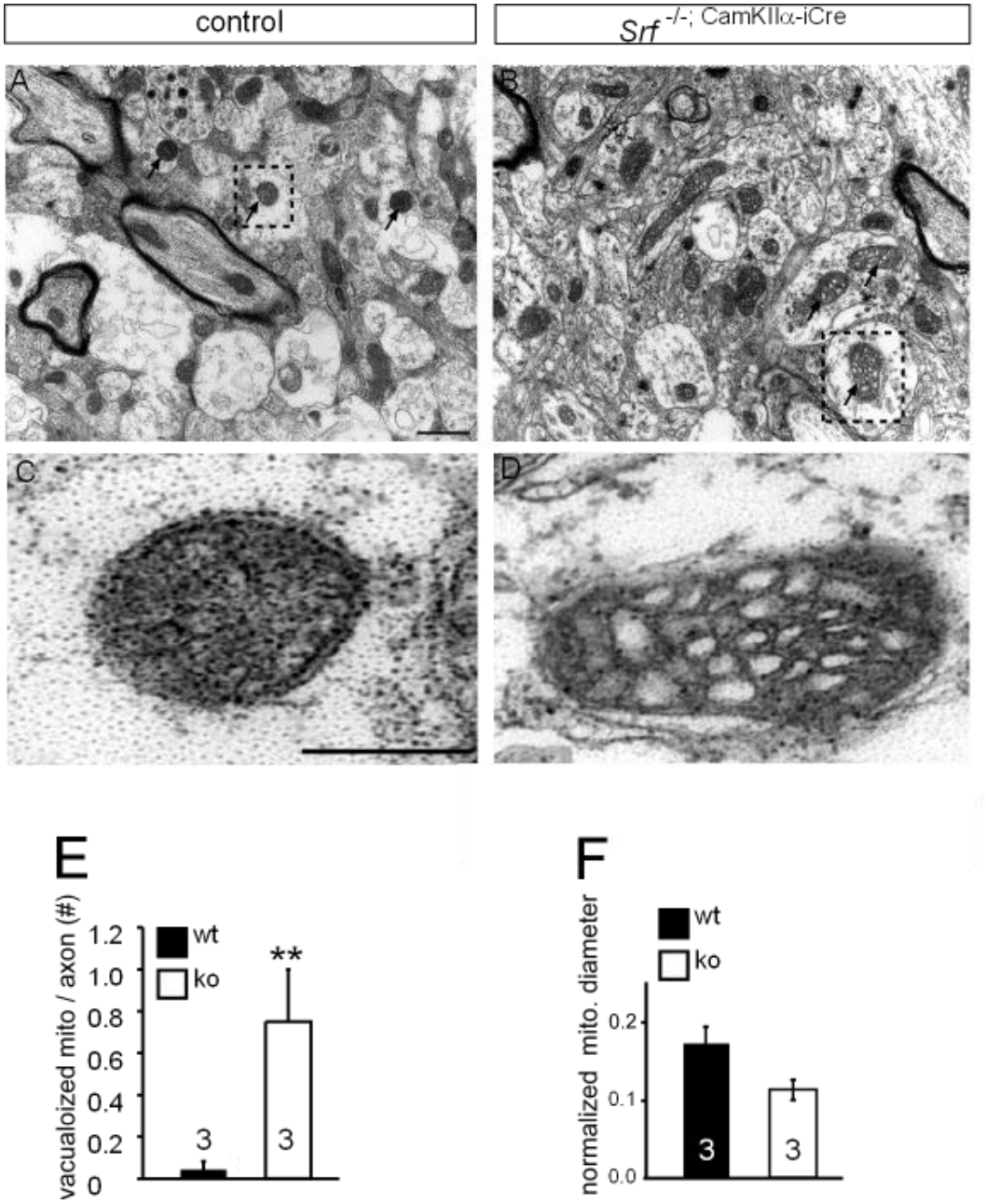

Figure 3.1 SRF-deficiency alters mitochondrial ultrastructure in corpus callosal cross-sections

(A, C) Axons of wild-type neurons contained round shaped mitochondria (A, arrows). Higher magnification (C) showed that these mitochondria were round in shape, had a clear double membrane and displayed an electron-dense granular matrix. In contrast, mitochondria in *Srf* mutant brain (B) were bottle-shaped and showed a disturbed ultrastructure with multiple vacuolizations inside (D). (E) Quantification of abnormal mitochondrial occurrence per axon. The number of vacuolized mitochondria was significantly increased in *Srf* mutant brains. (F) If normalized to increased axonal diameter in *Srf* mutant tissue, mitochondrial diameter was not increased in *Srf* mutant tissue. Scale bars (A, B) = 1 µm, (C, D) = 0.5 µm.

differently (Figure 3.1 B, D). They were overall bottle-shaped and ultrastructurally displayed an altered membrane topology with multiple balloon-like inclusions, which were not as electron dense as the surrounding matrix (Figure 3.1 D). Quantification revealed that the number of these abnormal mitochondria displaying clear vacuolization was significantly increased in *Srf* mutant tissue (Figure 3.1 E).

At first sight, it seemed that also the mitochondrial diameter was increased in case of SRF deficiency. However, if normalized to the generally increased axonal diameters in *Srf* mutant tissue, this observation could not be verified (Figure 3.1 F). One should notice that SRF deficiency led to a decreased myelination reflected by less axons surrounded with an electron dense myelin sheath in Figure 3.1 B. This effect has been reported before (Stritt et al., 2009), however no influence of myelination on the occurrence of abnormal mitochondria could be detected as mitochondrial vacuolization took place in myelinated as well as non-myelinated axons in *Srf* mutant tissue. This argues for a myelin-independent effect of SRF on mitochondria.

3.1.1.2 Mitochondrial distribution but not amount is impaired in *Srf* mutant brain

Besides ultrastructure, mitochondrial distribution is one important feature addressing proper mitochondrial function in neuronal cells as these rely on well-defined positioning of functional mitochondria. To address this question, immunohistochemical staining of mitochondria (TOM20) as well as neuronal nerve fibers (neurofilament H / SMI32) was performed for cortical sections and the mitochondrial distribution pattern analyzed (see Figure 3.2).

As expected, in wild-type cortical tissue mitochondria were highly abundant and were distributed throughout the whole neurite (arrows in Figure 3.2 A). In contrast, SRF-deficiency resulted in an accumulation of mitochondria proximally to the cell body as less mitochondria could be observed in distal parts of the neurite (arrows in Figure 3.2 B). Quantification showed that in *Srf* mutant tissue the number of mitochondria around the cell body was increased whereas mitochondrial abundance in areas further away than 60 µm was decreased significantly (Figure 3.2 E).

At first sight, the mitochondrial distribution pattern in Figure 3.2 suggests that mitochondrial amount is overall decreased in *Srf* mutant tissue as the TOM20 signal seems to be less in

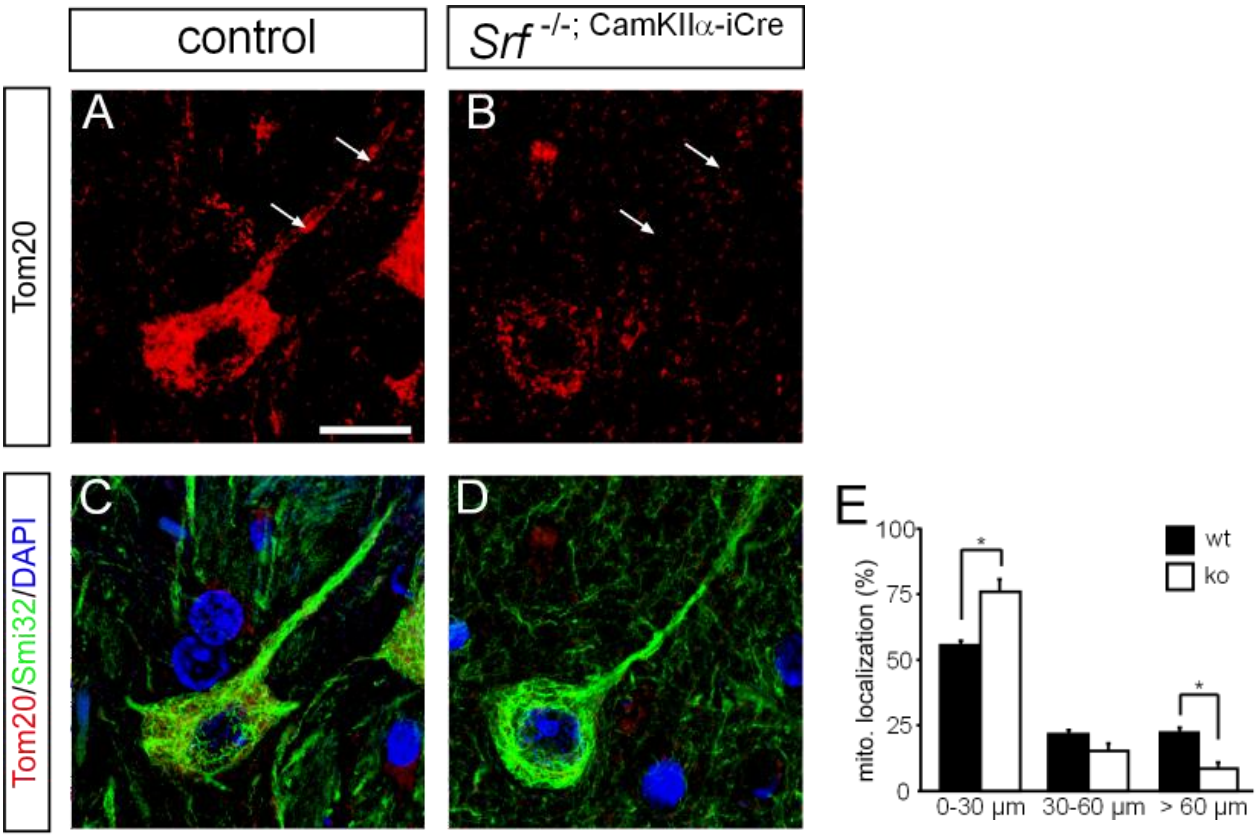

Figure 3.2 SRF-deficiency impairs mitochondrial distribution *in vivo*

(A, C) Wild-type neurons showed a normal distribution pattern of TOM20-stained mitochondria (arrows in A). Contrastingly, (B, D) show a SRF-deficient neuron with decreased number of mitochondria in a neurofilament H / SMI32-positive neurite (arrows in B). (E) Quantification of mitochondrial localization. Numbers of mitochondria were counted for areas maximum 30 µm, 30-60 µm and more than 60 µm away from the cell body. In *Srf* mutant tissue mitochondria accumulated proximally to the cell body and the number of mitochondria further away than 60 µm was significantly reduced in SRF-deficient tissue. Scale bar (A-D) = 10 µm.

case of SRF deficiency. However, immunoblotting of whole tissue extracts (including neurons and glia cells) for mitochondria and other cellular organelles (such as for Golgi apparatus by GM130) showed no obvious decrease (see Figure 3.3). As expected, immunoblotting of hippocampal and cortical tissue showed two hallmarks of *Srf* ablation: a decrease in pan-actin levels and an increase in inactivated phospho-cofilin levels.

Of note, tubulin dynamics did not seem to be impaired upon SRF deficiency. Neither total β-tubulin nor acetylated tubulin levels (indicating stabilized microtubular structures) were affected. One should remember that microtubules are believed to serve as the main cytoskeletal component for mitochondrial trafficking (and hence distribution). Thus, as SRF ablation did not seem to affect microtubules another mechanism needs to be responsible for the observed disturbed mitochondrial distribution pattern in *Srf* mutant tissue.

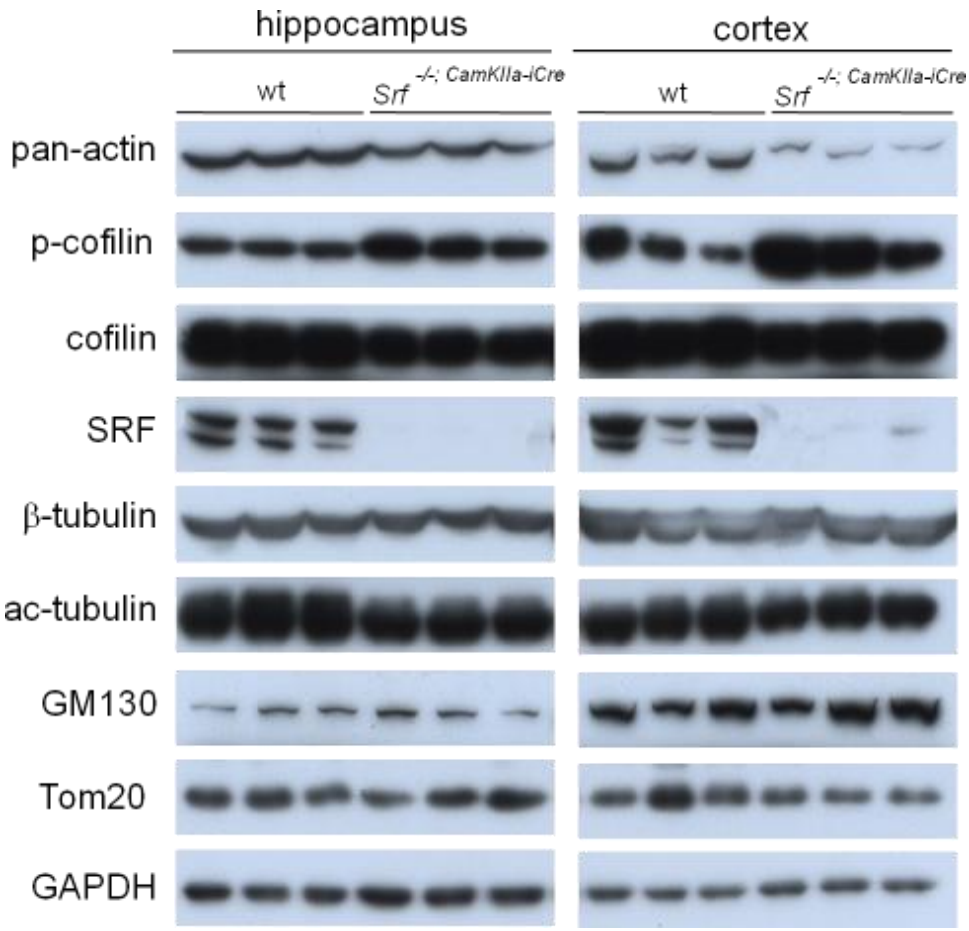

Figure 3.3 Immunoblotting of *Srf* wild-type and *Srf* mutant tissue

Immuboblotting reveals a decrease of pan-actin in *Srf* mutant tissue. Phospho-cofilin levels, indicating inactivated cofilin, were increased upon SRF deficiency. In contrast, no change in abundance of mitochondria (TOM20) or Golgi-apparatus (GM130) was observed as well as no change in tubulin dynamics (assessed by total β-tubulin and acetylated tubulin).

3.1.1.3 SRF deficiency decreases ATP content and ATP production rate of tissue extracts

Although overall abundance of mitochondria did not seem to be decreased in *Srf* mutant tissue, ultrastructural disorganization of mitochondrial membrane topology as well as altered mitochondrial distribution might lead to impaired ATP production. As in neuronal tissue mitochondria are the main ATP producers (see chapter 1.3), defects in ATP content and production rate should directly correlate with mitochondrial functionality *in vivo*.

To address this question mitochondrial fractions of wild-type and *Srf* mutant hippocampal tissue of P14-old mice were prepared (procedure see chapter 2.7.4.4). This resulted in a

cytosolic and a mitochondrial fraction, whose ATP production properties could be assayed luminometrically.

Initially, ATP content of wild-type and *Srf* mutant hippocampal tissue was measured. Interestingly, ATP content (normalized to the whole protein amount) was significantly reduced in case of SRF ablation, suggesting impaired mitochondrial function *in vivo* (see Figure 3.4 A). However one cannot rule out that other metabolic pathways, independently from mitochondrial activity, are affected as well. For this reason, ATP production of mitochondrial fractions was measured in an *in vitro* based assay (detailed procedure see chapter 2.7.4.4). Right after adding substrates to the mitochondrial fractions ATP production started rapidly and slowed down after approximately 100 s (see Figure 3.4 B). Figure 3.4 B shows that mitochondrial ATP production activity was impaired in fractions derived from *Srf* mutant tissue. Of note, no obvious ATP production was detectable in cytosolic fractions (data not shown).

Although it is likely that these effects are mainly due to impaired mitochondrial ultrastructure in *Srf* mutant tissue, it is worth mentioning that this approach does not take into account the mixture of miscellaneous cell types in hippocampal tissue lysates. Beside neurons these contain mostly glia cells, which are highly metabolically active. Maybe the observed impaired ATP production might be ascribed to non-neuronal cell types, although this is rather improbable.

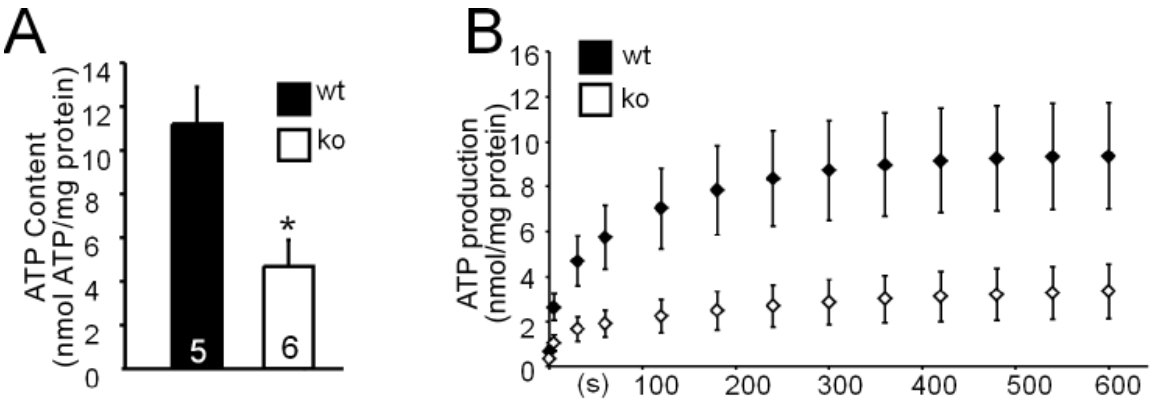

Figure 3.4 Measurement of ATP content and ATP production rate of hippocampal tissue

(A) ATP content was significantly decreased in hippocampal tissue derived from *Srf* mutant animals. (B) ATP production rate of mitochondrial fractions was impaired upon SRF ablation.

3.1.2 *In vitro* Effects of SRF on Mitochondria

As SRF seems to have an effect on mitochondria *in vivo* it is reasonable that an SRF mediated impact on mitochondrial dynamics is also observable *in vitro*. Investigation of mitochondrial dynamics in neurons mainly focuses on mitochondrial key features like **size**, **(ultra)structure**, **distribution** and **trafficking**.

To investigate these properties *in vitro* cell culture experiments were performed. Firstly, hippocampal neurons from *Srf* mutant animals were cultivated and compared to wild-type control neurons with regard to the mentioned mitochondrial characteristics (loss-of-function approach). Later, it was tried in gain-of-function experiments to rescue the mitochondrial phenotype by overexpressing constitutively SRF-VP16 in SRF-deficient neurons.

3.1.2.1 SRF deficiency impairs mitochondrial size, occupancy and ultrastructure *in vitro*

To assess the mechanisms by which SRF influences mitochondrial behavior in neurons in a loss-of-function approach neurons lacking SRF were cultivated *in vitro*. As reported before (Knöll et al., 2006), these neurons display defects in neurite outgrowth and show a different growth cone morphology. Notably, all these well described phenotypes could be observed in this study as well. To visualize mitochondria, neurons were electroporated with pDSRed2Mito, which is a red fluorescent protein (RFP) harboring a cytochrome c-localization sequence, thereby shuttling into mitochondria and staining them in red.

In wild-type neurons mitochondria were equally distributed throughout the whole neurite (see Figure 3.5 A, C) with an average size of 3 µm² [± 0.29 µm², SEM] (see Figure 3.5 E). In contrast to that, mitochondrial size was significantly reduced upon SRF-deficiency [0.82 µm² ± 0.28 µm²]. Furthermore, mitochondria in SRF-deficient neurons were clustered around the nucleus in the cell body and did not enter the neurite (Figure 3.5 B), indicating trafficking impairments in these cells as well. However, one can argue that the restriction of mitochondria in the cell body is due to the fact that neurites are shorter in *Srf* mutant neurons and mitochondria are less likely to travel into these protrusions. To address this issue, mitochondrial distribution is quantified by determination of the occupancy, i.e. the relative amount of the neurite covered by mitochondria (for detailed quantification

procedure see chapter 2.8.5.1). Thereby, this quantification takes into account that neurites are shorter in *Srf* mutant neurons. It turns out that mitochondrial occupancy significantly decreased from 41.3 % ± 3.3 % in wild-type neurons to 24.5 % ± 4.2 % in SRF-deficient neurons (see Figure 3.5 F). Furthermore, conditional SRF ablation in cultivated neurons after two weeks *in vitro* showed again mitochondrial fragmentation, although neurites were fully developed (data not shown).

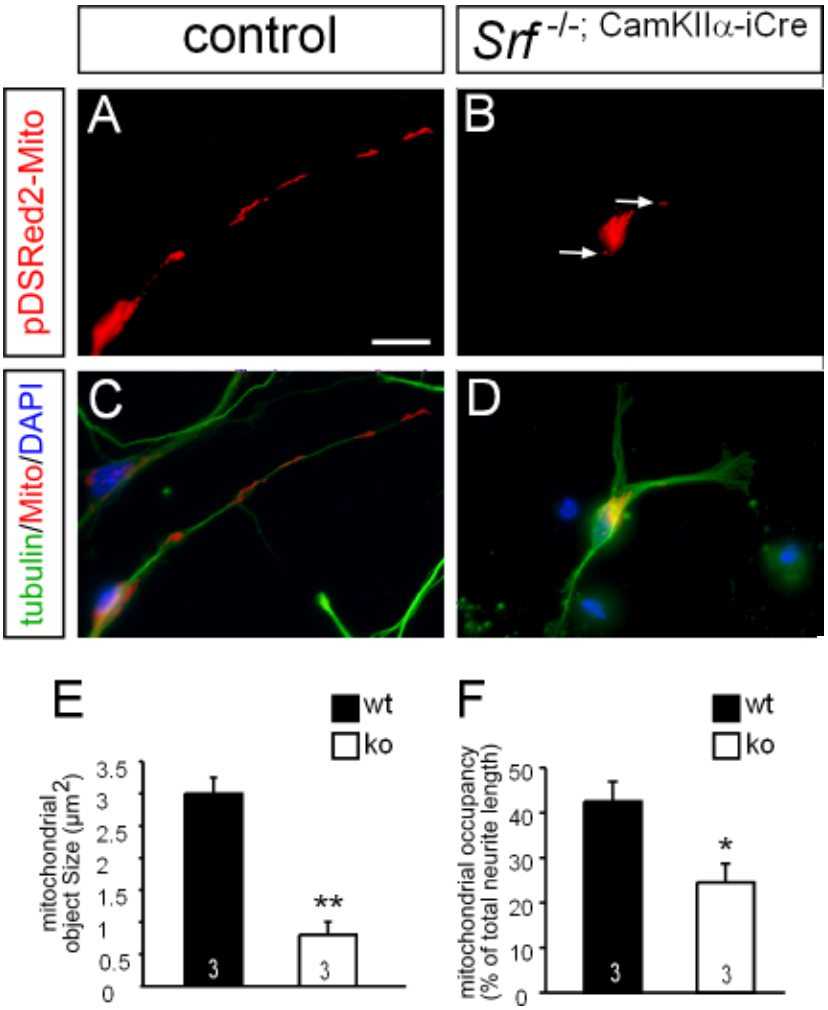

Figure 3.5 Mitochondrial size and occupancy are impaired in SRF-deficient neurons

(A-D) Neurons electroporated with pDSRed2Mito showed red stained mitochondria. In wild-type neurons (A, C) these mitochondria were equally distributed throughout the neurite. (B, D) SRF deficiency resulted in shorter neurites and misshaped growth cones. Furthermore, mitochondria were smaller and clustered in the nucleus (arrows). (E) Quantification of mitochondrial object size revealed that mitochondria were significantly smaller in SRF-deficient neurons. (F) Mitochondrial occupancy was significantly decreased upon *Srf* knockout. Scale bar (A-D) = 10 µm.

To investigate whether SRF ablation also influences mitochondrial ultrastructure with regard to inner membrane topology *in vitro* cultures of wild-type and *Srf* mutant neurons were visualized via electron microscopy. In wild-type neurons mitochondria displayed a clear double membrane and well-shaped cristae (Figure 3.6 A, C) in an electron-dense matrix. In contrast to that, SRF-deficient neurons contained mitochondria showing membrane disarrangements and invaginations into the cristae space (Figure 3.6 B, D, arrows). These invaginations were not as electron-dense as the matrix indicating that the content of these bubble-like structures is rather of cytoplasmic origin. In this regard, these invaginations seemed to originate from a mitochondrial membrane folding inside allowing cytoplasmic content to flow into the matrix space. Interestingly, the membrane topology right aside of these invaginations was maintained, suggesting that this invagination process required controlled membrane reorganization rather than simply disrupting mitochondrial

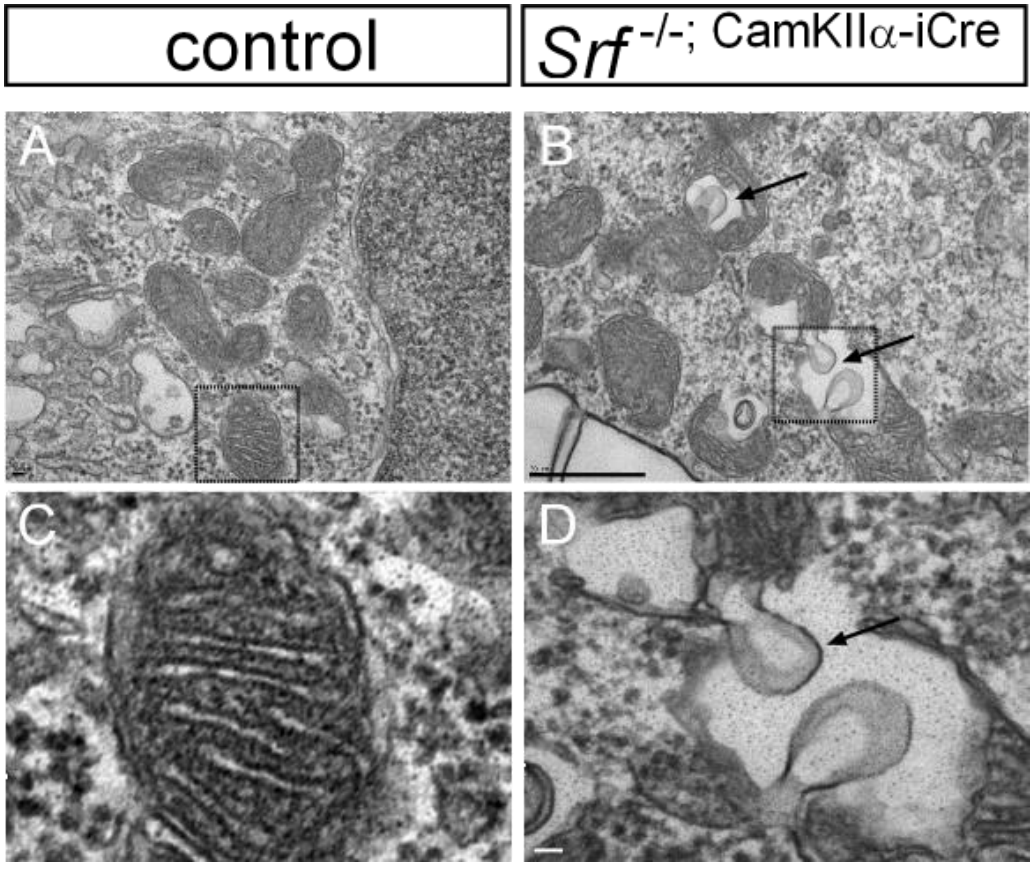

Figure 3.6 Electron microscopy of neurons in culture

(A, C) Mitochondria in wild-type neurons displayed a double-membrane as well as clearly defined cristae morphology. (B, D) Mitochondria in SRF-deficient neurons showed membrane disarrangements and invaginations into the cristae space that were not as electron dense as the matrix (arrows). Scale bars (A,B) = 3 µm, (C, D) = 0.5 µm.

membranes and destroying the matrix.

Although one might remember the electron microscopy performed with corpus callosal cross-sections (Figure 3.1), these *in vitro* membrane disarrangements are different. Whereas *in vivo* mitochondria are filled with multiple vesicles, mitochondria *in vitro* have one or two invaginations without impairing the surrounding matrix. Nevertheless, these two observed types of membrane disarrangements interfering with the electron density of the matrix might be based on similar cellular processes.

3.1.2.2 SRF-deficiency impairs mitochondrial trafficking

As the observed impairments in mitochondrial occupancy are likely to be based upon mitochondrial trafficking, disturbances of mitochondrial movement was analyzed in more detail. For this, time-lapse videomicroscopy was applied allowing for live-cell visualization of mitochondrial trafficking (Figure 3.7).

In Figure 3.7 A and B typical wild-type and *Srf* mutant neurons are depicted. In wild-type control neurons mitochondria were mobile for the whole recording time (only 45 s of a whole 5 min video recording are shown). Interestingly, mitochondria did not move uni-directionally but in a saltatory fashion with phases of moving, pausing and directional changes. However, in *Srf* mutant neurons this trafficking pattern was impaired. Mitochondria were rather stationary for the whole recording time (Figure 3.7 D), albeit enough space for travelling was available.

Quantification of mitochondrial movement velocities revealed that the average velocity in wild-type neurons dropped from 0.104 µm/s ± 0.003 µm/s to 0.084 µm/s ±0.003 µm/s in *Srf* deficient neurons (Figure 3.7 D). This does not seem to be a drastic decrease, which is due to the quantification parameters: A cut-off of 0.05 µm/s was used to take into account only fast moving mitochondria. Thereby, even in SRF-deficient neurons mitochondria with rather high velocities were quantified. Nevertheless, these “non-moving” mitochondria were also quantified as thresholding resulted in a rather low percentage of moving mitochondria in SRF-deficient neurons (Figure 3.7 F). In wild-type neurons 72.8 % ± 5.2 % of the mitochondria were moving (i.e. moved for more than three consecutive frames with a velocity higher than

0.05 µm/s). In contrast, in SRF-deficient neurons 41.9 % ± 4.5 % of all mitochondria were moving.

Thereby, these observed trafficking impairments might lead to the observed mitochondrial occupancy defects (see Figure 3.5).

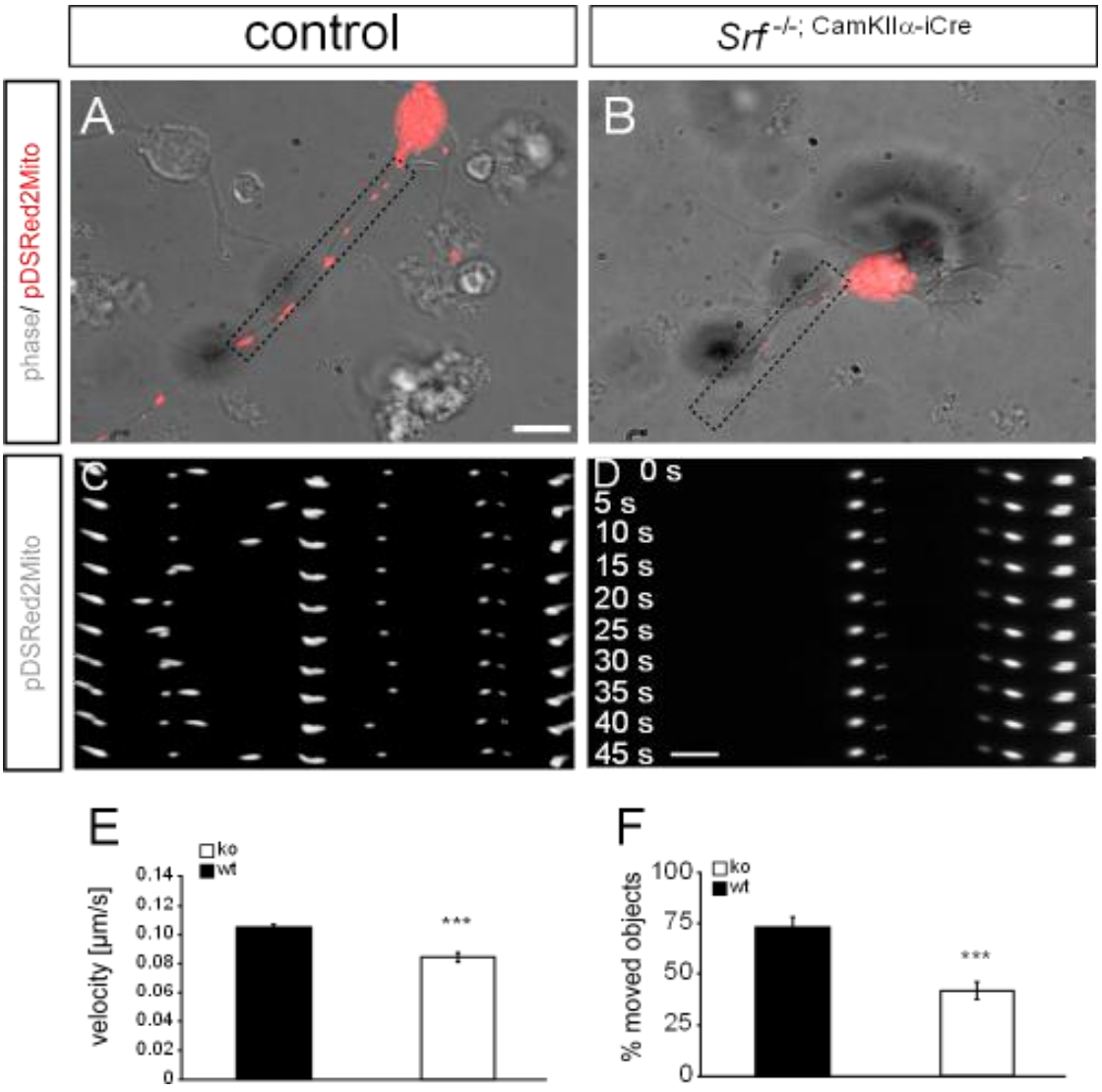

Figure 3.7 Time-lapse videomicroscopy of wild-type and SRF-deficient neurons

(A) Phase contrast picture of a wild-type neuron expressing pDSRed2Mito allowing for visualization of red-stained mitochondria. (B) Mitochondria in a *Srf* mutant neuron were smaller and clustered around the nucleus. (C) Mitochondrial signals taken from the dashed area in (A). With increasing time mitochondria moved along the neurite. (D) Time series of mitochondria from the dashed area in (B) showing stationary mitochondria in *Srf* mutant neurons. (E) Mitochondrial movement velocity was significantly decreased in *Srf* mutant neurons. (F) Relative amount of moved mitochondria was significantly reduced upon SRF ablation. Scale bars (A, B) = 10 µm, (C, D) = 3 µm.

3.1.2.3 SRF-mediated effects on distribution are mitochondria specific

As SRF deficiency influences the actin cytoskeleton in general it is tempting to assume that the observed mitochondrial phenotypes are due to general microfilament disturbances and reflects a secondary phenotype. To address this important question whether SRF has a direct or indirect effect on mitochondria synaptic vesicles were monitored with special regard to distribution and trafficking. For this, a RFP-labeled synaptophsin was overexpressed in neurons leading to red-stained synaptic vesicles.

In wild-type neurons synaptic vesicles were distributed throughout the whole cell with distinct accumulation in the cell body area (Figure 3.8 A, C). Quantification revealed that most of the vesicles were located in the perinuclear space (48.0 % ± 4.5 %) and only a small fraction could be found in the growth cone area (9.2 % ± 3.3 %, see Figure 3.8 E). This distribution pattern could be found in *Srf* mutant neurons as well, although these neurons displayed the same morphological phenotype as the *Srf* mutant neurons before that were labeled for mitochondria (compare Figure 3.8 B, D with Figure 3.5 B, D). Furthermore, there was only a slight but not significant increase of synaptic vesicle amount in the cell body area of *Srf* mutant neurons (51.5 % ± 2.0 % of all synaptic vesicles were located in the cell body area). This speaks in favor of SRF not controlling synaptic vesicle trafficking, which was monitored by videomicroscopy again. In line, these experiments showed that neither the amount of moving synaptic vesicles (96 % ± 2 % in wild-type vs. 99 % ± 0.4 % in *Srf* mutant, see Figure 3.8 F) nor the velocity of moving vesicles was decreased (1.5 µm/s ± 0.12 µm/s in wild-type vs. 1.7 µm/s ± 0.06 µm/s in *Srf* mutant, see Figure 3.8 G).

This experiment shows that the previously observed mitochondrial phenotypes in SRF-deficient neurons cannot be totally ascribed to the altered neuronal morphology.

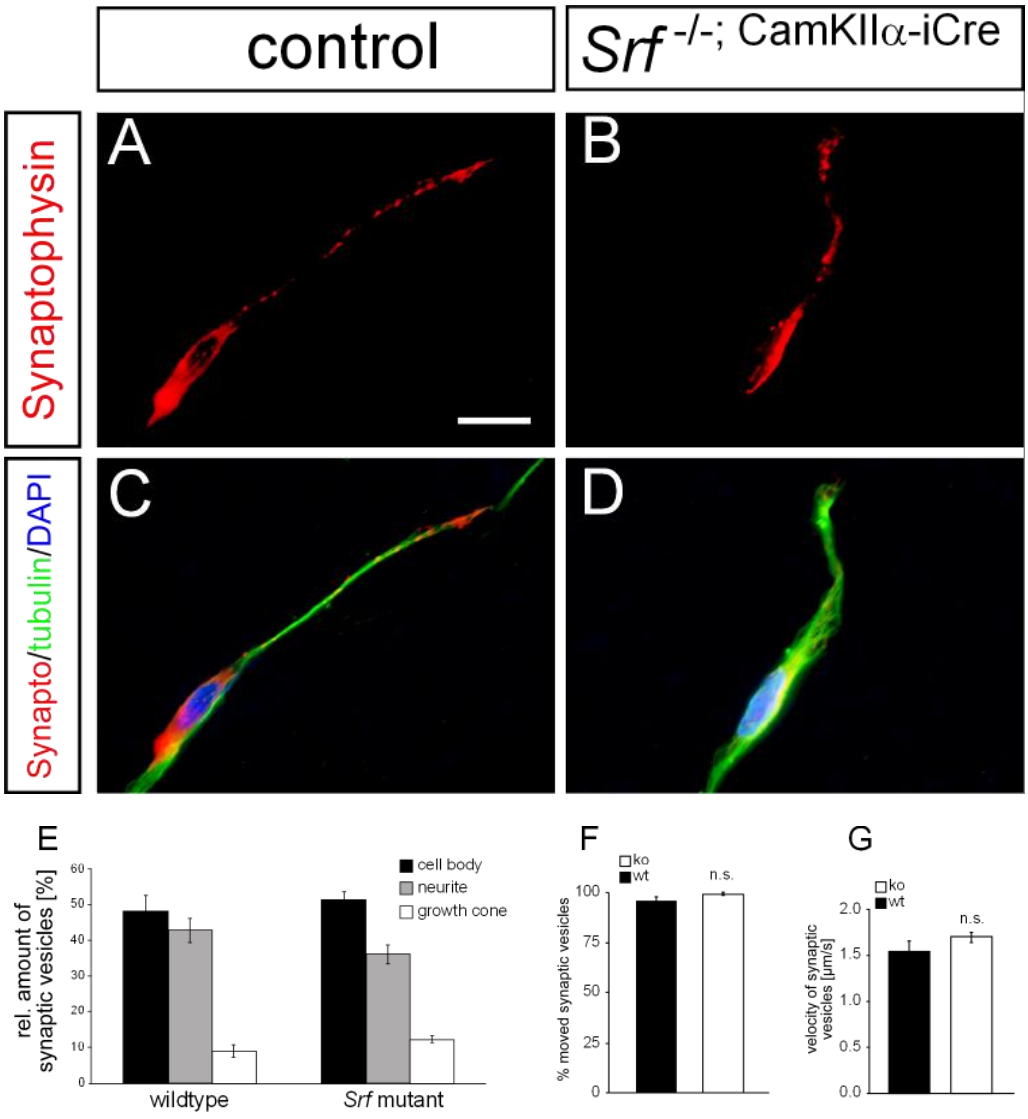

Figure 3.8 Distribution and trafficking of synaptic vesicles in neurons

(A, C), Wild-type neurons expressing RFP-labeled synatophysin showed synaptic vesicles distributed throughout the whole neurite with distinct accumulation in the cell body. (B, D) Albeit *Srf* mutant neurons displayed shorter neurite morphology, synaptic vesicles were distributed in the whole cell. (E) Quantification of synaptic vesicle amount in different cellular compartments revealed no difference between wild-type and *Srf* mutant. (F) Almost all synaptic vesicles were moving in wild-type and SRF-deficient neurons. (G) No difference in movement velocities of synaptic vesicles could be observed. Scale bar (A-D) = 10 µm.

3.1.2.4 Constitutively active SRF-VP16 restores normal mitochondrial size and occupancy in an SRF-deficient background *in vitro*

The loss-of-function experiments performed so far provide evidence that SRF is necessary for proper mitochondrial function in neurons. Consequentially, in a gain-of-function approach these effects should be reversed. To address this issue, a constitutively active SRF-VP16-mutant was applied (introduced in chapter 1.1.1). SRF-ΔMADS-VP16 serves as a proper control as it only lacks the MADS-box and is thereby incapable of DNA-binding.

Wild-type neurons overexpressing SRF-ΔMADS-VP16 showed no obvious phenotype (Figure 3.9 A, E, I). Mitochondria were normal in size (3 µm² ± 0.3 µm²) and normally distributed (occupancy of 40.5 % ± 3.2 %). Notably, overexpression of constitutively active SRF-VP16 in a wild-type background resulted in large network-like structures of mitochondria (Figure 3.9 B, F, J). Thereby, mitochondrial size almost doubled in these neurons (6 µm² ± 0.9 µm², see Figure 3.9 M) and occupancy significantly increased to 71 % ± 9 % (see Figure 3.9 N).

Of note, SRF-VP16 was able to rescue the mitochondrial phenotype in an *Srf* mutant background. While *Srf* mutant neurons expressing SRF-ΔMADS-VP16 displayed mitochondrial fragmentation (mitochondrial size at 0.82 µm² ± 0.23 µm², Figure 3.9 M) and decreased occupancy (24.5 % ± 4.2 %, Figure 3.9 N), *Srf* mutant neurons expressing SRF-VP16 showed a normal phenotype indistinguishable from wild-type neurons (Figure 3.9 D, H, L). In these neurons mitochondrial size was significantly increased at 3.1 µm² ± 0.1 µm² (Figure 3.9 M) and occupancy restored (50 % ± 1.2 %, Figure 3.9 N) in comparison to SRF-deficient neurons.

To control for the VP16-specificity another VP16-fused transcription factor CREB-VP16 was applied. Of note, CREB-VP16 had no effect on mitochondrial size or on mitochondrial occupancy (Figure 3.9 M, N). This indicates that the observed effects of SRF-VP16 are not a due to a general activity of any transcription factor. Furthermore, it strengthens the specificity of SRF to modulate mitochondrial dynamics as not every constitutively active transcription factor (such as CREB-VP16) can induce mitochondrial changes *in vitro*.

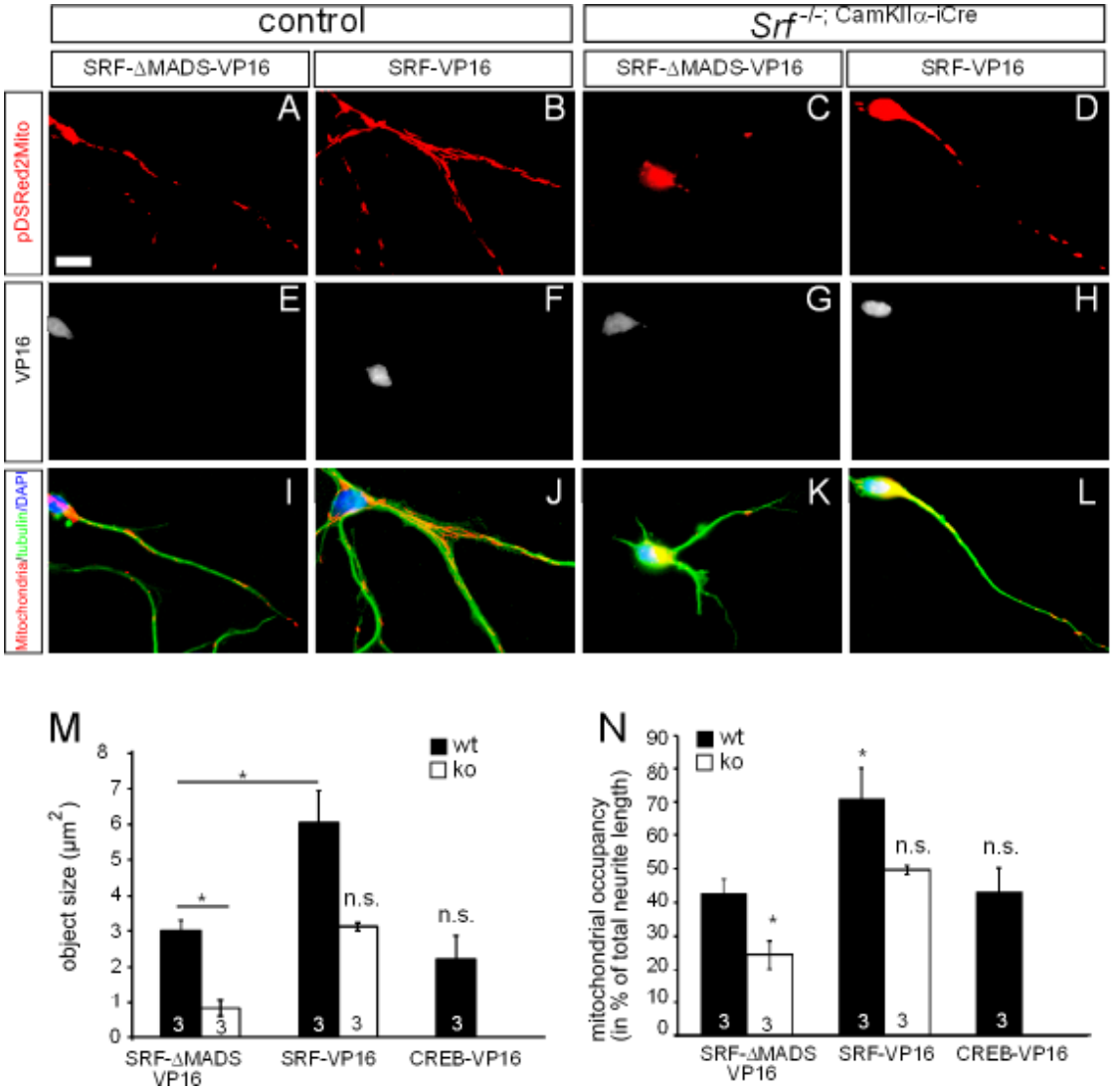

Figure 3.9 Rescue of mitochondrial size and occupancy upon overexpression of SRF-VP16

(A, C, E) show wild-type neurons expressing the SRF-ΔMADS-VP16 control construct. Neurons and mitochondria looked normal. (B, F, J) Wild-type neurons overexpressing constitutively active SRF-VP16 showed large network-like mitochondrial structures. (C, G, K), SRF-deficient neurons expressing SRF-ΔMADS-VP16 displayed the knockout phenotype with shorter neurites and perinuclear clustering of fragmented mitochondria. (D, H, L) Overexpression of SRF-VP16 rescued the morphological as well as the mitochondrial phenotype in *Srf* mutant neurons. (M) Quantification of mitochondrial object size. SRF-VP16 increased mitochondrial size in wild-type neurons and rescued mitochondria in *Srf* mutant neurons. CREB-VP16 did not have an effect. (N) Quantification of mitochondrial occupancy. SRF-VP16 restored normal occupancy in *Srf* mutant neurons and increased occupancy in wild-type neurons significantly. CREB-VP16 had no effect. Scale bar (A-L) = 10 µm.

Beside size and distribution, mitochondrial ultrastructure was rescued by overexpression of SRF-VP16 (see Figure 3.10). Wildtype neurons showed a normal membrane topology with a clear double membrane and an electron dense matrix pervaded by well-organized cristae (Figure 3.10, A). In contrast, SRF deficiency resulted in membranous invaginations, disturbing the membrane topology and disrupting cristae morphology (Figure 3.10 B, arrows). In wildtype neurons SRF-VP16 overexpression had no obvious effect on ultrastructure (Figure 3.10 C), whereas SRF-VP16 was able to rescue membrane disturbances in *Srf*-mutant neurons (Figure 3.10 D).

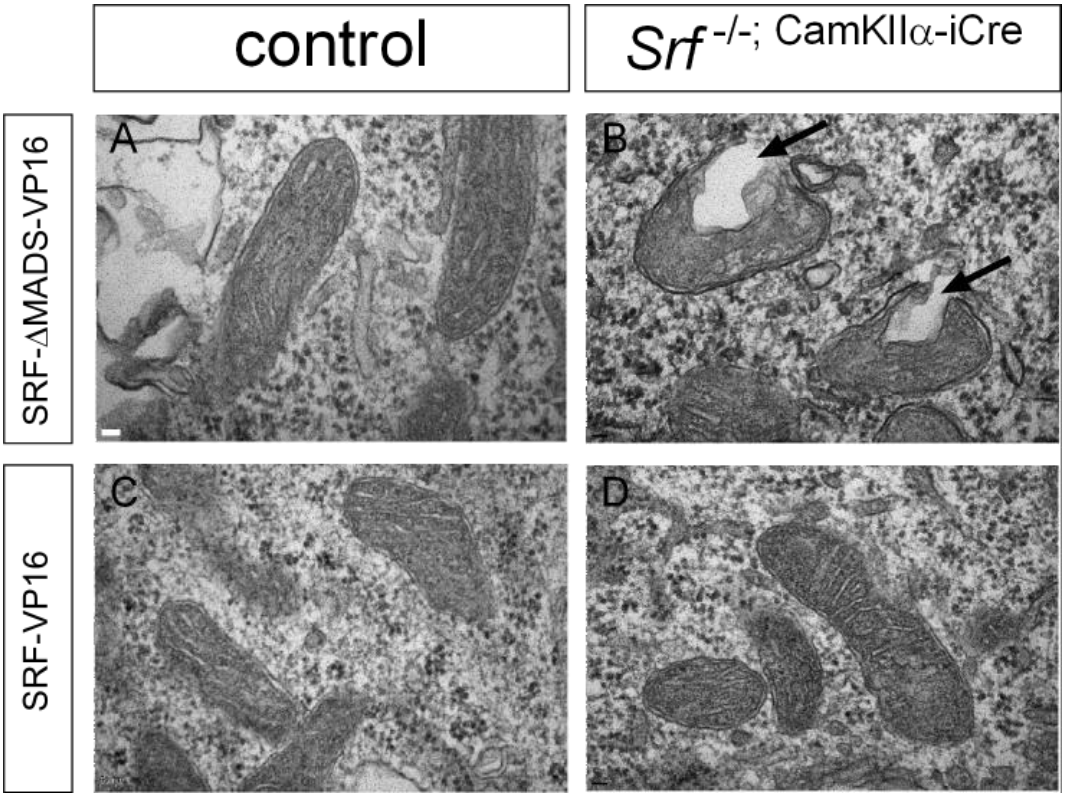

Figure 3.10 Rescue of mitochondrial ultrastructure by overexpression of SRF-VP16

(A) Wildtype neurons expressing the SRF-ΔMADS-VP16 control construct displayed normally shaped mitochondria with a clear double membrane and well-organized cristae morphology. (B) SRF-deficient neurons showed disturbances in membrane topology and invaginations into the matrix space (arrows). (C) SRF-VP16 had no obvious effect on membrane topology of wildtype neurons. (D) In *Srf*-mutant neurons SRF-VP16 overexpression restored normal membrane topology and inhibited formation of invaginations. Scale bar (A-D) = 50 nm.

3.1.2.5 SRF-VP16 rescues mitochondrial trafficking in *Srf* mutant neurons

As overexpression of SRF-VP16 rescues mitochondrial occupancy it is likely that trafficking of mitochondrial objects is also restored upon SRF-VP16 expression.

Figure 3.11 shows a visualization of the performed time-lapse videomicroscopy experiments. The mitochondrial trafficking pattern is shown in kymographs displaying time on the y-axis and distance on the x-axis. Every white signal represents a mitochondrial object and the more the mitochondria move the more staggered the mitochondrial movement pattern gets in the kymograph.

Obviously, wild-type neurons expressing an SRF-ΔMADS-VP16 control construct displayed a normal movement behavior of moving and stopping mitochondria. The average movement velocity was at 0.12 µm/s ± 0.03 µm/s (see Figure 3.11 E) and 71.6 % ± 2 % of mitochondria were engaged in movement (Figure 3.11 F). As expected, SRF-deficiency together with overexpression of the SRF-ΔMADS-VP16 control construct led to impaired mitochondrial trafficking (Figure 3.11 B): Mitochondrial velocity decreased significantly to 0.09 µm/s ± 0.03 µm/s and only 46.9 % ± 8.2 % of mitochondria were moving. This is consistent with the previous time-lapse recording of mitochondrial movement (Figure 3.7) indicating that SRF-ΔMADS-VP16 indeed serves as a non-functional control construct.

Notably, overexpression of SRF-VP16 drastically increased mitochondrial trafficking (Figure 3.11 C). Mitochondrial velocity was significantly increased compared with wild-type control to 0.18 µm/s ± 0.02 µm/s. Furthermore, 86 % ± 1.6 % of mitochondria were engaged in transport. It is important to note that this quantification takes into account only small, thereby fast moving mitochondria in the periphery of the neuron. As many of the mitochondria form the observed large network-like structures (Figure 3.9) and are not engaged in movement, these mitochondria were not quantified for their trafficking properties.

Additionally, the trafficking enhancing effect of SRF-VP16 restored mitochondrial movement even in the background of SRF deficiency. Thereby, mitochondrial velocity was at wild-type levels (0.13 µm/s ± 0.01 µm/s) and 80 % ± 3.4 % of mitochondria were moved.

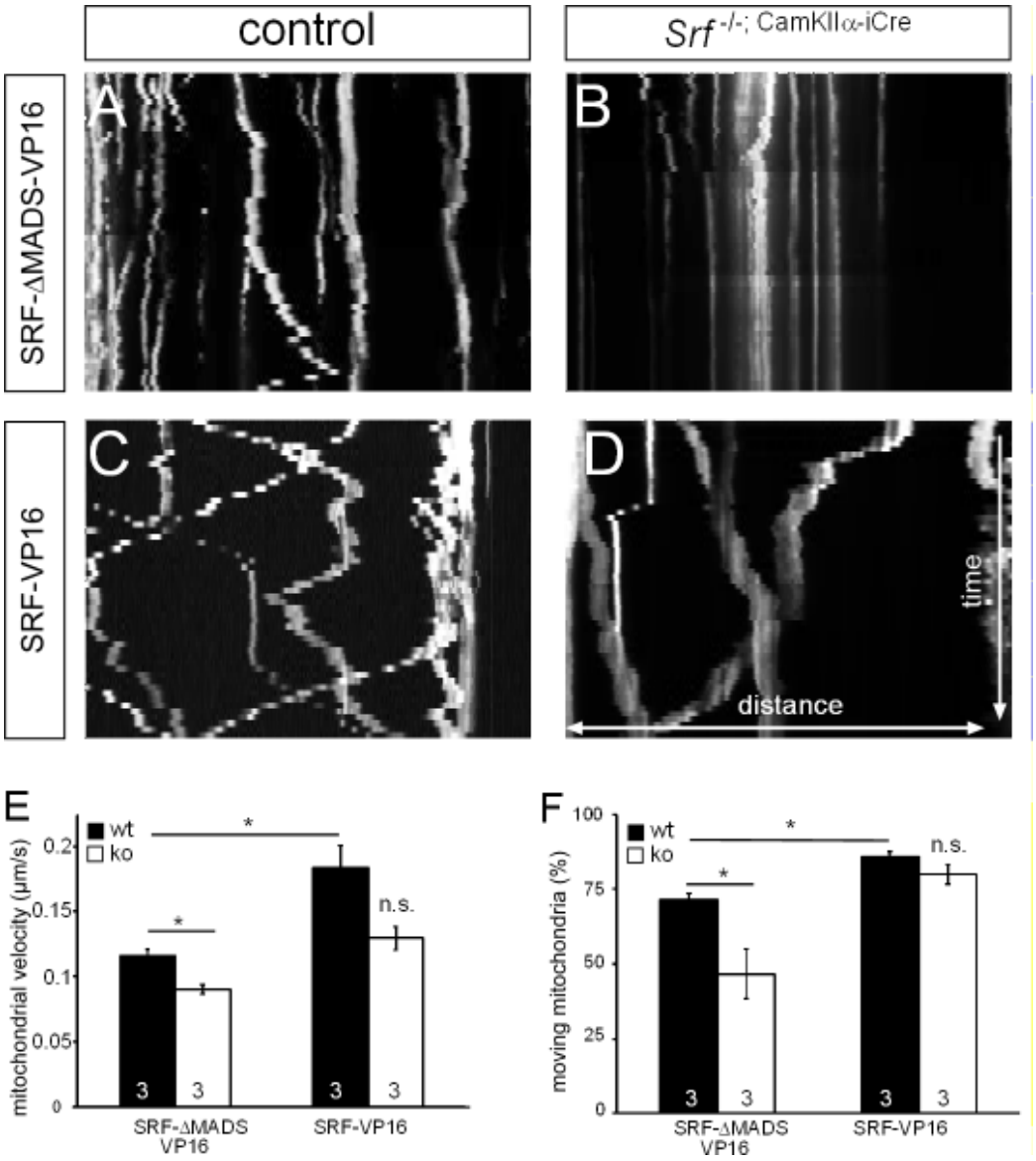

Figure 3.11 Rescue of mitochondrial trafficking upon SRF-VP16 overexpression

(A) Kymograph showing mitochondrial trafficking pattern in wild-type neurons. A wild-type neuron expressing the SRF-ΔMADS-VP16 control construct showed a normal mitochondrial trafficking pattern with moving and stopping mitochondria. (B) A SRF-deficient neuron expressing SRF-ΔMADS-VP16 displayed impaired mitochondrial movement with most of the mitochondria not moving. (C) Wild-type neurons overexpressing SRF-VP16 showed drastically increased mitochondrial movement. (D) Overexpression of SRF-VP16 in an *Srf* mutant neuron rescued mitochondrial movement. (E) Quantification of mitochondrial velocity. SRF ablation together with SRF-ΔMADS-VP16 expression led to significantly slower velocities. SRF-VP16 overexpression in wild-type neurons significantly increased velocities and rescued mitochondrial movement in *Srf* mutant neurons. (F) Quantification of the number of mitochondria engaged in movement. SRF deficiency decreased the relative amount of moved mitochondria significantly, whereas SRF-VP16 increased the number of moving mitochondria in wild-type neurons and rescued mitochondrial trafficking in *Srf* mutant neurons.

Thus, taking together the effects of SRF-VP16 with regard to mitochondrial size, occupancy and trafficking SRF-VP16 rescued mitochondrial properties in an *Srf* mutant background. Furthermore, in wild-type neurons SRF-VP16 expression led to a drastic increase of all observed mitochondrial parameters resulting in a new mitochondrial phenotype forming syncytial structures with fast moving mitochondria in the periphery.

However, the exact mechanism by which SRF exerts its function on mitochondria is not understood so far. Indeed, a direct mechanism involving SRF controlling the expression of mitochondrial target genes seems rather improbable as RT-PCR did not reveal any effect of SRF on mitochondrial related structural, fusion/fission or trafficking genes (data not shown). Thereby, it is more likely that SRF influences mitochondrial dynamics indirectly by changes in microfilament dynamics. For this reason, the impact of the actin cytoskeleton on mitochondrial dynamics shall be addressed in more detail in the next chapter.

3.2 Impact of the Actin Cytoskeleton on Mitochondrial Dynamics

As SRF is one of the major gene transcriptional regulators of the actin cytoskeleton it is likely that the observed phenotypes, including mitochondrial fragmentation, perinuclear clustering and impaired trafficking, rely on changes in the actin microfilament. SRF deficiency results in a decrease of β-actin as the latter is a direct target gene of SRF (Figure 3.3). Thus, one possible explanation would be that an impairment in functional actin treadmilling or an overall decrease of filamentous actin influences mitochondrial size and distribution.

There are many possible mechanisms to influence the G/F-actin ratio in the cell mainly relying on application of actin drugs that lead to a depolymerisation of F-actin, thereby increasing G-actin levels (e.g. by administration of latrunculin) or on the other hand stabilize F-actin (e.g. jasplakinolide). Although all of these drugs are rather specific in their way of interfering with actin treadmilling, in this project another, more sensitive way of shifting the G/F-actin ration was used. For this, actin point-mutants were overexpressed that differ in their way of stabilizing F-actin (see Figure 3.12, after (Posern et al., 2002)).

As depicted, several well described actin mutants are used to modify the G/F-actin ratio. Overexpression of actin S14C or actin G15S results in an increase of F-actin. Both actin mutants are stably incorporated into filamentous actin and stabilize its conformation.

However, both actin mutants differ in their way of interacting with actin binding proteins. Most important for this work, actin S14C does interact with cofilin, whereas actin G15S does not (Posern et al., 2004). Additionally, overexpression of actin R62D leads to an increase of monomeric G-actin as this point mutant cannot be built into filamentous actin. Notably, actin R62D does not disrupt existing F-actin but just increases the G-actin pool because of its incapability of polymerization (Posern et al., 2002).

Thus, overexpression of these actin mutants allow for investigating whether mitochondrial size and distribution are dependent on the G/F-actin status in the cell.

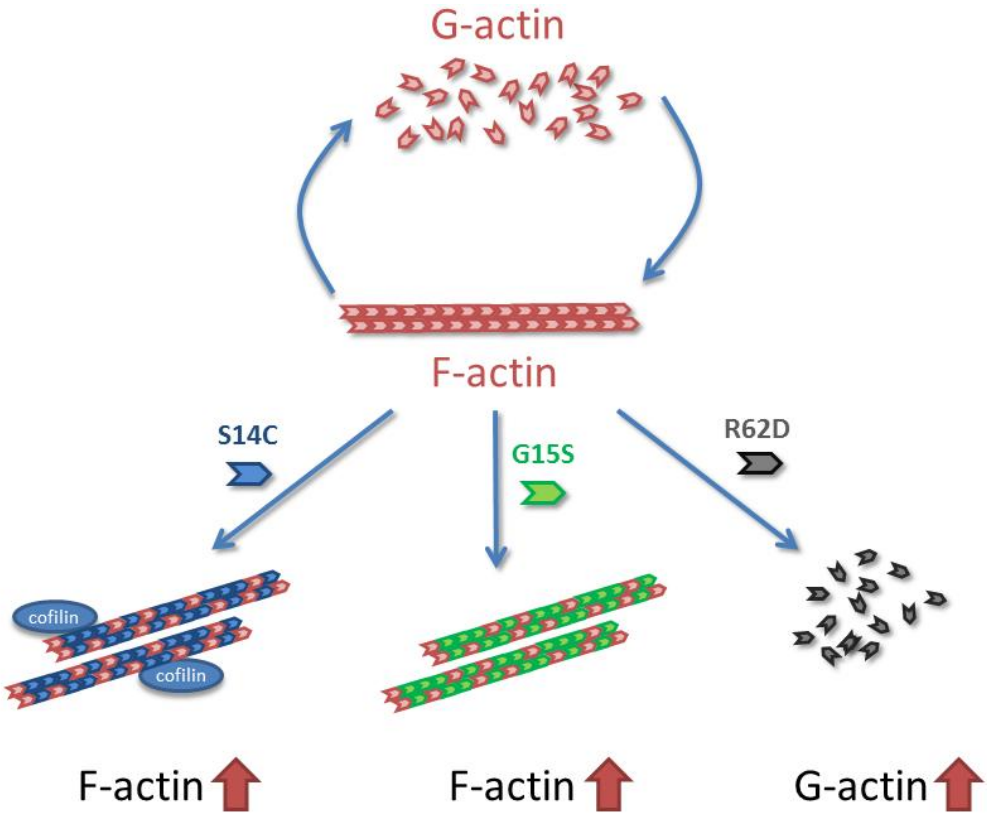

Figure 3.12 Actin point-mutants shift the actin treadmilling process

Actin treadmilling involves turnover of F-actin polymers to monomeric G-actin. Application of point-mutated actin proteins interfere with this process. Actin S14C as well as actin G15S favor F-actin assembly and form actin filaments, yet differ in their binding properties with regard to cofilin (actin S14C does bind cofilin, whereas actin G15S does not). Actin R62D cannot be built into F-actin, thereby overexpression of R62D increases the pool of monomeric G-actin.

3.2.1 Mitochondrial size is dependent on the G/F-actin ratio in the cell

To investigate, whether mitochondrial size is G-actin dependent, wild-type neurons were treated with the actin depolymerizing drug latrunculin (Figure 3.13 B, G). Immediately after 20 min of incubation mitochondria got fragmented and their size decreased significantly from 2.2 µm² ± 0.1 µm² in wild-type control neurons to 1 µm² ± 0.01 µm² in latrunculin stimulated neurons (Figure 3.13 K). However, mitochondrial occupancy was not changed between wild-type neurons (46,1 % ± 2.7 %) and latrunculin-stimulated neurons (44.2 % ± 2.4 %, see Figure 3.13 L). Although mitochondria were smaller in latrunculin-treated neurons, these cells obviously contained more (albeit smaller) mitochondria that in sum compensated the decrease in mitochondrial size and led to a "normal" occupancy. Of note, overall morphology of latrunculin-treated neurons was not changed, at least after a short period of stimulation (20 min).

Overexpression of the aforementioned actin mutants influenced, at least in part, mitochondrial size and occupancy. These actin mutants are FLAG-tagged, thereby they were stained by a FLAG-specific antibody in immunocytochemistry. Of note, overexpression of actin R62D changed the morphology of wild-type neurons (Figure 3.13 C, H), thereby phenocopying *Srf* mutant neurons as reported before (Stern et al., 2009). Additionally, mitochondrial size was decreased significantly to 1.3 µm² ± 0.09 µm² (Figure 3.13 K). Furthermore, mitochondrial occupancy was significantly decreased as well (to 17.9 % ± 3.2 %).

Interestingly, the two F-actin favoring actin mutants actin G15S and actin S14C differed in their way they influenced mitochondrial size and occupancy. Overexpression of actin G15S led to a significant increase of mitochondrial size (4.4 µm²± 0.04 µm²) and occupancy (62 % ± 3.8 %) (see Figure 3.13 D, I, K, L). In contrast, actin S14C did not seem to have an effect neither on mitochondrial size (2.2 µm² ± 0.08 µm²) nor on occupancy (41 % ± 1.8 %) (Figure 3.13 E, J, K, L). This shows that increasing the F-actin pool alone is not sufficient to increase mitochondrial size. It is likely that recruitment of actin binding proteins such as cofilin might co-regulate mitochondrial size dependent on the polymerization status of actin. Nevertheless, this experiment shows that the polymerization status of actin influences mitochondria. Increase in G-actin levels leads to smaller mitochondria, whereas increase of F-actin levels (without cofilin binding, see actin G15S) increases mitochondrial size.

As shown in Figure 3.13, overexpression of actin R62D did lead to a neuronal phenotype reminiscent of SRF-deficient neurons (compare with Figure 3.5). Thus, it is interesting whether this artificial increase in G-actin levels is sufficient to abrogate the SRF-VP16 effect with regard to mitochondria (formation of syncytial network-like mitochondrial structures).

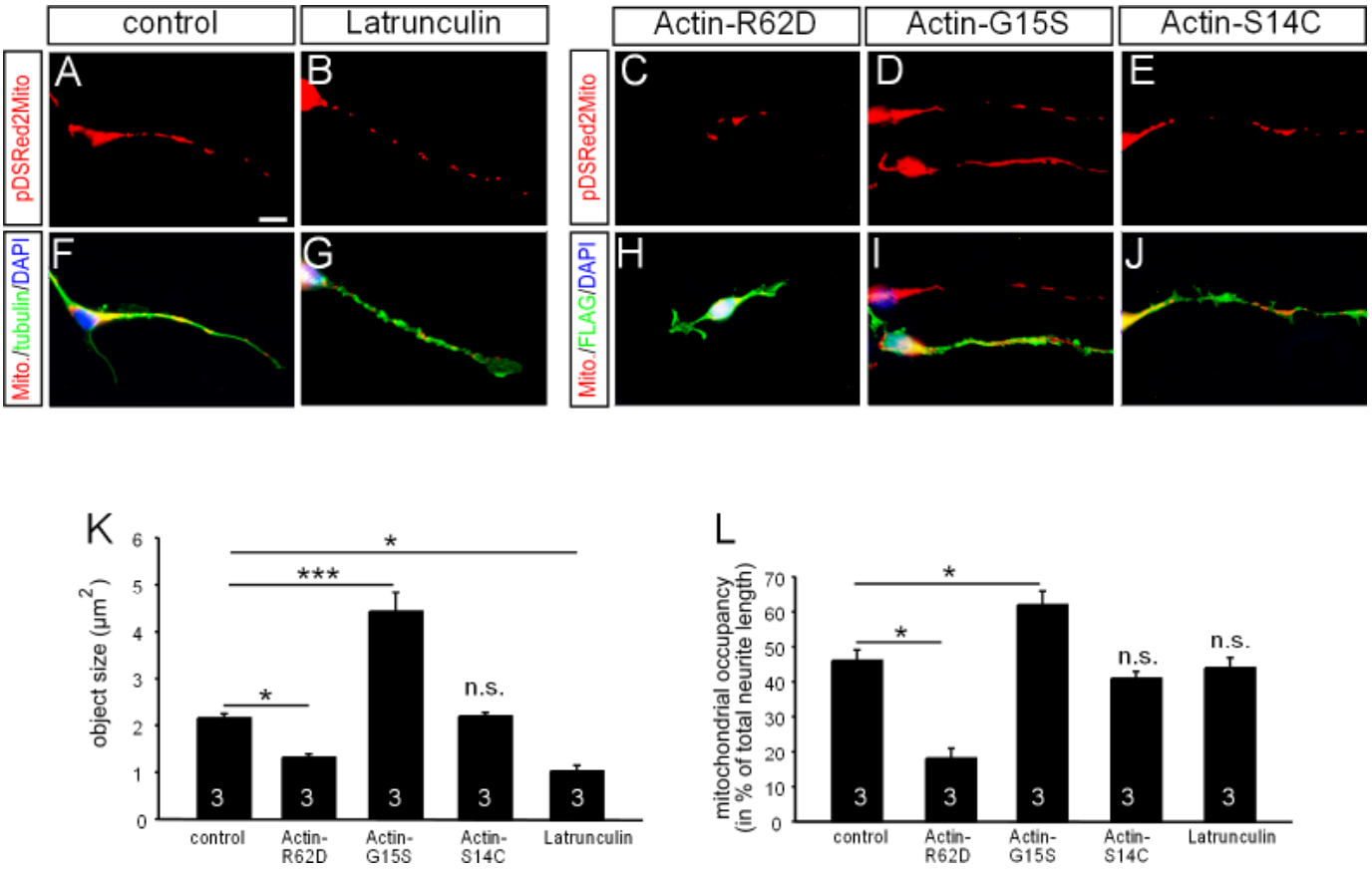

Figure 3.13 Shifting the G/F-actin ratio influences mitochondrial size and occupancy

(A, F) Control neurons electroporated with pDSRed2Mito only displayed normal mitochondria. (B, G) Application of the actin depolymerizing drug latrunculin led to mitochondrial fragmentation. (C, H) Overexpression of actin R62D resulted in neurons that phenocopied SRF-deficient neurons with regard to overall morphology, mitochondrial size and occupancy. (D, I) A neuron overexpressing actin G15S displayed enlarged mitochondria. (E, J) Overexpression of actin S14C did not have an impact on mitochondria. (K) Quantification of mitochondrial object size. Whereas increasing the G-actin pool by overexpression of actin R62D or administration of latrunculin decreased mitochondrial size significantly, overexpression of actin G15S increased mitochondrial size more than twofold. Actin S14C did not influence mitochondrial size. (L) Quantification of mitochondrial occupancy. Actin R62D decreased, actin-G15S increased mitochondrial occupancy significantly. Actin S14C and latrunculin administration did not alter mitochondrial occupancy. Scale bar (A-J) = 10 µm.

As shown in Figure 3.14, wild-type neurons were co-electroporated with actin R62D and SRF-VP16 or SRF-ΔMADS-VP16 as control. Control neurons overexpressing SRF-ΔMADS-VP16 together with actin R62D displayed the aforementioned phenotype with shorter neurites, mitochondrial fragmentation and perinuclear clustering of mitochondria (Figure 3.14 A, C, E, G). Quantifications shown in Figure 3.14 I and J revealed that mitochondrial size was decreased to 1.0 µm² ± 0.06 µm² and mitochondrial occupancy was reduced to 17.2 % ± 1.5 %. Interestingly, neurons co-expressing actin R62D and SRF-VP16 showed the same phenotype (Figure 3.14 B, D, F, H). In spite of SRF-VP16 expression, these neurons showed fragmented mitochondria (0.97 µm² ± 0.33 µm²) and decreased mitochondrial occupancy (18.4 % ± 3.5 %). Although not quantified, it is obvious, that the overall phenotype of actin R62D expressing neurons did not get rescued upon SRF-VP16 expression (see Figure 3.14 A, B).

This experiment shows that increased G-actin levels are sufficient to abolish the SRF-VP16 effect. Thus, it is reasonable to state that the observed mitochondrial phenotypes upon SRF-VP16 expression are based on functional actin treadmilling. Shifting the G/F-actin ratio towards G-actin, thereby interfering with functional treadmilling, seems to be adequate to overcome SRF-VP16 mediated effects. In this regard, SRF-VP16 is most likely to exert its effect on mitochondria via influencing the G/F-actin ratio.

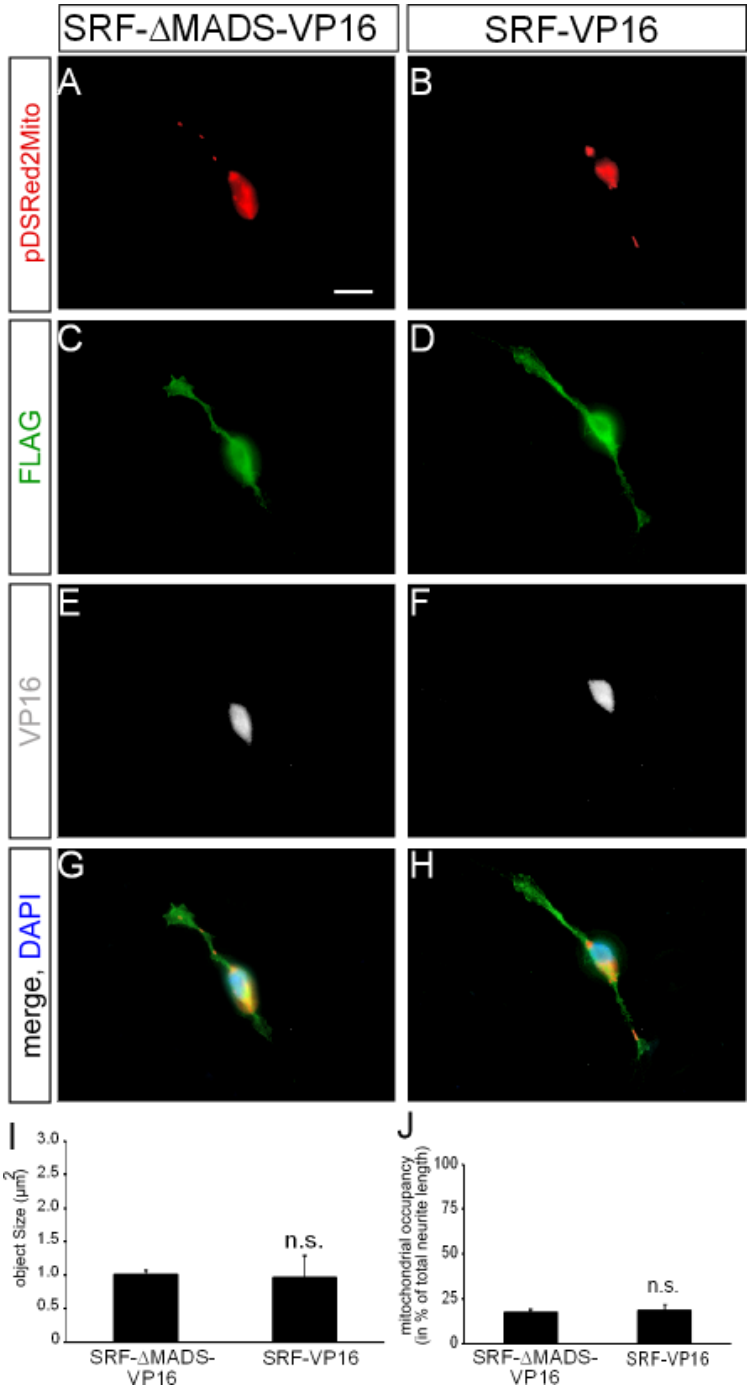

Figure 3.14 Overexpression of actin R62D abrogates the SRF-VP16 effects on mitochondria

(A, C, E, G) A wild-type neuron overexpressing actin R62D together with the SRF-ΔMADS-VP16 control construct phenocopied the *Srf* mutant phenotype. Neurites were shorter, mitochondria were smaller and clustered in the cell body. (B, D, F, H) Even in presence of constitutively active SRF-VP16 neurons co-expressing actin R62D exhibited the same phenotype as without SRF-VP16. (I) Quantification of mitochondrial object size. Mitochondria were fragmented upon actin R62D expression regardless of SRF-VP16 expression. (J) Quantification of mitochondrial occupancy. Actin R62D overexpression decreased occupancy albeit SRF-VP16 expression. Scale bar (A-H) = 10 µm.

3.2.2 Actin dynamics modulate mitochondrial dynamics in growth cones

One important cellular compartment in neurons that is highly dependent on microfilament formation is the growth cone (see chapter 1.2.2). For this reason, this particular subcellular structure was investigated in more detail with special focus on mitochondrial localization in growth cones. As it is believed that the actin microfilament serves as a docking station to arrest mitochondria in a position their energy production is needed (Mironov, 2007; MacAskill and Kittler, 2009), the question arises whether interfering with actin polymerization in the growth cone affects mitochondrial positioning. It is known that actin growth cone dynamics is modulated upon stimulation with guidance cues such as BDNF or ephrin-A5 (Meier et al., 2011). Whereas BDNF increases filopodia formation (Chen et al., 2006; Stern et al., 2009), stimulation with ephrins leads to a transient F-actin decrease (Marsick et al., 2012). Thereby, stimulation with these guidance cues allows for selective F-actin assembly or disassembly in the growth cone.

To analyze, whether selective F-actin formation or F-actin depolymerization has an effect on mitochondria, neurons were stimulated with BDNF for 60 min or with ephrin-A5 for 10 min. Thereby, this short ephrin-A5 administration should only result in a F-actin depolymerization without a full growth cone collapse observed after longer times of ephrin-A5 stimulation (Meier et al., 2011).

Unstimulated wild-type neurons displayed growth cones with only few mitochondria entering the growth cone area (Figure 3.15 A, D). Quantification revealed that on average only 1 mitochondrion enters the growth cone area (1.1 ± 0.3 mitochondria / growth cone, Figure 3.15 G). BDNF stimulation increased growth cone size as reported before (Meier et al., 2011). Furthermore, mitochondria got recruited to BDNF stimulated growth cones and on average 3.3 ± 0.4 mitochondria were located in the growth cone area (Figure 3.15 B, E, G). Ephrin-A5 stimulation on the other hand led to a reduction of the growth cone area and a removal of mitochondria from the growth cone as only 0.3 ± 0.09 mitochondria could be found on average in the growth cone area (Figure 3.15 C, F, G).

To exclude that the quantified increase of mitochondrial recruitment to growth cones (in case of BDNF stimulation) or the withdrawal of mitochondria from growth cones after ephrin-A5 stimulation is due to the size-rearrangements elucidated by the two guidance cues, mitochondrial number was normalized to the growth cone size. In doing so, the previous phenotype was confirmed. Whereas in control neurons 0.32 ± 0.04 mitochondria

could be found in 10 µm² growth cone area, this value was significantly increased after BDNF stimulation (0.57 ± 0.08 mitochondria / 10 µm² growth cone) or significantly decreased upon ephrin-A5 administration (0.15 ± 0.01 mitochondria / 10 µm² growth cone, Figure 3.15 H). In sum, attractive (BDNF) and repulsive (ephrin-A5) guidance cues attracted and displaced mitochondria from growth cones, respectively.

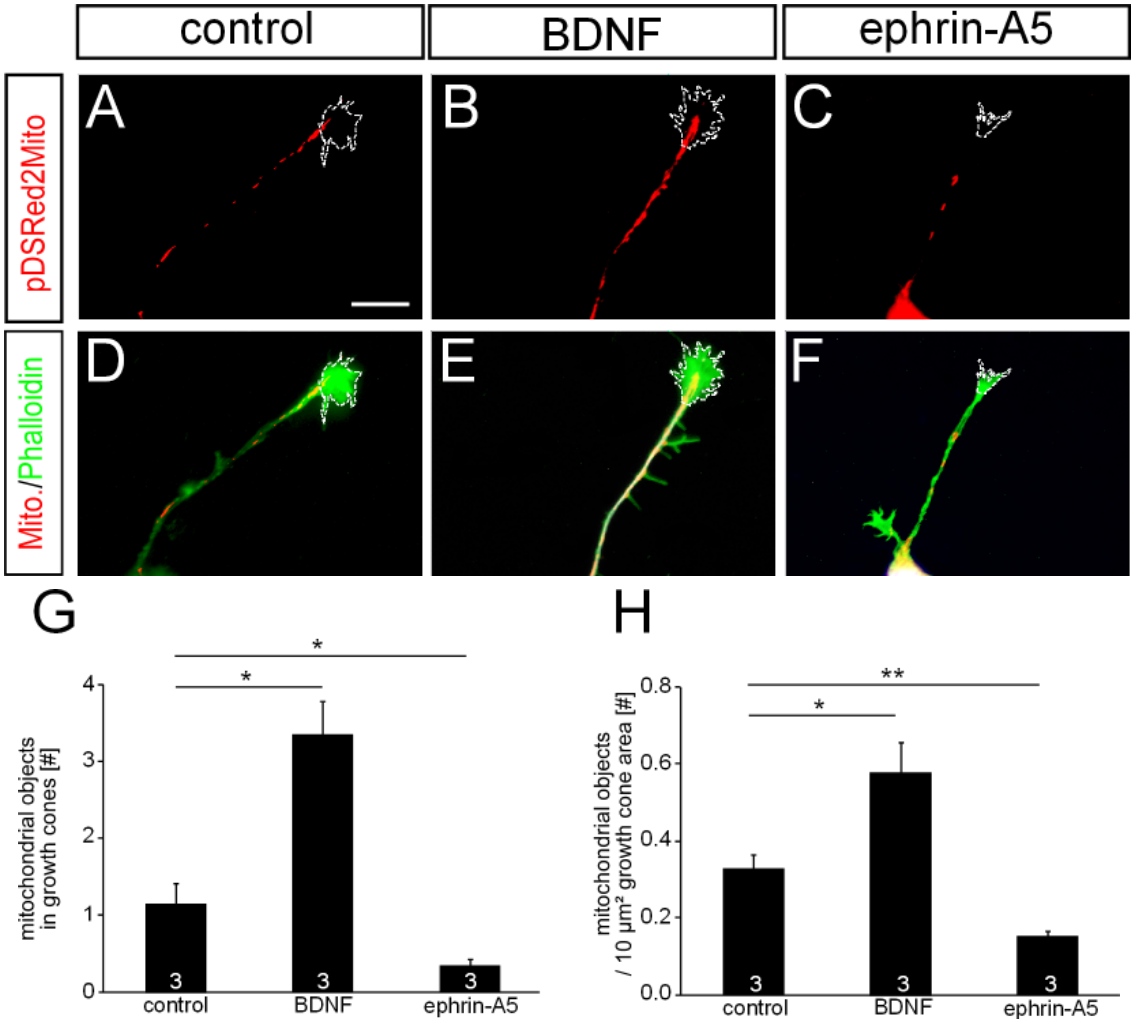

Figure 3.15 Stimulation of growth cones with BDNF or ephrin-A5 influences growth cone mitochondrial dynamics

(A, D) An unstimulated wild-type growth cone contained only few mitochondria. (B, E) BDNF stimulation led to growth cone enlargement and recruitment of mitochondria into the growth cone area. (C, F) Ephrin-A5 stimulation decreased growth cone size and led to withdrawal of mitochondria from the growth cone area. (G) BDNF significantly increased, whereas ephrin-A5 significantly decreased the number of mitochondria in growth cones. (H) Quantification of the number of mitochondrial objects normalized to growth cone area. Again, BDNF significantly increased and ephrin-A5 significantly decreased mitochondrial object number in growth cones. Scale bar (A-F) = 10 µm

To analyze more directly, whether actin treadmilling underlies these phenotypes, actin point mutant were used again. In line with previous data, Figure 3.16 B, C shows that increasing the F-actin pool by overexpressing actin G15S led to larger growth cones and a significant increase of mitochondrial localization in the growth cone (6.1 ± 1.3 mitochondria / growth cone in actin G15S overexpressing neurons compared to 1.1 ± 0.3 mitochondria / growth

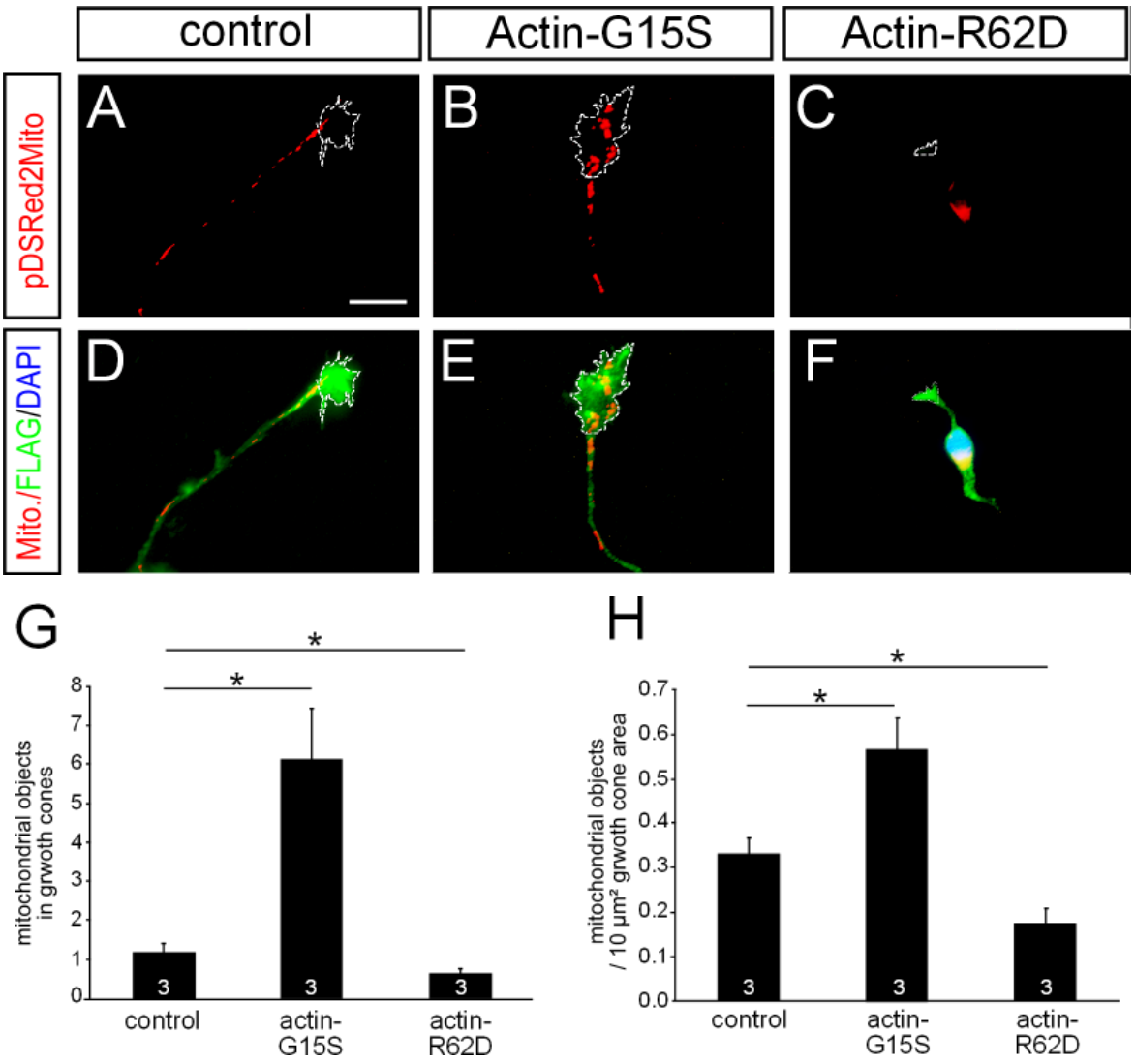

Figure 3.16 Actin mutants influence mitochondrial recruitment to growth cones

(A, D) A wild-type neuron showing recruitment of mitochondria to a growth cone. (B, E) Overexpression of actin G15S increased growth cone size and the number of mitochondria in the growth cone. (C, F) Actin R62D decreased mitochondrial occupancy in growth cones. (G) Number of mitochondria in growth cones was significantly increased upon actin G15S overexpression and significantly decreased upon actin R62D overexpression. (H) Normalization of mitochondrial number to growth cone size. Actin G15S increased, whereas actin R62D decreased mitochondrial occupancy in growth cones. Scale bars (A-F) = 10 µm.

cone in control neurons, Figure 3.16G). Contrastingly, actin R62D overexpression resulted in a significant removal of mitochondria from the growth cones (Figure 3.16 C, F, G). Thereby, only 0.6 ± 0.14 mitochondria were located in the growth cone.

To take into account that growth cone size was altered upon overexpression of the actin point mutants mitochondrial number in growth cones was normalized to the growth cone area. Again, actin G15S significantly increased mitochondrial occupancy in growth cones (from 0.32 ± 0.04 mitochondria / 10 µm² growth cone in wild-type neurons to 0.56 ± 0.07 mitochondria / 10 µm² growth cone, Figure 3.16 H). In line, actin R62D decreased mitochondrial occupancy to 0.17 ± 0.04 mitochondria / 10 µm² growth cone area (Figure 3.16 H).

Taken together, the performed experiments suggest that actin treadmilling is crucial to control mitochondrial dynamics. Enhancing F-actin polymerization (e.g. by overexpressing actin G15S) led to an increase in mitochondrial size and occupancy. Additionally, BDNF stimulation revealed that not only an artificial increase in the F-actin levels by overexpressing actin mutants but also a more physiological related F-actin regulation was sufficient to recruit mitochondria to F-actin dependent growth cones.

In contrast, increasing the G-actin pool did not only impair the overall neuronal morphology as described previously (Stern et al., 2009) but also decreased mitochondrial size and occupancy. Furthermore, decreasing the amount of F-actin by selective depolymerization in the growth cone upon ephrin-A5 stimulation revealed that F-actin seems to be necessary for subcellular mitochondrial localization.

This speaks in favor of a model, in which mitochondria are recruited to F-actin rich areas. Additionally, F-actin polymerization seems to be involved in controlling mitochondrial size. Nevertheless, F-actin polymerization alone cannot explain the observed increase in mitochondrial size and occupancy as actin S14C, another F-actin favoring actin mutant but capable of binding to cofilin, did not influence mitochondrial size. Interestingly, changes in cofilin activity are one hallmark of SRF ablation (Alberti et al., 2005). For this reason, the following experiments focus on cofilin's contribution to mitochondrial dynamics.

3.3 Cofilin Activity and its Influence on Mitochondrial Size and Distribution

As described in chapter 1.2.3 cofilin is a major regulator of the polymerization status of actin microfilaments. Cofilin itself is mainly regulated by phosphorylation at the serine residue 3, thereby phosphorylation leads to an inactivation of cofilin. Phospho-cofilin is incapable of F-actin binding, whereas unphosphorylated cofilin binds to F-actin and exerts its actin severing function leading to smaller actin fragments (Andrianantoandro and Pollard, 2006). Cofilin is phosphorylated by LIM kinase (LIMK) and is dephosphorylated upon slingshot phosphatase (Ssh) activity (Huang et al., 2006).

Interestingly, the phosphorylation status of cofilin is increased in case of SRF ablation as shown by immunoblotting of hippocampal and cortical tissue (Figure 3.3) in line with reports before (Alberti et al., 2005). Recent research revealed that SRF normally inhibits LIMK activity in neurons, thereby SRF ablation leads to hyperphosphorylated cofilin levels (Mokalled et al., 2010).

To investigate the role of cofilin in more detail with regard to mitochondrial dynamics, several point mutated cofilin mutants (Agnew et al., 1995; Garvalov et al., 2007) were used as well slingshot constructs allowing for dephosphorylation of cofilin (see Figure 3.17).

A non-phosphorylatable cofilin mutant (**cofilin-S3A**) was used to give rise to a putative constitutively active cofilin mutant. Due to lacking the critical serine residue, this cofilin-S3A is active and always exerts its F-actin severing function. As in *Srf* deficient neurons cofilin is hyperphosphorylated indicating permanent inactivation of cofilin, overexpression of cofilin-S3A should rescue the phenotype in an SRF-deficient background.

In contrast to that, a phopshomimetic **cofilin-S3E** mutant was used to recapitulate the hyperphosphorylated cofilin status of *Srf* mutant cells. In this mutant the serin residue is changed to a glutamate residue, thereby this cofilin mutant serves as a phosphomimetic cofilin protein. In principal, this cofilin-S3E mutant should induce an SRF-knockout phenotype if overexpressed in wild-type neurons.

Another way to restore normal cofilin function in *Srf* mutant neurons is performed by overexpressing active slingshot phosphatase (Ssh). In principal, this reduces phospho-cofilin levels that should reverse the neuronal and mitochondrial phenotype in case of SRF ablation. This implies that increased phospho-cofilin levels are the critical factor to induce the

phenotypes in *Srf* mutants. In this context, two different slingshot mutants were applied: An active full-length version (**SshL**) and an inactive control (**SshS**). Thus, overexpression of SshL should rescue *Srf* mutant neurons.

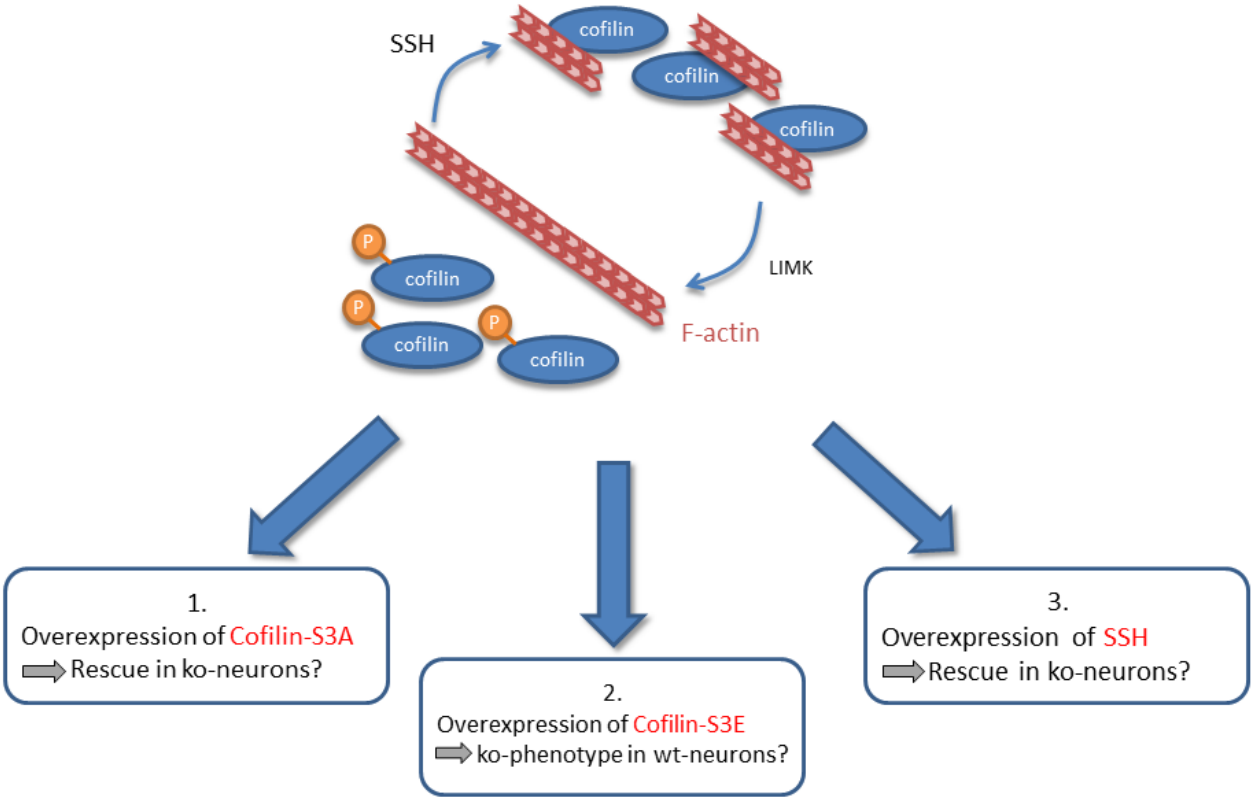

Figure 3.17 Scheme of the experimental approaches modulating cofilin activity in neurons

Under physiological conditions cofilin activity is regulated by phosphorylation. Whereas LIM kinase (LIMK) phosphorylates and deactivates cofilin, dephosphorylation by slingshot phosphatase (Ssh) reactivates cofilin that binds to F-actin and severs microfilaments. Different cofilin point mutants as well as slingshot phosphatase were used to investigate the role of cofilin with regard to mitochondrial dynamics. Details see text.

3.3.1 Phospho-cofilin levels are increased in SRF-deficient cells

Although it was shown that phospho-cofilin levels are increased in SRF-deficient tissue (Figure 3.3), it was additionally investigated if this holds true on single cell level, too. For this, an immunocytochemical staining for phospho-cofilin was performed (Figure 3.18).

As expected, phospho-cofilin levels were rather low in case of wild-type neurons expressing the inactive SRF-ΔMADS-VP16 construct (Figure 3.18 E). Mitochondrial dynamics with regard to size and occupancy seemed normal (Figure 3.18 A). Overexpression of the constitutively active SRF-VP16 construct led to increased mitochondrial size as observed in previous experiments (Figure 3.9) and further decreased phospho-cofilin levels (Figure 3.18 F).

In contrast, SRF-deficient neurons expressing SRF-ΔMADS-VP16 showed drastically increased phospho-cofilin levels (Figure 3.18 G) in addition to overall impaired neuronal morphology and mitochondrial size (Figure 3.18 C). Conversely, overexpression of SRF-VP16 was able to rescue neuronal morphology (as described before) and also reduced phospho-cofilin levels in the cell (Figure 3.18 H).

Quantification of phospho-cofilin intensities was performed by SlideBook-based analysis. In doing so, the sum of all cofilin-intensities in the cell was quantified (see Figure 3.18 Q). It turned out that phospho-cofilin levels compared to wild-type neurons (2.1 ± 0.1 A.U.) were significantly increased in *Srf* mutant neurons (10.7 ± 0.05 A.U.). In turn, overexpression of SRF-VP16 significantly decreased phsopho-cofilin intensities both in wild-type and *Srf* mutant neurons (0.6 ± 0.06 A.U. and 2.2 ± 0.5 A.U., respectively). To check whether the observed changes in phospho-cofilin intensities were based upon changes in cofilin expression, cofilin intensities were quantified as well. It turned out that cofilin levels were unchanged between wild-type and SRF-deficient cells and independent of SRF-VP16 or SRF-ΔMADS-VP16 expression (Figure 3.18 R).

Thereby, this experiment shows that even on a single cell level an increase of phospho-cofilin levels can be observed in SRF-deficient cells that is rescued to wild-type levels upon SRF-VP16 overexpression. In this context, mitochondrial size and occupancy seems to be correlated to phospho-cofilin levels, as higher phospho-cofilin intensities could be observed in cells with smaller mitochondria.

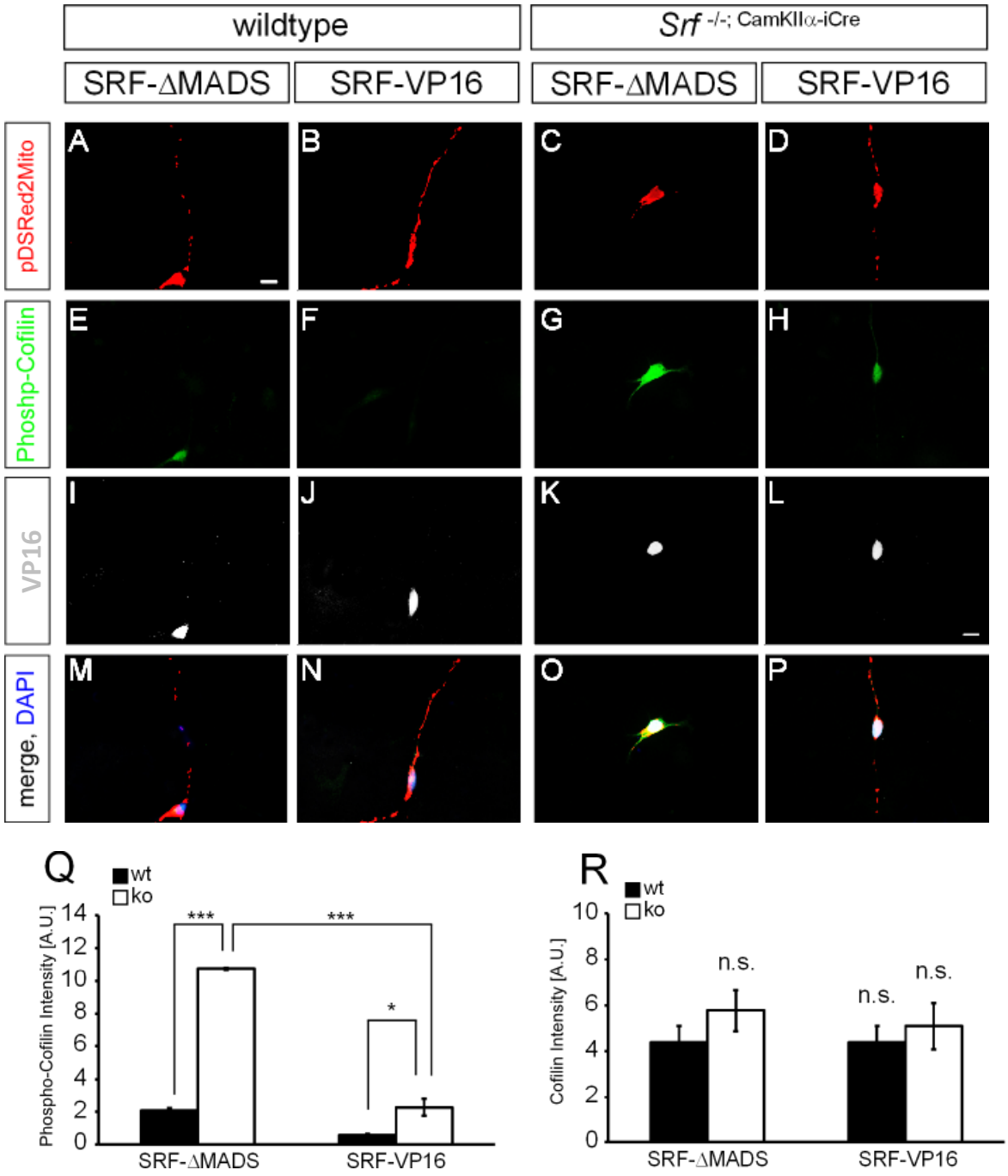

Figure 3.18 Phospho-cofilin status is changed on single cell level upon SRF deficiency

(A, E, I, M) Wild-type neurons expressing a non-functional SRF-ΔMADS-VP16 construct displayed normal mitochondria and low phospho-cofilin levels. (B, F, J, N) Overexpression of SRF-VP16 in wild-type neurons resulted in an increase of mitochondrial size and further decreased phospho-cofilin levels. (C, G, K, O) SRF-deficient neurons expressing the SRF-ΔMADS-VP16 construct showed mitochondrial fragmentation and increased cofilin levels. (D, H, L, P) Overexpression of SRF-VP16 in *Srf* mutant neurons rescued mitochondrial size, neuronal morphology and restored phospho-cofilin levels. (Q) Quantification revealed that phospho-cofilin was significantly increased in *Srf* mutant neurons. This was rescued by overexpression of SRF-VP16 that significantly decreased phospho-cofilin levels in wild-type and SRF deficient background. (R) Quantification of cofilin levels. No change was observed in any condition. Scale bar (A-P) = 10 µm.

3.3.2 Non-phosphorylatable cofilin-S3A rescues mitochondrial size and occupancy in *Srf* mutant neurons

To narrow down whether the mitochondrial defects in *Srf* mutant cells are really based upon cofilin activity, different cofilin mutants were used. First of all, a non-phosphorylatable, thereby permanently active cofilin-S3A GFP-tagged mutant was overexpressed in wild-type as well as SRF-deficient neurons (Figure 3.19). In a control experiment wild-type as well as SRF-deficient neurons overexpressed GFP alone.

GFP-expressing wild-type neurons displayed a normal neuronal morphology and mitochondria at an average size of 3 µm² ± 0.3 µm² (Figure 3.19 A, E, I) and an occupancy of 41.3 % ± 4.4 % (Figure 3.19 J). In contrast, *Srf* mutant neurons displayed their typical

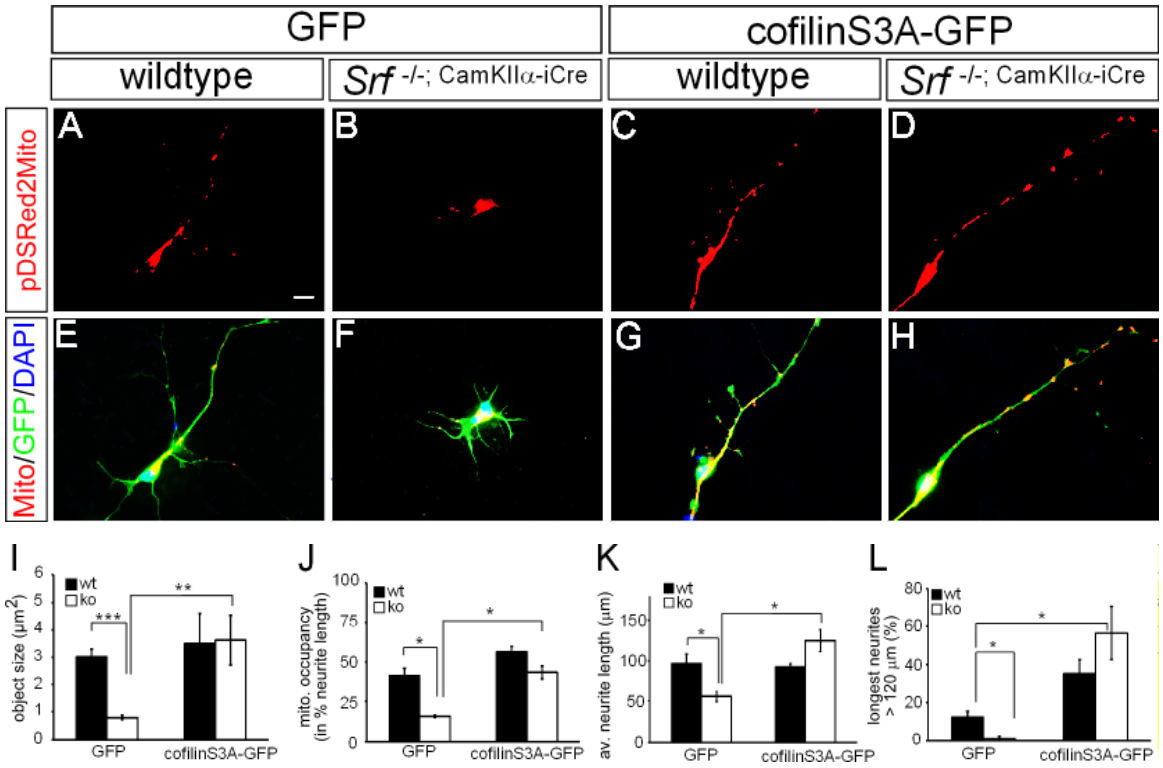

Figure 3.19 Effect of cofilin-S3A on mitochondrial dynamics and neuronal morphology

(A, E) Wild-type neurons expressing GFP showed a normal neuronal morphology and normal mitochondria. (B, F) SRF ablation led to neurite shortening, mitochondrial fragmentation and cell-body restriction of mitochondrial distribution. (C, G) Cofilin-S3A did not have a drastic effect on mitochondrial size in wild-type cells. (D, H) Overexpression of cofilin-S3A rescued neurite length, mitochondrial size and occupancy in SRF-deficient neurons. (I) Mitochondrial size was significantly decreased upon SRF ablation and could be rescued by cofilin-S3A. (J) SRF deficiency led to a significant decrease of mitochondrial occupancy that got rescued upon cofilin-S3A overexpression. (K) Rescue of neurite length upon cofilin-S3A overexpression. (L) Cofilin-S3A also increased the presence of long neurites (longer than 120 µm) compared to wild-type GFP-expressing neurons. Scale bar (A-H) = 10 µm.

impaired morphology (Figure 3.19 B, F), mitochondrial fragmentation (0.8 µm² ± 0.09 µm², Figure 3.19 I) and decreased mitochondrial occupancy (15.7 % ± 0.7 %, Figure 3.19 J).

Interestingly, overexpression of cofilin-S3A was sufficient to rescue the neuronal morphology in *Srf* mutant neurons as well as mitochondrial parameters (Figure 3.19 D, H). Thereby, mitochondrial size increased to 3.6 µm² ± 0.9 µm² (Figure 3.19 I) and occupancy was at 43.2 % ± 4 % (Figure 3.19 J). Of note, in spite of a slight increase in the quantified mitochondrial parameters, cofilin-S3A in wild-type neurons (see Figure 3.19 C, G) had neither a significant effect on mitochondrial size (3.5 µm² ± 1.1 µm²) nor on occupancy (56.6 % ± 3.3 %).

Furthermore, the potential of cofilin-S3A to rescue neurite length was examined. Whereas wild-type neurons had an average length of 96.7 µm ± 11.2 µm, SRF deficiency resulted in significantly shorter neurites (average length of 55.4 µm ± 6.3 µm, see Figure 3.19 K). Obviously, overexpression of cofilin-S3A did not impact neurite length in wild-type neurons (92.2 µm ± 4.4 µm). However, cofilin-S3A was able to rescue neurite length in an SRF-deficient background and increased neurite length to 125 µm ± 13.5 µm. As reported before (Garvalov et al., 2007), cofilinS3A had an effect on the amount of very long neurites that was increased in wild-type neurons expressing cofilin-S3A. For this reason, the relative amount of longest neurites (i.e. neurites longer than 120 µm) was quantified. As expected, this value decreased from 12.2 % ± 2.9 % in wild-type neurons to 1.1 % ± 0.7 % in *Srf* mutant neurons (Figure 3.19 L). Interestingly, cofilin-S3A significantly increased the relative amount of neurites longer than 120 µm in a wild-type as well as SRF-deficient background (35.3 % ± 7.4 % and 56.6 % ± 13.8 %, respectively, see Figure 3.19 L).

In sum, this experiment shows that non-phosphorylatable cofilin-S3A is able to overcome the morphological and mitochondrial phenotype of SRF-deficient neurons. On this account, it is likely, that the phenotype of *Srf* mutant neurons depends on the decrease of active cofilin upon hyperphosphorylation of this actin severing protein. Consequently, increasing the amount of active cofilin alleviates the phenotpyes of SRF-deficient neurons.

3.3.3 Cofilin-S3E decreases mitochondrial size and occupancy and circumvents SRF-VP16 mediated effects on mitochondria

As constitutively active cofilin-S3A was able to rescue mitochondrial size and occupancy in *Srf* mutant neurons, it is likely that a permanently inactive cofilin mutant recapitulates the phenotype of SRF-deficient neurons in a wild-type background. For this, a phosphomimetic cofilin-S3E mutant was overexpressed that behaved like phosphorylated cofilin and is thereby permanently inactive.

As a control, GFP was co-expressed with SRF-ΔMADS-VP16 (Figure 3.20 A, E, I, M). In these cells mitochondria were of normal size (2.2 µm² ± 0.2 µm², Figure 3.20 Q) and displayed normal occupancy (39.6% ± 1.8 %, Figure 3.20 R). As expected, SRF-VP16 induced formation of large mitochondria in GFP expressing wild-type neurons (Figure 3.20 B) that led to a significant increase in mitochondrial size to 4.3 µm² ± 0.3 µm² (Figure 3.20 Q) and an occupancy of 58.5 % ± 2.2 % (Figure 3.20 R).

Interestingly, overexpression of cofilin-S3E in control neurons co-expressing SRF-ΔMADS-VP16 impaired mitochondrial parameters without influencing the overall neuronal morphology (Figure 3.20 C, G, K, O). Still, neurons showed long neurites, whereas mitochondrial size was significantly decreased to 1.2 µm² ± 0.1 µm² (Figure 3.20 Q) as well as occupancy (25.2 % ± 1 %, Figure 3.20 R).

More important, cofilin-S3E was also able to abrogate the effect of SRF-VP16 on mitochondrial parameters (Figure 3.20 D, H, L, P). Neurons co-expressing constitutively active SRF-VP16 and constitutively inactive cofilin-S3E failed to form large mitochondria (mitochondrial size at 1.3 µm² ± 0.2 µm²) and mitochondrial occupancy was significantly decreased in comparison to SRF-ΔMADS-VP16 and GFP co-expressing neurons (occupancy of 26.2 % ± 2.4 %, Figure 3.20 R).

Thus, this experiment has two major implications: First, constitutively inactive cofilin-S3E is not able to induce a neuronal morphology reminiscent of SRF-deficient neurons. It impacts only mitochondrial parameters such as size and occupancy. Second, cofilin-S3E is able to circumvent SRF-VP16's ability to induce large mitochondria. Thus, it is likely that the SRF-VP16 function relies on a functional regulation of cofilin activity. This speaks in favor of a model in which SRF-mediated control of mitochondrial size is dependent on functional cofilin activity and subsequent proper regulation of actin treadmilling.

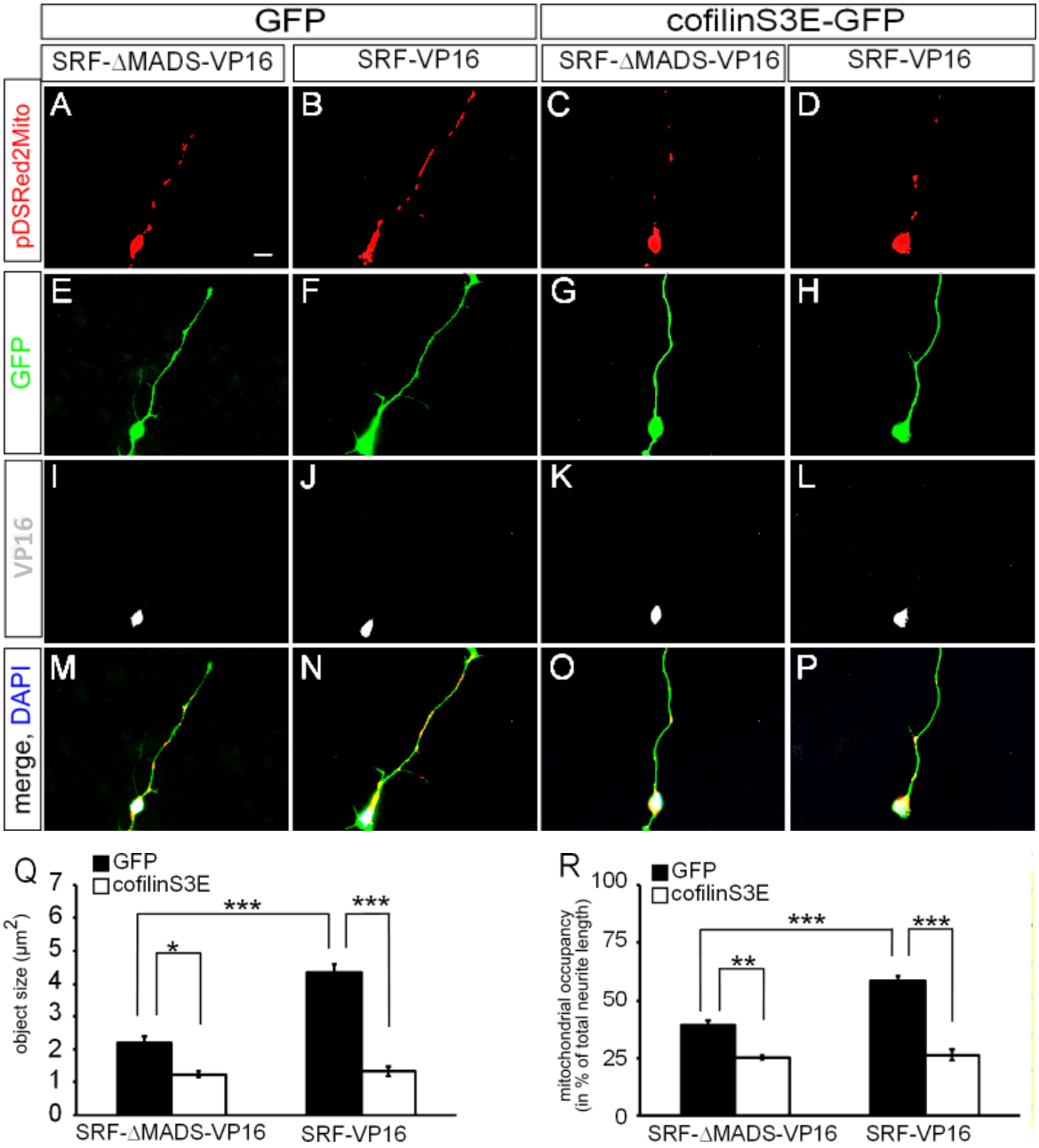

Figure 3.20 Cofilin-S3E decreases mitochondrial size and circumvents the SRF-VP16 effect

(A, E, I, M) Wild-type neurons co-expressing GFP and SRF-ΔMADS-VP16 displayed a normal phenotype. (B, F, J, N) Overexpression of SRF-VP16 and GFP led to an increase in mitochondrial size and occupancy. (C, G, K, O) Co-expression of SRF-ΔMADS-VP16 and cofilin-S3E led to mitochondrial fragmentation without impairing neurite length. (D, H, L, P) Cofilin-S3E was able to abrogate the SRF-VP16 mediated effect on mitochondria. (Q) Quantification of mitochondrial size. In SRF-ΔMADS-VP16-expressing neurons cofilin-S3E significantly decreased mitochondrial size. Whereas SRF-VP16 overexpression in GFP-expressing cells significantly increased mitochondrial size, this effect was abolished upon co-expression with cofilin-S3E. (R) Mitochondrial occupancy was significantly decreased in control neurons upon cofilin-S3E expression. The SRF-VP16 mediated increase of mitochondrial occupancy was abrogated by cofilin-S3E expression. Scale bar (A-P) = 10 µm.

3.3.4 Active Slingshot phosphatase restores phospho-cofilin levels and mitochondrial shape in *Srf* mutant neurons

Whereas the previous experiments rely on non-functional or constitutively active cofilin mutants, respectively, another way to interfere with cofilin phosphorylation is via overexpression of slingshot phosphatase. This enzyme catalyzes specifically the dephosphorylation and subsequent activation of cofilin (see chapter 1.2.3). Two different slingshot constructs were used in this approach: a full-length and thereby active version slingshot L (SshL) and a short, consequently inactive mutant slingshot S (SshS).

Wild-type neurons expressing inactive SshS displayed normal neuronal morphology (Figure 3.21 A, E, I) and relatively low levels of phospho-cofilin (Figure 3.21 E). In SRF-deficient neurons expressing SshS (Figure 3.21 B, F, J) phospho-cofilin levels were increased and neuronal morphology impaired as observed previously. In detail, mitochondrial size decreased significantly from 2.8 µm² ± 0.1 µm² in wild-type neurons to 0.78 µm² ± 0.06 µm² in SRF-deficient neurons (Figure 3.21 M). As well, mitochondrial occupancy dropped significantly from 47 % ± 3.3 % in wild-type neurons to 12.8 % ± 0.5 % in *Srf* mutant neurons (Figure 3.21 N). Furthermore, in wild-type neurons neurites were of an average length of 81.4 µm ± 2.4 µm and neurite length was significantly decreased to 47.9 µm ± 6.8 µm in *Srf* mutant neurons (Figure 3.21 O). This correlated with a significant increase in summarized phospho-cofilin levels from 1.8 ± 0.7 A.U. in wild-type neurons to 5.9 ± 2.1 A.U. in *Srf* mutant neurons (Figure 3.21 P). However, total cofilin levels were unchanged (4.4 ± 0.7 A.U. vs. 3.7 ± 0.06 A.U.).

Interestingly, overexpression of active SshL had only mild, thereby not significant effects on neuronal and mitochondrial morphology (Figure 3.21 C, G, K). Although mitochondrial size (4.2 µm² ± 0.5 µm², Figure 3.21 M) as well as mitochondrial occupancy (58.6 % ± 4.3 %, Figure 3.21 N) was increased, none of these parameters was significantly altered. This was also true for neurite length (87.5 µm ± 3 µm, Figure 3.21 O) and phospho-cofilin intensity (0.56 ± 0.23 A.U., Figure 3.21 P). Nevertheless, SshL was able to rescue mitochondria and neurite length in an SRF-deficient background. These neurons displayed a normal morphology as well as normally shaped and distributed mitochondria (Figure 3.21 D, H, L). Mitochondrial size was restored up to wild-type levels (2.6 µm² ± 0.4 µm², Figure 3.21 M) as was occupancy (41 % ± 2.3 %, Figure 3.21 N).

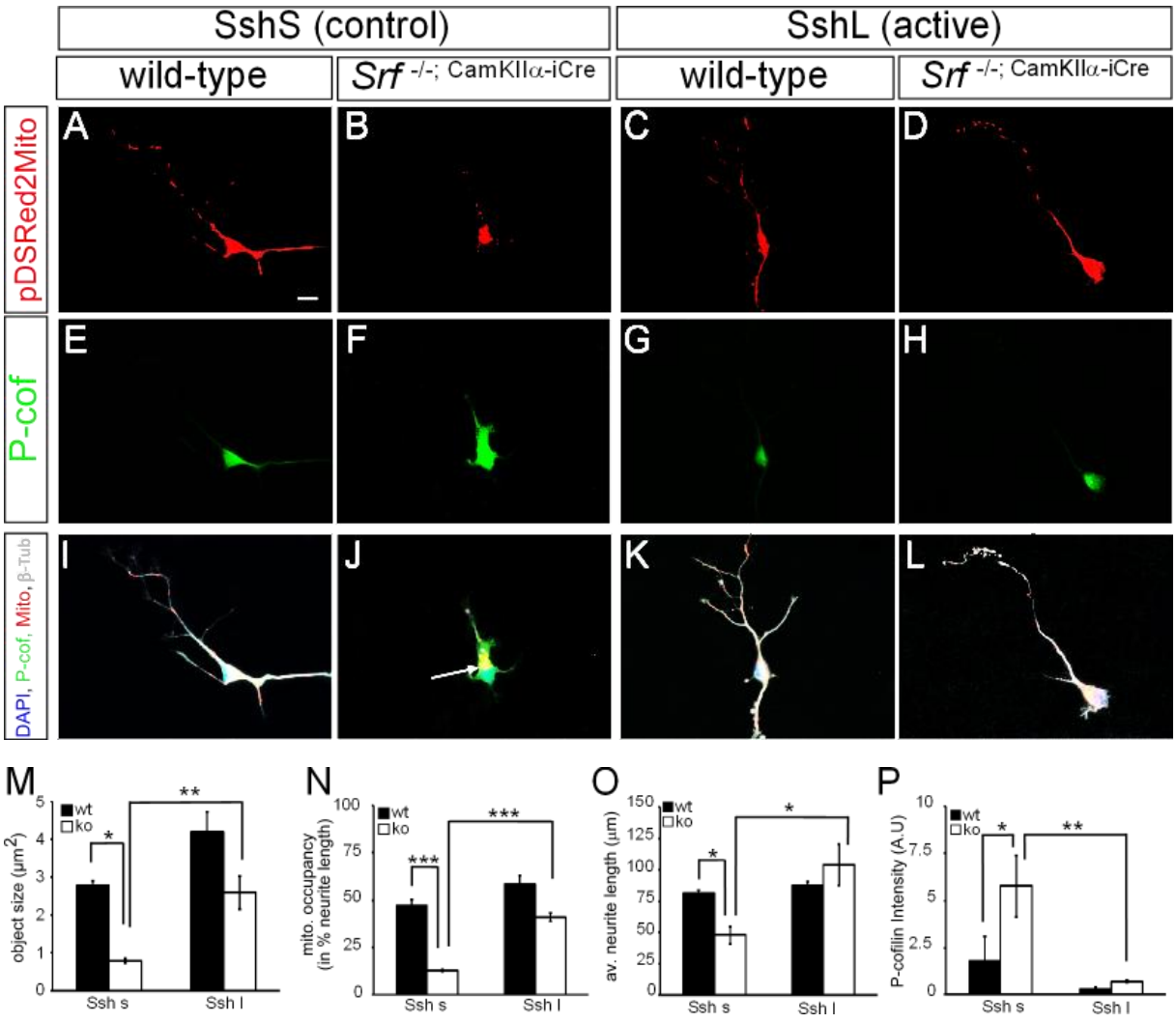

Figure 3.21 Overexpression of active slingshot SshL rescues mitochondria and neuronal morphology in SRF-deficient neurons

(A, E, I) Wild-type neurons expressing an inactive control slingshot (SshS) displayed normal neuronal morphology and mitochondrial size. (B, F, J) *Srf* mutant neurons expressing SshS showed increased phospho-cofilin levels, impaired morphology and mitochondrial fragmentation as well as perinuclear clustering. (C, G, K) Expression of active slingshot SshL in wild-type neurons decreased phospho-cofilin levels but did not obviously alter neuronal and mitochondrial morphology. (D, H, L) SshL overexpression was sufficient to rescue mitochondria and neuronal morphology in an SRF-deficient background. (M) Mitochondrial size was significantly decreased upon SRF ablation but got rescued by expression of SshL. Expression of SshL in wild-type neurons increased mitochondrial size but not significantly. (N) Mitochondrial occupancy decreased in *Srf* mutant neurons and got rescued upon SshL expression. (O) SRF-deficient neurons displayed significantly shorter neurites, which were rescued by SshL. In wild-type neurons SshL had no effect on neurite length. (P) Phospho-cofilin levels were significantly increased in SRF-deficient neurons. SshL expression decreased phospho-cofilin levels both in wild-type and *Srf* mutant neurons. Scale bar (A-L) = 10 µm.

Furthermore, neurite length was increased and even exceeded the wild-type level (104 µm ± 16.3 µm, Figure 3.21 O). Again, this correlated with a significant reduction of phospho-cofilin levels (1.4 ± 0.16 A.U., Figure 3.21 P). Cofilin levels were unchanged (3.7 ± 0.06 A.U. in wild-type neurons expressing SshL and 3.5 ± 0.3 A.U. in SRF-deficient neurons expressing SshL).

As decreasing phospho-cofilin levels is sufficient to overcome mitochondrial fragmentation as well as impaired neurite outgrowth in SRF-deficient neurons, this experiment shows that the morphological and mitochondrial phenotype induced by SRF ablation is likely to be based upon mis-regulated cofilin activity. Although it has been shown before that hyperphosphorylation is a hallmark of SRF deficiency (Alberti et al., 2005) which relies on mis-regulation of LIMK (Mokalled et al., 2010), this is the first proof of principle experiment showing a direct rescue of SRF-deficiency upon decreasing phospho-cofilin levels by slingshot phosphatase. This draws to the conclusion that SRF exerts its impact on morphological and mitochondrial dynamics in neurons via regulation of cofilin. This is supported by the fact that overexpression of SRF-VP16 led to a decrease of phospho-cofilin levels and rescued the neuronal phenotype (Figure 3.18). Additionally, constitutively active cofilin-S3A rescued the neuronal phenotype, whereas non-functional cofilin-S3E prevented SRF-VP16 from its impact on mitochondria.

All of these findings strongly suggest that the SRF-cofilin-actin axis is crucial for controlling mitochondrial function. However the direct link between cofilin regulation of actin treadmilling and its connection to mitochondrial dynamics is not addressed by these experiments.

3.4 Neuroprotective Implications of SRF's Function on Mitochondria

Many neurodegenerative diseases rely on dysfunctional mitochondria as neurons are completely dependent on mitochondrial ATP production (see chapter 1.3). One of these diseases that have a direct impact on mitochondria is Huntington's disease. Interestingly, the cause of this disease is well understood: Abnormal N-terminal expansions of glutamate in the huntingtin protein cause pathological aggregations of this protein, thereby interfering with multiple cellular functions, e.g. mitochondrial trafficking (Bossy-Wetzel et al., 2008). Furthermore, it is believed that poly-glutamatergic huntingtin exerts its major pathological function by interfering with gene transcription in the nucleus.

The neurodegenerative function of huntingtin as well as its impact on mitochondria has been studied in detail. Of note, Orr et al. have reported that overexpression of an aggregation-competent huntingtin protein causes mitochondrial fragmentation and decreases neurite occupancy, which is reminiscent of the observed phenotypes in SRF-deficient neurons (compare Figure 3.22 taken from Orr et al., 2008 with Figure 3.5).

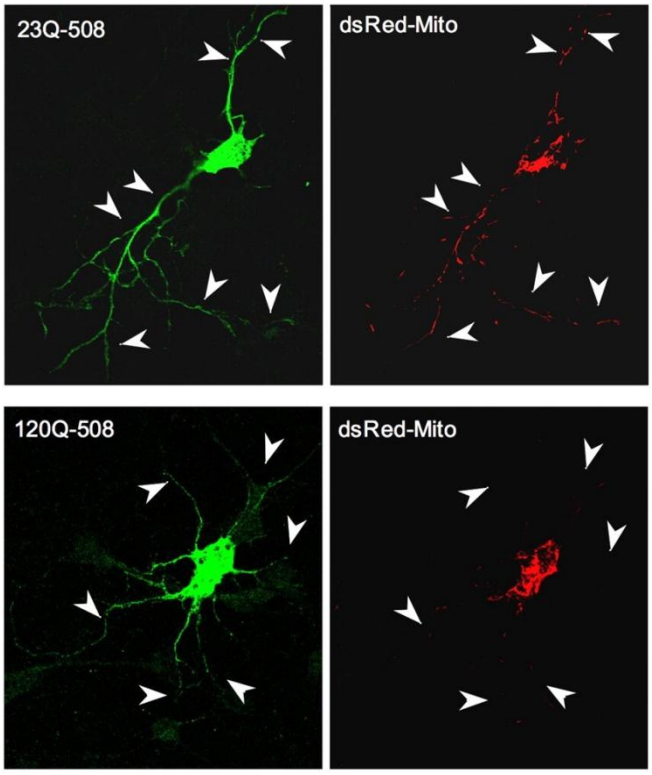

Figure 3.22 Mutant huntingtin decreases mitochondrial distribution in neurons

Normal huntingtin (23Q-508, labeled in green) has no effect on dsRed-Mito labeled mitochondria, whereas aggregation competent 120Q-508 huntingtin (green) decreases mitochondrial distribution and leads to perinuclear clustering of mitochondria as observed in *Srf* mutant neurons (Orr et al., 2008)

For this reason, it was investigated whether the observed mitochondrial phenotypes induced by overexpression of mutant huntingtin could be rescued upon overexpression of SRF-VP16. As reported in chapters 3.1.2.4 and 3.1.2.5, SRF-VP16 increased mitochondrial size, occupancy and trafficking and rescued mitochondria in an SRF mutant background. Hence, one could assume that SRF-VP16 also alleviates impaired mitochondrial function in this neurodegeneration associated *in vitro* model.

3.4.1 Constitutively active SRF-VP16 alleviates mutant huntingtin effects on mitochondria *in vitro*

To check a possible neuroprotective function of SRF-VP16 in case of mutant huntingtin overexpression two huntingtin constructs were applied. A GFP-tagged huntingtin construct of 23 glutamate residues (GFP-HTT23) resembled normal huntingtin without aggregation competence. On the other hand, a GFP-tagged mutant huntingtin with 130 glutamate residues (GFP-HTT130) induced formation of huntingtin aggregates and was shown to impair mitochondrial dynamics *in vitro* (Orr et al., 2008).

In a control experiment wild-type neurons overexpressed aggregation incompetent GFP-HTT23 together with the transcriptionally inactive SRF-ΔMADS-VP16 construct. These neurons displayed normally sized mitochondria and occupancy (Figure 3.23 A, E). Thus, GFP-HTT23 had no effect on mitochondria *in vitro* as their size was of 2.8 µm² ± 0.3 µm² (Figure 3.23 I) and occupancy was of 46.9 % ± 1.4 % (Figure 3.23 J). In presence of GFP-HTT23 SRF-VP16 could exert its impact on mitochondria (Figure 3.23 B, F) and significantly increased mitochondrial size to 7.3 µm² ± 1.5 µm² (Figure 3.23 I) and occupancy to 73.2 % ± 2.3 % (Figure 3.23 J).

On the other hand, overexpression of aggregation competent GFP-HTT130 in SRF-ΔMADS-VP16 control neurons impaired mitochondrial size and distribution (Figure 3.23 C, G). Thereby, mitochondrial size was significantly decreased to 1.6 µm² ± 0.06 µm² (Figure 3.23 I) and occupancy significantly dropped to 17.7 % ± 0.6 % (Figure 3.23 J). Interestingly, SRF-VP16 could positively affect mitochondrial size and occupancy even in the background of GFP-HTT130 presence (Figure 3.23 D, H). Mitochondrial size was not only rescued to normal levels (which is approximately 3 µm²) but further increased to 6 µm² ± 0.6 µm² (Figure 3.23 I), which was significant compared to control neurons, too. Additionally, mitochondrial

occupancy was also rescued to 57 % ± 3.6 % (Figure 3.23 J), thereby significantly increased compared to neurons expressing GFP-HTT130 as well as control neurons expressing GFP-HTT23.

To check whether this SRF-VP16 effect was specific for SRF mediated transcriptional activity

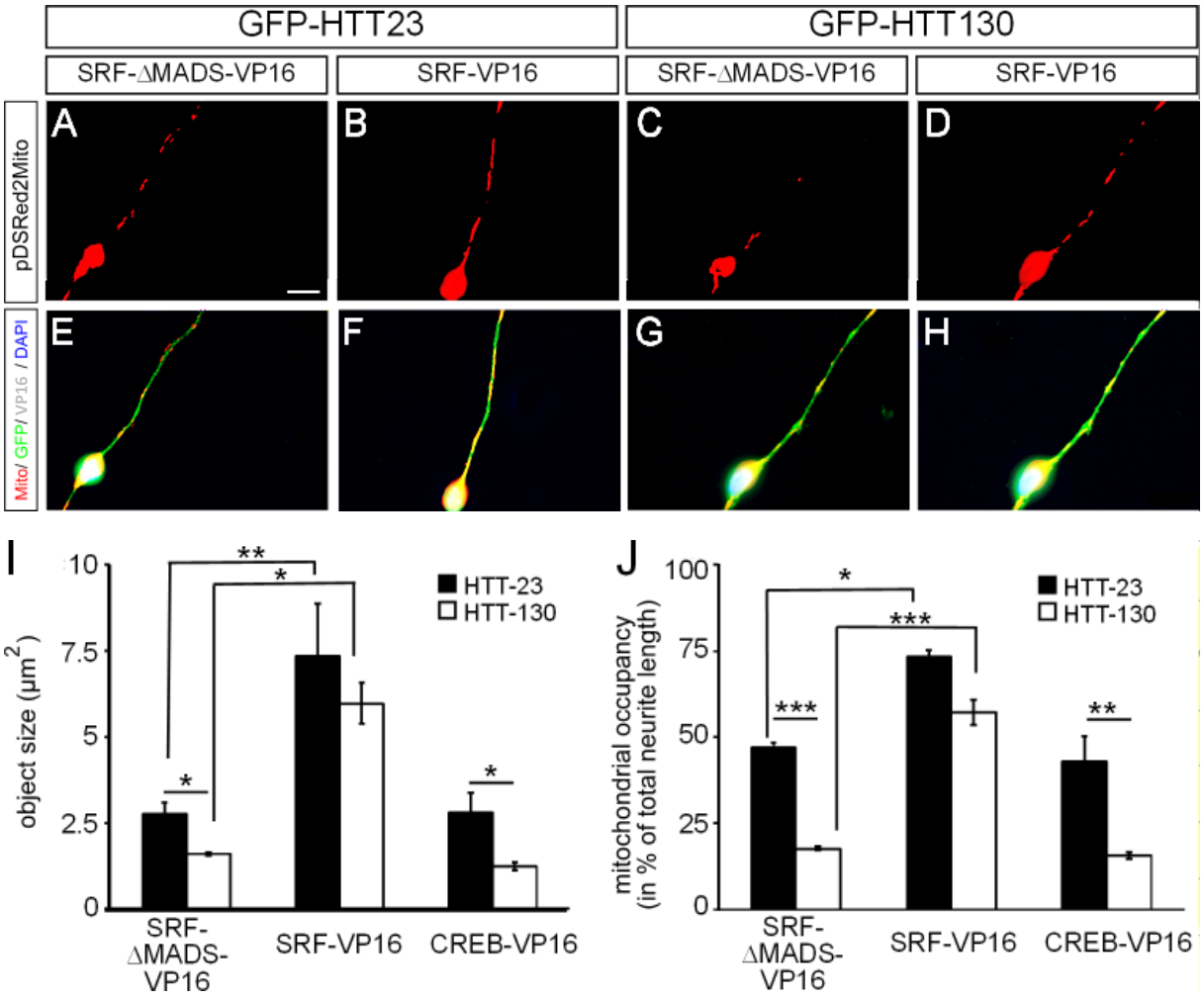

Figure 3.23 Overexpression of SRF-VP16 alleviates mutant huntingtin effects on mitochondria

(A, E) Aggregation incompetent GFP-HTT23 had no effect on mitochondria in wild-type neurons expressing SRF-ΔMADS-VP16. (B, F) SRF-VP16 overexpression in presence of GFP-HTT23 induced mitochondrial enlargement. (C, G) In presence of the control construct SRF-ΔMADS-VP16 aggregation-competent GFP-HTT130 decreased mitochondrial size and occupancy without disturbing the overall neuronal morphology. (D, H) SRF-VP16 restored mitochondrial size and occupancy in presence of GFP-HTT130. (I) Overexpression of GFP-HTT130 significantly decreased mitochondrial size in SRF-ΔMADS-VP16 expressing cells. SRF-VP16 significantly increased mitochondrial size in GFP-HTT23 and GFP-HTT130 expressing cells. Overexpression of CREB-VP16 could not rescue mitochondrial fragmentation upon GFP-HTT130 overexpression. (J) Mitochondrial occupancy significantly decreased upon GFP-HTT130 overexpression in SRF-ΔMADS-VP16 control neurons. SRF-VP16 significantly increased occupancy either in presence of GFP-HTT23 and GFP-HTT130. CREB-VP16 overexpression failed to overcome the GFP-HTT130 effect. Scale bar (A-H) = 10 µm.

or just due to a general transcriptional effect of VP16, the same experiment was performed with CREB-VP16. However, CREB-VP16 overexpression failed to rescue mitochondrial size in GFP-HTT130 expressing neurons (size decreased from 2.8 µm² ± 0.6 µm² in GFP-HTT23 expressing neurons to 1.3 µm² ± 0.01 µm² in GFP-HTT130 expressing neurons, Figure 3.23 I). Additionally, mitochondrial occupancy could not be rescued upon CREB-VP16 overexpression (occupancy decreased from 43 % ± 7.2 % in control neurons to 15.5 % ± 0.9 % in GFP-HTT130 expressing neurons, Figure 3.23 J).

Mutant huntingtin does not only impair mitochondrial size and distribution *in vitro* but also influences mitochondrial trafficking as reported before (Orr et al., 2008). Indeed, mis-regulation of mitochondrial transport is believed to be one of the main reasons by which huntingtin exerts its neuropathological function (Gauthier et al., 2004; Chang et al., 2006). Therefore, it was investigated whether SRF-VP16 could also rescue GFP-HTT130 mediated impaired mitochondrial trafficking. Again, time-lapse videomicroscopy was performed to analyze mitochondrial trafficking in living neurons. Trafficking behavior is visualized by kymographs in Figure 3.24. Whereas SRF-ΔMADS-VP16 overexpressing control neurons showed massive impairment of mitochondrial movement upon GFP-HTT130 expression (Figure 3.24 A), mitochondrial trafficking was rescued upon SRF-VP16 overexpression (Figure 3.24 B). Thereby, mitochondrial velocity was significantly increased from 0.33 µm/s ± 0.01 µm/s to 0.68 µm/s ± 0.05 µm/s (Figure 3.24 C). This shows that also

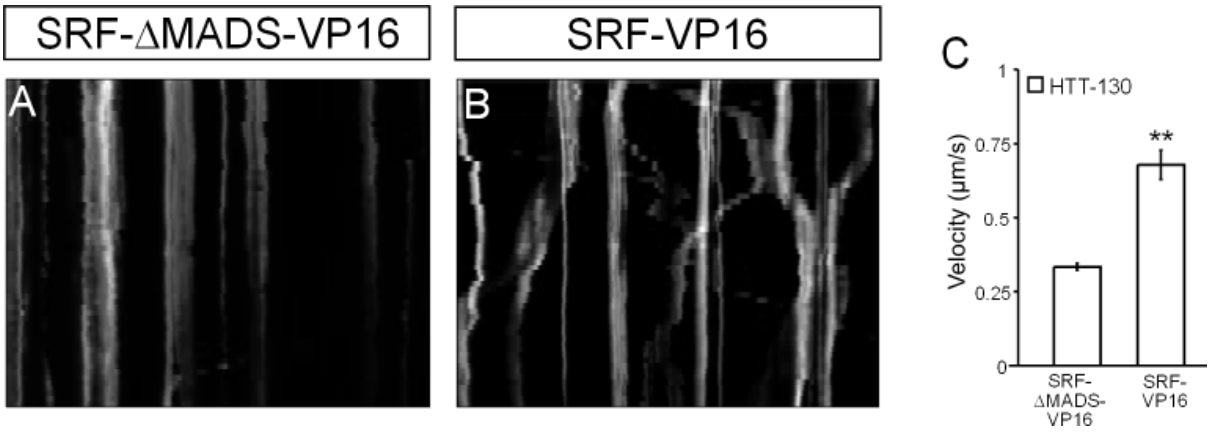

Figure 3.24 SRF-VP16 restores mitochondrial movement in GFP-HTT130 expressing neurons

(A) Kymograph displaying mitochondrial movement in control neurons expressing GFP-HTT130. Vertical lines of mitochondrial objects indicate massive impairment of mitochondrial movement. (B) SRF-VP16 rescued mitochondrial movement in GFP-HTT130 expressing neurons. (C) Mitochondrial velocity was significantly increased in GFP-HTT130 expressing neurons upon SRF-VP16 overexpression.

impaired mitochondrial trafficking (that might account for abnormal mitochondrial distribution and occupancy, see Figure 3.23 J) could be restored by SRF-VP16. Thus, it is shown for the first time that SRF has a neuroprotective effect in an *in vitro* model connected with a neurodegenerative disease (in this case Huntington's).

3.4.2 SRF expression is impaired in an *in vivo* Huntington model

As constitutively active SRF alleviates mutant huntingtin function *in vitro*, one possibility mutant huntingtin exerts its pathological function might be downregulating SRF. It has been reported before that huntingtin modulates gene expression in the nucleus (Bossy-Wetzel et al., 2008), thus, mis-regulating SRF could be one possibility how mutant huntingtin impairs mitochondrial dynamics. To address this question a Huntington's disease mouse model was investigated. These R6/2 mice are transgenic for first exon of the human huntingtin gene showing $(CAG)_{115}$-$(CAG)_{150}$ expansions (Mangiarini et al., 1996). This abnormal glutamate expanded huntingtin transgene is expressed ubiquitously; therefore, R6/2 mice exhibit abnormal neurological functions that are related to huntingtin accumulations. To check for down-regulation of SRF in these mice immunohistochemical staining of the hippocampus was performed as well as hippocampal protein lysates checked by immunoblotting (Figure 3.25).

These experiments showed that along with formation of huntingtin aggregates (positive ubiquitin signal, compare Figure 3.25 C and D) the SRF signal was reduced in the hippocampal CA1 region (Figure 3.25 E and F). In line, the amount of SRF was reduced in hippocampal protein lysates from huntingtin transgenic animals shown by immunoblotting (Figure 3.25 I). Interestingly, other transcription factors (as RelA, c-Jun or MRTF-A) were unchanged in huntingtin-transgenic animals.

This speaks in favor of a model in which mutant huntingtin reduces SRF expression. Consequently, this would lead to mitochondrial impairments as investigated in chapters 3.1.1 and 3.1.2.1. In line, overexpression of constitutively active SRF-VP16 *in vitro* was able to rescue these effects as it circumvented SRF down-regulation upon mutant huntingtin expression. Thus, for the first time a direct involvement of the transcription factor SRF in a neuropathological context is shown.

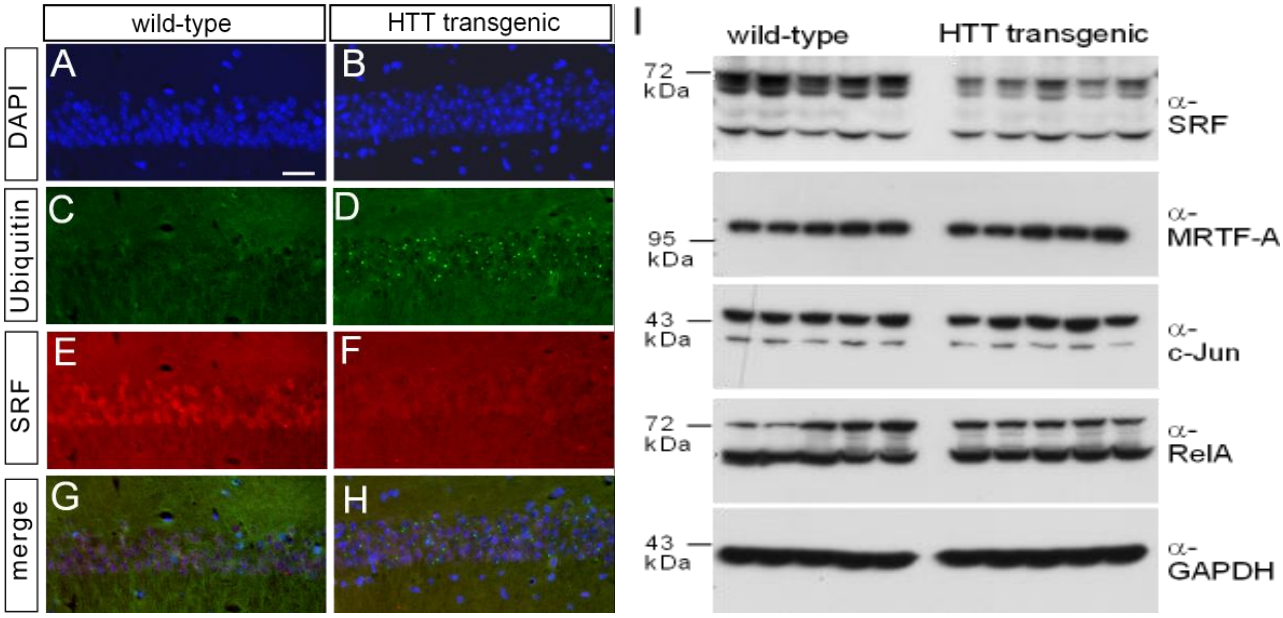

Figure 3.25 SRF-expression is down-regulated in a Huntington mouse model

(A, C, E, G) In wild-type hippocampal sections SRF is expressed the CA1 region, whereas no ubiquitin staining indicates absence of huntingtin aggregates. (B, D, F, H) In huntingtin-transgenic mice ubiquitin staining revealed presence of huntingtin aggregates and SRF signal was reduced. (I) Immunoblotting of hippocampal protein lysates showed that SRF expression was reduced in huntingtin-transgenic animals, whereas the expression of other transcription factors was unchanged. Scale bar (A-H) = 20 µm.

3.4.3 SRF-VP16 protects mitochondria against depolarizing agents

Overexpression of mutant huntingtin serves as an *in vitro* model of Huntington's disease. As SRF-VP16 seems to have a neuroprotective function in this context, it was further investigated if SRF-VP16 could exert its beneficial impact on mitochondria in a more artificial context. For this, the toxic agent FCCP was applied on wild-type neurons and mitochondrial response observed. FCCP uncouples the respiratory chain, thereby leading to a decrease in membrane potential. It was shown *in vitro* that application of FCCP induces mitochondrial fragmentation (Cereghetti et al., 2010), therefore it was investigated whether this effect could be prevented by SRF-VP16 as well.

Figure 3.26 shows the performed experiment. In line with previous experiments, non-stimulated neurons (Figure 3.26 A, E, I) responded to SRF-VP16 overexpression (shown in Figure 3.26 B, F, J) with mitochondrial enlargement (from 1.4 µm² ± 0.1 µm² to 2.6 µm² ± 0.5 µm², Figure 3.26 M) and an increase in mitochondrial occupancy (from 38,8 % ± 2 % to 55 % ± 4.3 %, Figure 3.26 N). Of note, these values are lower as observed in previous experiments. This might be due to additional DMSO application in the non-stimulated neurons as a control agent as FCCP was dissolved in DMSO. Thereby, mitochondrial parameters might be affected by this, nevertheless the SRF-VP16 effect could still be observed. In FCCP-stimulated neurons expressing the SRF-ΔMADS-VP16 control construct (Figure 3.26 C, G, K) mitochondrial fragmentation was induced (mitochondrial size was decreased to 0.67 µm² ± 0.04 µm², Figure 3.26 M). Furthermore, mitochondrial distribution was impaired and mitochondrial occupancy was decreased to 21.2 % ± 0.3 % (Figure 3.26 N). Again, SRF-VP16 overexpression led to mitochondrial enlargement and redistribution to normal values (Figure 3.26 D, H, L). In doing so, mitochondrial size was significantly increased to 1.9 µm² ± 0.2 µm² (Figure 3.26 M) as was mitochondrial occupancy (48 % ± 2 %, Figure 3.26 N).

Thus, this experiment shows that SRF-VP16 can exert its beneficial impact on mitochondria in an artificial *in vitro* system in which mitochondrial function is impaired by uncoupling agents such as FCCP. This suggests that the influence on mitochondria by SRF is likely to be a general cellular mechanism to control proper mitochondrial function. Therefore, the latter experiments support a model in which SRF has a neuroprotective function and it is interesting to see whether this SRF based mechanism is crucial for other mitochondria affecting diseases.

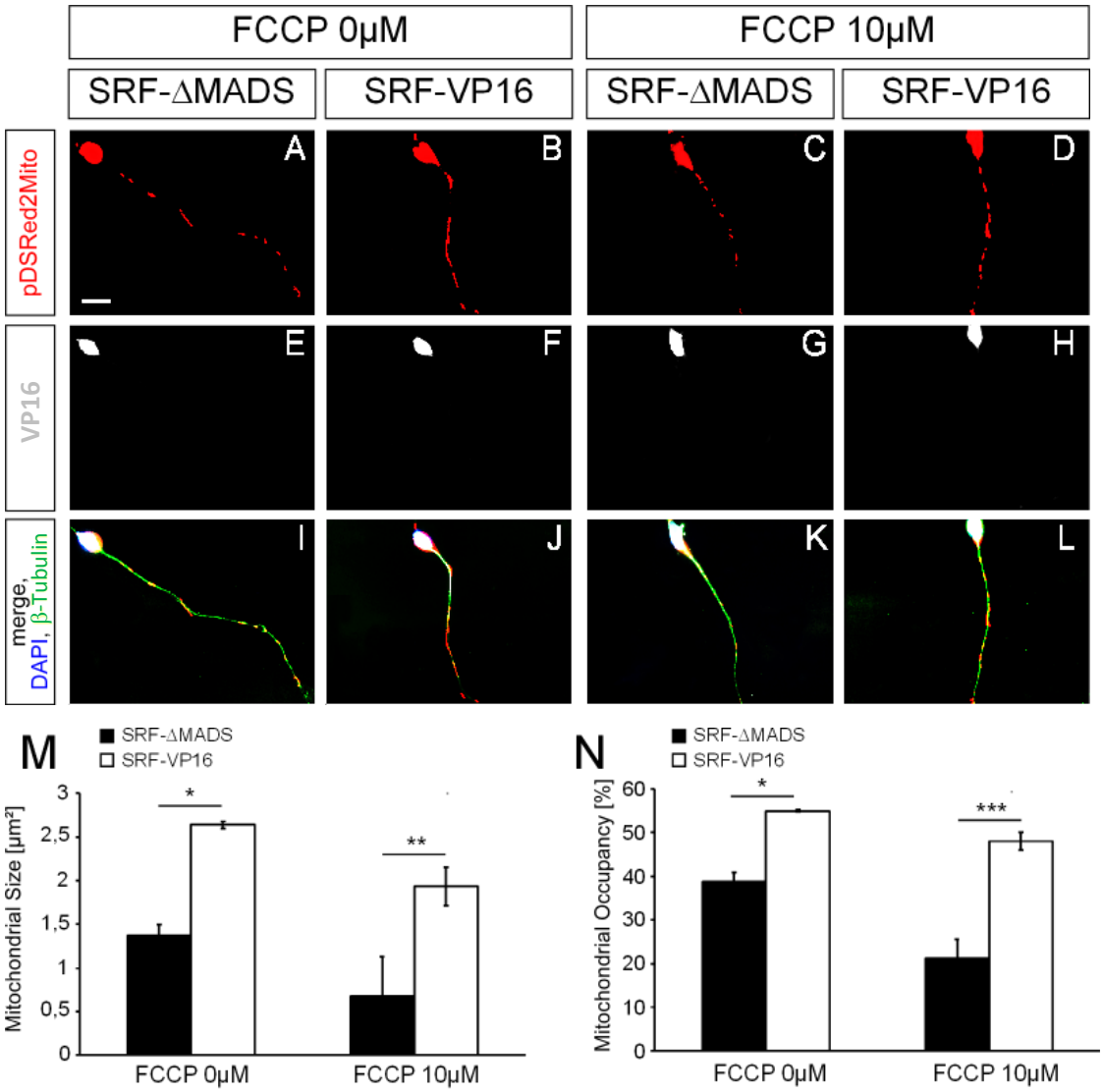

Figure 3.26 SRF-VP16 rescues mitochondrial fragmentation upon FCCP administration

(A, E, I) Control neurons without FCCP stimulation showed normal mitochondria. (B, F, J) Overexpression of SRF-VP16 without FCCP stimulation led to mitochondrial enlargement. (C, G, K) Stimulation of SRF-ΔMADS-VP16 expressing neurons with FCCP resulted in mitochondrial fragmentation. (D, H, L) Mitochondrial size and distribution were rescued upon SRF-VP16 overexpression in case of FCCP stimulation. (M) SRF-VP16 increased mitochondrial size and rescued mitochondria in presence of FCCP. (N) Mitochondrial occupancy was increased by SRF-VP16 in non-stimulated neurons. Furthermore, SRF-VP16 restored normal occupancy in FCCP-stimulated neurons. Scale bar (A-L) = 10 µm.

4. Discussion

4.1 Impact of SRF on mitochondrial dynamics

Much is known about SRF's contribution to neuronal function and morphology (see chapter 1.1.4). Recent research mostly focused on neuronal morphology and motility dependent on SRF loss-of-function. In this regard, it has been shown that SRF-deficiency impairs neurite outgrowth and axonal guidance (Knöll et al., 2006; Wickramasinghe et al., 2008), neuronal migration (Alberti et al., 2005) as well as hippocampal lamination (Stritt and Knöll, 2010) and myelination (Stritt et al., 2009; Lu and Ramanan, 2012). Interestingly, no attention has been paid on mitochondrial dynamics dependent on SRF function in neurons, although it is known that mitochondrial activity is necessary for proper neuronal function. At this point, this important issue is addressed for the first time.

This work shows that SRF is one important regulator of mitochondrial dynamics in neurons. Whereas SRF loss-of-function results in impaired mitochondrial structure, distribution and trafficking, SRF gain-of-function (upon overexpression of constitutively active SRF-VP16) reveals mitochondrial enlargement and increased trafficking.

4.1.1 SRF influences mitochondrial (ultra)structure and size

To address the question whether SRF has an influence on mitochondrial structure in neurons, forebrain specific *Srf* knockout mice were investigated (chapter 3.1.1). For this, corpus callosal cross-sections were analyzed ultrastructurally by electron microscopy. This method allows for detailed observation of membrane topology of cellular organelles. It was shown that SRF-deficiency resulted in abnormal vacuolization inside the mitochondria (Figure 3.1). Thereupon, mitochondria displayed multi-vesicularization and these balloon-like inclusions were not as electron-dense as the rather granular matrix. Furthermore, these mitochondria deviated from the normal cross-sectioned round shaped wild-type mitochondria and were tubular-like shaped. Although their size also seemed to be increased, this could not be confirmed by normalization to increased cross-sectioned neurite diameter. Obviously, besides altered mitochondrial ultrastructure severe de-myelination was observed in these cross-sections as reported before (Stritt et al., 2009). As myelination and mitochondrial function seems to be intertwined (Mahad et al., 2008), one might ask whether

the observed mitochondrial aberrations are a direct SRF effect or result secondarily from the de-myelination. However, abnormal mitochondria were observed in non-myelinated as well as myelinated axons arguing for a direct SRF-dependent effect on mitochondria.

As ultrastructure is fundamental for proper mitochondrial function, it is reasonable that the observed changes in ATP content and production of *Srf* mutant brain tissue (see Figure 3.4) rely on these changes. However, even though ATP production is decreased upon SRF ablation, only whole tissue extracts were analyzed. Due to the fact that these homogenates also contain glial cells, the observed changes in ATP content could be also contaminations of non-neuronal origin that can also be affected indirectly by neuron-specific SRF ablation (Stritt et al., 2009). Nevertheless, this seems improbable as mitochondrial ultrastructural alterations were only observed in *Srf* mutant axons.

Mitochondrial ultrastructure was also changed *in vitro* albeit these changes did not recapitulate the *in vitro* phenotype in detail. Here, mitochondria generally contained one or two cristae invaginations that were not as electron-dense as the matrix (see Figure 3.6). This speaks in favor of a cytoplasmic origin of this vacuolization, whereas *in vivo* mitochondria displayed multi-vacuolization and enclosed vesicles (see Figure 3.1). Nonetheless, it seems likely that the underlying mechanisms controlling mitochondrial ultrastructure might be similar.

In general, the mitochondrial phenotype *in vitro* supports the *in vivo* observations as mitochondria are also inaccurately distributed and structurally altered. Additionally, the effect on mitochondrial size seemed to be more pronounced *in vitro*, as electron microscopy revealed that *in vivo* mitochondria did not seem to be fragmented but rather enlarged (see Figure 3.1). However, this did not hold true if normalized to the increased axonal diameter. Additionally, TOM20 (translocator of outer membrane 20) staining of mitochondria *in vivo* did not show obvious changes in mitochondrial size (see Figure 3.2). On the other hand, mitochondria *in vitro* were severely fragmented (see Figure 3.5). In line, SRF gain-of-function supports a model in which SRF controls mitochondrial size: Whereas SRF-ablation decreased mitochondrial size, constitutively active SRF-VP16 led to “megamitochondrial” network-like structures (see Figure 3.9). However, total amount of mitochondria was not changed upon SRF-ablation as immunoblotting of tissue and cell culture revealed (see Figure 3.3 and data not shown).

As changes in mitochondrial size are the major hallmark of changes in SRF activity the question arises: How can SRF exert its function on mitochondrial structure and size?
In this regard, it is important to understand whether the SRF-effect on mitochondria is direct or indirect. For this, it was checked whether SRF influenced other organelles with regard to their size, distribution and amount. No changes for markers of the Golgi-apparatus or the microtubule-cytoskeleton could be detected by immunoblotting of *Srf* mutant tissue (see Figure 3.3). Although no changes could be observed for the total amount of the mitochondrial marker TOM20, electron-microscopy did show structural changes of mitochondria and immunohistochemistry revealed mitochondrial distribution defects. One explanation could be that mitochondria are so abundant in all kind of cells that a slight decrease of mitochondrial abundance in neurons would be undetectable due to the high amount of mitochondria in glial cells. One the other hand, mitochondrial amount could be really unchanged in SRF-deficient neurons and SRF-mediated effects only impinged on mitochondrial structure and distribution.
In vitro experiments showed no changes for size and abundance of synaptic vesicles (see Figure 3.8). Furthermore, another constitutively active transcription factor, CREB-VP16, failed to have an effect on mitochondria (see Figure 3.9). This suggests that the observed *in vitro* phenotypes are specific with regard to the influenced organelle (mitochondria) as well as the operating transcription factor.
Again, one might argue that the observed mitochondrial fragmentation is an indirect effect of SRF ablation as the latter results in severe morphological impairments of *Srf* mutated neurons that could influence e.g. mitochondrial distribution (see Figure 3.5). However, in a side project *Srf* was knocked out in neurons that had been cultivated for two weeks *in vitro*, thereby showed a fully developed neurite network formation. Again, mitochondria displayed fragmentation, although to a lesser extent (data not shown). This argues that neuronal morphology might be contributing but not be the predominant cause of mitochondrial fragmentation.

As mitochondria show fragmentation and perinuclear clustering upon SRF deficiency, one possible reason might be changes in the expression of fusion / fission proteins that regulate mitochondrial size. However, neither quantitative PCR (qPCR) nor immunoblotting revealed any changes in the expression of fusion / fission related proteins on mRNA or protein level,

respectively. Furthermore, qPCR-based analysis of mitochondria related genes (with regard to metabolism, membrane structure or transcriptional regulators) that might be affected by SRF showed no significant changes for any of them (data not shown).
Thus, albeit SRF seems to have mitochondria specific effects, these are likely to be mediated indirectly. Thereby, the question arises how specificity can be maintained, while SRF has no direct effect on mitochondrial target gene expression.

4.1.2 SRF affects mitochondrial distribution and trafficking

Besides structure, SRF influenced mitochondrial distribution and transport in neurons. This is reasonable as both processes are connected: Functional trafficking is prerequisite for proper distribution. Therefore, the performed experiments are consistent: Mitochondrial trafficking is impaired *in vitro* as is distribution (see Figure 3.5 and Figure 3.7). Distribution is also altered *in vivo* leading to more mitochondria in the perinuclear space (see Figure 3.2).
As these effects could be rescued upon overexpression of the constitutively active SRF-VP16 but not CREB-VP16 these phenotypes seemed to be SRF-specific again (see Figure 3.9 and Figure 3.11). However, it is still unclear how SRF influenced mitochondrial trafficking as no changes in expression of transport proteins could be observed by qPCR (data not shown). Again, one might argue that the decrease in velocity and relative amount of moved mitochondria was due to the severely impaired neuronal morphology (see Figure 3.7). But still, trafficking of synaptic vesicles was not altered upon SRF ablation (see Figure 3.8 F, G) arguing for a mitochondria specific effect of SRF regardless of neuronal morphology.

Taken together, SRF ablation led to mitochondrial impairments with regard to distribution, trafficking, size and (ultra)structure. Whereas the exact mechanism of SRF towards mitochondria is not clear, SRF's impact on organelles seemed to be mitochondria specific. While mitochondrial related genes with regard to structure, fusion / fission, trafficking, metabolism and transcriptional regulation were not affected by SRF, cytoskeletal rearrangements might account for mitochondrial alterations. As SRF is one major controller of actin microfilaments (see chapter 1.1.2.2), it is tempting to assume that alterations in actin dynamics might underlie the observed mitochondrial impairments. The performed immunoblotting showed that levels of pan-actin were decreased and levels of inactivated

phospho-cofilin were increased upon SRF-deficiency *in vivo* (see Figure 3.3). Furthermore, it was shown that SRF-VP16 increases levels of F-actin (Schratt et al., 2002), which might be important to understand the SRF-effect on mitochondria.

Of note, in the literature only little attention has been paid on actin's contribution to functional mitochondria, therefore this might be one possible explanation underlying the mitochondrial phenotype in case of SRF ablation.

4.2 Influence of actin dynamics on mitochondria

In contrast to the microtubule cytoskeleton, the actin microfilament has not been investigated extensively with regard to mitochondrial dynamics. It is believed that most of mitochondrial trafficking in neurons is mediated via kinesin- and dynein-driven transport along microtubules (MacAskill and Kittler, 2009), whereas actin is thought to mediate short range movements and is involved in fine-tuned mitochondrial positioning in F-actin rich areas, e.g. growth cones (Sheng and Cai, 2012).

However, little is known about actin's contribution to mitochondrial remodeling. To date, it is believed that an increase in F-actin-based mitochondrial arresting leads to the recruitment of the fission machinery and results in mitochondrial fragmentation. This is supported by research showing mitochondrial enlargement upon increased mitochondrial trafficking (Saotome et al., 2008; Russo et al., 2009; Pathak et al., 2010). Furthermore, in an epithelial cell line F-actin assembly is required for recruitment of the fission protein Drp1 (De Vos et al., 2005). This speaks in favor of a model in which F-actin formation leads to mitochondrial arresting, thereby recruitment of fission proteins and subsequent mitochondrial fragmentation. If this is true, F-actin disassembly would increase mitochondrial transport and lead to mitochondrial enlargement.

In order to check for the contribution of G/F-actin treadmilling to mitochondrial remodeling, actin mutants were applied that are either polymerization incompetent (actin R62D) or favor F-actin assembly (actin S14C or actin G15S). In any case point-mutated actin proteins got overexpressed that led to a shift in the G/F-actin ratio. In turned out that increasing the G-actin pool by overexpression of actin R62D significantly decreased mitochondrial size and

occupancy in neurons (Figure 3.13 C, H, K, L). Interestingly, overexpression of actin R62D circumvented the SRF-VP16 effect on mitochondria (Figure 3.14) arguing that SRF exerts its function on mitochondria via functional actin treadmilling. This is another hint supporting the aforementioned hypothesis that SRF impacts mitochondria indirectly via the actin cytoskeleton. However, overexpression of F-actin favoring actin G15S as well as wild-type actin failed to rescue neurite outgrowth and mitochondrial dynamics observed upon SRF deficiency (data not shown, (Stern et al., 2009)). This suggests that impaired functional actin treadmilling is important but not the only factor underlying impaired neurite outgrowth and mitochondrial fragmentation upon SRF ablation. It is likely that other factors, e.g. actin binding proteins, play a decisive role in regulating these processes.

Furthermore, mitochondrial fragmentation was also observed after stimulation with latrunculin, an F-actin disrupting drug. In contrast, increasing the F-actin pool by overexpression of actin G15S led to mitochondrial enlargement, whereas the F-actin favoring mutant actin S14C had no effect on mitochondrial size (Figure 3.13). It is important to note that these actin mutants were overexpressed throughout the whole neuron and were not restricted to F-actin-rich areas (e.g. the growth cone). Thereby, these point-mutated actins could possibly exert an “abnormal” effect on mitochondria because normally neurites are rather actin free.

For this reason it was investigated whether these actin mutants had an effect on mitochondria in an area that is known to be reliant and filled with actin, i.e. the growth cone (detailed introduction into actin dynamics in growth cones see chapter 1.2.2 and Figure 1.6). It turned out that increasing the F-actin pool by overexpression of actin G15S resulted in growth cone enlargement and recruitment of mitochondria to the growth cone area (Figure 3.16 B, E). Contrastingly, increasing the G-actin pool led to neurons phenocopying SRF-deficient neurons with smaller growth cones and perinuclear clustering of mitochondria (Figure 3.16 C, F). Whereas these experiments were based upon overexpression of artificial actin point-mutants, a more physiological stimulation of actin treadmilling was achieved using BDNF- and ephrin-A5-administration. BDNF, an attractive guidance cue inducing F-actin rich filopodia in growth cones (Meier et al., 2011), led to mitochondrial recruitment to growth cones (Figure 3.15 B, E). In contrast, ephrin-A5 (leading to disruption of F-actin in the growth cone) withdrew mitochondria from growth cones (Figure 3.15 C, F). This is in line with previous reports showing NGF mediated F-actin dependent anchoring of mitochondria

(Chada and Hollenbeck, 2003). Furthermore, it was shown that WAVE1, a controller of F-actin polymerization, is required for attraction of mitochondria to dendritic spines and filopodia (Sung et al., 2008).

However, this study shows data contradicting the existing model of F-actin based arresting of mitochondria and recruitment of fission proteins (De Vos et al., 2005; Russo et al., 2009). In this case, mitochondria should be smaller after of F-actin assembly (actin G15S overexpression) or larger after increasing the G-actin pool (by actin R62D overexpression).

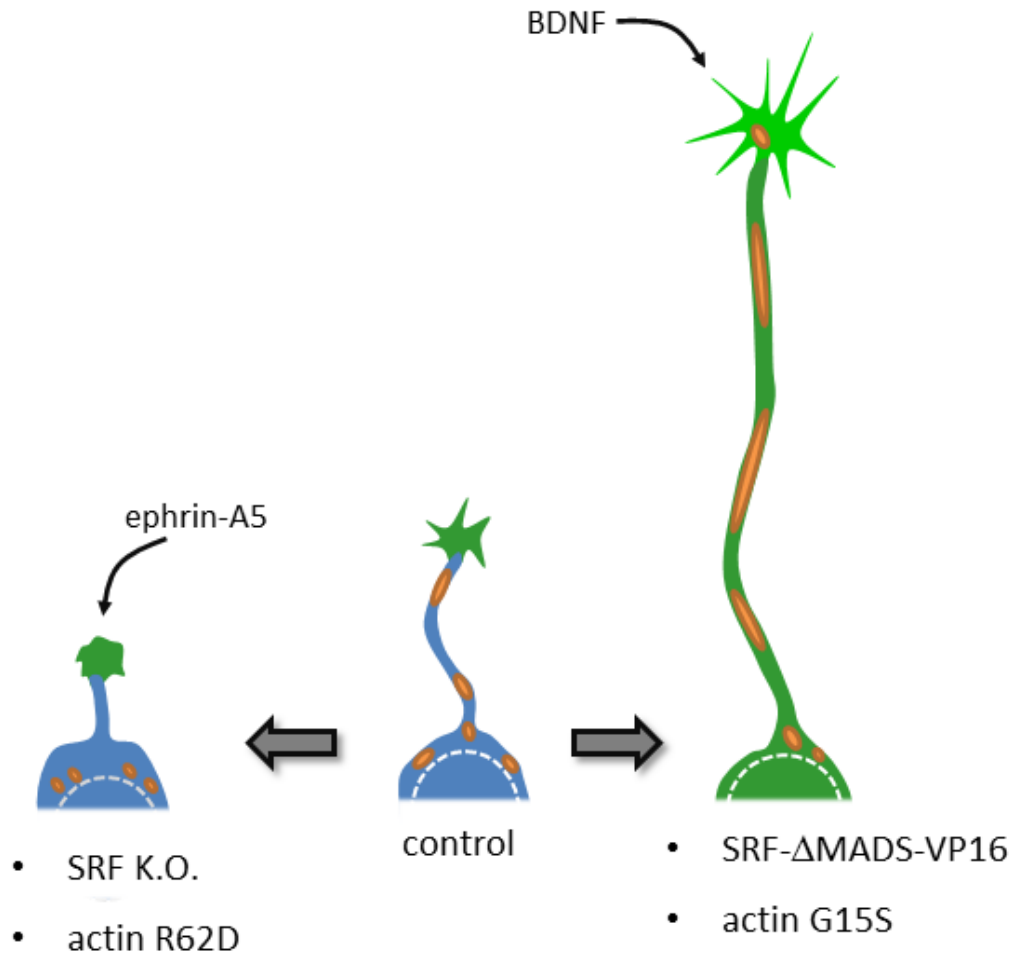

Figure 4.1 Model of actin-effects on mitochondrial size

In control neurons mitochondria are normal in size and equally distributed throughout the neurite with only few mitochondria entering the growth cone area.
Increasing the F-actin pool or overexpression of SRF-VP16 leads to mitochondrial enlargement as well as enhanced neurite outgrowth. Stimulation with BDNF increases growth cone area and recruits mitochondria to growth cones.
SRF-deficiency as well as increasing the G-actin pool by overexpression of actin R62D impairs neurite outgrowth and leads to mitochondrial fragmentation. Selective F-actin depolymerization in the growth cone by ephrin-A5 stimulation withdraws mitochondria from growth cones.

Indeed, here it is shown that it is just the other way round. For this reason, this work supports another model in which increasing the F-actin pool leads to mitochondrial enlargement and recruitment to growth cones (see Figure 4.1).

How could actin mediate its effect on mitochondria?

In contrast to microtubules, only a few adaptor molecules have been identified that mediate mitochondrial interaction with the actin cytoskeleton. This involves myosin motor proteins like myosin XIX (Quintero et al., 2009), myosin V (Naisbitt et al., 2000) or WAVE1 (Sung et al., 2008), the latter might be serving as a "real anchor" involved in arresting of mitochondria. Thus, there might be some adaptor molecules that are involved in actin-mitochondria interactions. However, so far it is not understood how actin influences mitochondrial size. Indeed, the suggested model of F-actin anchoring of mitochondria and subsequent recruitment of fission proteins seems questionable as this project suggests that F-actin formation leads to mitochondrial enlargement.

Of note, it is also controversial how SRF comes into play. In this context, the question arises whether SRF-mediated transcriptional activation (e.g. upon overexpression of SRF-VP16) leading to F-actin formation is causing mitochondrial enlargement or whether it is the other way round: Formation of F-actin could also activate SRF-mediated gene transcription. This has been reported for the used actin point mutants. Actin G15S (favoring F-actin) activates SRF-dependent gene expression, whereas actin R62D (increasing the G-actin pool) decreases SRF transcriptional activity in neurons (Stern et al., 2009). Additionally, actin S14C does not activate SRF transcriptional activity which would explain the missing effects of actin S14C on mitochondria. Furthermore, latrunculin decreases SRF transcriptional activity by increasing the amount of G-actin monomers and inhibiting the dissociation of G-actin from MRTFs. Thereby MRTFs cannot translocate into the nucleus and do not initiate SRF-mediated gene transcription (Miralles et al., 2003; Posern et al., 2004). Thus, it could also be the case that increasing or decreasing the F-actin amount leads to mitochondrial effects indirectly via altered SRF transcriptional activity. Nonetheless, it still seems unclear how SRF would then influence mitochondria because neither mitochondrial target genes nor expression of fusion / fission proteins were affected by SRF.

Additionally, the effects of SRF on mitochondrial trafficking are somehow contradicting the abovementioned picture. It is believed that actin-based mitochondrial trafficking rather

opposes fast axonal transport mediated by microtubule motor proteins. Disruption of F-actin leads to enhanced mitochondrial movement (Morris and Hollenbeck, 1995) and actin is believed to arrest mitochondria (Chada and Hollenbeck, 2004). Currently it is assumed that actin-based motor proteins (namely myosin V) compete with microtubule motors distracting mitochondria from microtubules to actin microfilaments (Pathak et al., 2010). Consequently, an increase in F-actin should result in decreased mitochondrial trafficking. This runs contrary to this study as it is proposed at this point that SRF activation (by SRF-VP16 overexpression) leads to F-actin formation and subsequent changes in mitochondrial dynamics (distribution and size). Additionally, SRF-VP16 does also lead to increased trafficking of small mitochondrial objects beside the syncytial "megamitochondria" (see chapter 3.1.2.5). Furthermore, SRF-deficient neurons (displaying impaired actin microfilaments) contain mainly stationary mitochondria. This is contradicting as an increase of SRF-activity and subsequent F-actin formation should result in arresting of mitochondria and SRF loss-of-function (therefore decreasing F-actin) should speed up mitochondria. For this reason, one can only speculate what might contribute to SRF-mediated changes in mitochondrial trafficking. As SRF did not seem to affect expression of motor proteins directly, it is possible that an indirect effect accounts for changes in mitochondrial trafficking. Maybe SRF increases general metabolic activity of the cell, which would be in line with the performed experiments showing decreased levels of ATP content and production in *Srf* mutant tissue (see Figure 3.4). Thereby, mitochondria must be transported faster to meet with regions of high energy turnover. SRF could also influence the recruitment of actin binding proteins to the actin cytoskeleton in such a way that mitochondrial arresting or transport along microfilaments is stopped.

Of note, actin point-mutants alone did not have an impact on mitochondrial trafficking beside their ability to change the overall neuronal morphology (data not shown). This supports a model in which the changes in mitochondrial movement are not based upon changes in the actin cytoskeleton but on another SRF-effect on the cell that is not understood so far.

Generally, the impact of actin binding proteins on the interplay of mitochondria and actin microfilaments is poorly understood. It is likely that these proteins are not only involved in managing the actin-status of the cell but are also required for the interaction with organelles like mitochondria.

4.3 Regulation of cofilin activity and its relevance for mitochondrial dynamics

Another possibility to explain SRF- and actin-mediated influences on mitochondrial dynamics goes via the actin binding protein cofilin. Of note, this work provides the first proof of principle that the observed morphological changes in *Srf* mutant neurons are due to alterations in cofilin phosphorylation and can be rescued upon restoring cofilin activity. Furthermore, cofilin has been shown to be involved in mitochondrial processes such as apoptosis (Klamt et al., 2009; Rehklau et al., 2011). Thus, this actin binding protein might be crucial for integrating the SRF transcriptional activity into changes in actin dynamics and subsequent impact on mitochondria.

As introduced in chapter 1.2.3, cofilin acts as an F-actin severing protein. Thereby, actin is cleaved into smaller oligomers that can form new seeds for polymerization or be further de-polymerized into monomers depending on the physiological circumstances (Condeelis, 2001). Additionally, at high concentrations cofilin seems to fulfill an actin-nucleating function besides its severing activity (Van Troys et al., 2008). Phosphorylation at the serine residue 3 is the major process by which cofilin gets inactivated (Van Troys et al., 2008). On the other hand, dephosphorylation and subsequent activation is mediated by slingshot phosphatase (Huang et al., 2006). Interestingly, hyperphosphorylated cofilin is one major hallmark of SRF deficiency (Alberti et al., 2005) but it was unclear whether this inactivation of cofilin is really crucial for developing the SRF-linked phenotype.

In this study it was shown that levels of phosphorylated cofilin are also increased in single *Srf* mutant neurons as observed by immunocytochemistry (see Figure 3.18). Interestingly, overexpression of constitutively active SRF-VP16 rescued neuronal morphology as well as mitochondrial dynamics and restored phospho-cofilin levels to a wild-type level (Figure 3.18 Q). This speaks already in favor of cofilin being involved in regulating neuronal and mitochondrial morphology which is further supported by applying cofilin mutant proteins. In doing so, a non-phosphorylatable (thereby permanently active) cofilin-S3A mutant rescued mitochondria and neurite outgrowth in an *Srf* mutant background (see Figure 3.19). On the other hand, a phosphomimetic (and consequently inactive) cofilin-S3E mutant decreased mitochondrial size and occupancy and circumvented the SRF-VP16 effect on mitochondria

(see Figure 3.20) without disturbing neurite outgrowth. Thus, these experiments strongly argue for a model in which the effects of SRF deficiency on neurons are due to alterations of the activation status of cofilin. This definitely holds true for the effects on mitochondria as all mitochondrial parameters were restored upon expression of constitutively active cofilin-S3A in an *Srf* mutant background and cofilin-S3E in turn negatively influenced mitochondrial size as well as occupancy. On the other hand, cofilin activity seemed to be necessary but not crucial for maintaining neuronal morphology as cofilin-S3E failed to negatively influence neurite outgrowth in wild-type neurons (see Figure 3.20). Overexpression of mutant cofilin proteins is always somewhat critical as it was reported that overexpression of wild-type cofilin induces cofilin-actin rod formation that impairs axonal trafficking (Cichon et al., 2011) and can be found in neurodegenerative diseases (Bamburg et al., 2010). Of note, also cofilin-S3A is reported to induce rod formation but to a less extent (Cichon et al., 2011). For this reason, in chapter 3.3.2 only neurons without rod formation were monitored.

Another way to interfere with cofilin activity goes via activation of slingshot phosphatase. Overexpression of an active form of slingshot phosphatase (SshL) rescued mitochondrial size and occupancy as well as neurite outgrowth in SRF-deficient neurons (see chapter 3.3.4, Figure 3.21). Furthermore, phospho-cofilin levels that were increased in *Srf* mutant neurons were restored to wild-type levels after overexpression of active SshL (Figure 3.21 P). This experiment strongly argues that the effects on mitochondria (fragmentation, perinuclear clustering) as well as neuronal morphology (impaired neurite outgrowth) upon SRF deficiency are based upon impaired cofilin activity. Again, this is a first proof of principle experiment showing a rescue of neurite outgrowth in *Srf* mutant neurons by SshL overexpression. So far it was unclear whether the observed increase in phospho-cofilin levels was just a side-effect of SRF ablation or whether this had any implication in mediating the observed phenotypes upon SRF deficiency. Now it seems obvious that cofilin indeed is the main player conducting impaired mitochondrial dynamics and neurite outgrowth in *Srf* mutant neurons.

How could cofilin exert its function on mitochondria?

As it was shown before, cofilin phosphorylation (and thereby activity) is changed upon SRF deficiency (Alberti et al., 2005). This results from a decrease in LIMK inhibition, subsequently cofilin gets hyperphosphorylated upon SRF ablation (Mokalled et al., 2010). So far, the direct impact of cofilin on mitochondrial size and distribution is not understood. One could assume

that cofilin acts directly on mitochondria as reported before in case of mitochondrial mediated apoptosis (Rehklau et al., 2011). However, changes in cofilin activity always have an influence on the actin cytoskeleton. Therefore, changes in cofilin activity could indirectly influence mitochondrial size via impairing actin treadmilling. For example, a decrease in cofilin phosphorylation (e.g. upon overexpression of SRF-VP16 or SshL) would activate cofilin and lead to an increased actin severing function. Hence, new seeds for F-actin polymerization would be generated that in turn would increase to pool of F-actin and lead to the observed mitochondrial phenotypes (e.g. mitochondrial enlargement) that have been linked to changes in the G/F-actin ratio.

However, overexpression of SRF-VP16 or SshL did only have a slight impact on cofilin phosphorylation in wild-type neurons as these cells had rather low basal levels of phospho-cofilin (see Figure 3.18 Q, Figure 3.21 P). Thus, it is hard to explain the severe effect SRF-VP16 has on mitochondria only because of changes in cofilin phosphorylation. Interestingly, active SshL has a positive effect on mitochondrial size in wild-type neurons but not significantly (Figure 3.21 M). Hence, this suggests that cofilin activity is one but not the only player in influencing mitochondrial size. Apparently, SRF seems to affect more than only cofilin activity. However, it is evidently that changes in cofilin phosphorylation account for the phenotype observed upon SRF ablation.

Taken together, it seems likely that SRF exerts (at least in part) its function on mitochondria via the cofilin-actin axis (see Figure 4.2). In wild-type neurons SRF inhibits LIMK activity that leads to low levels of phosphorylated cofilin. Unphosphorylated cofilin can bind to F-actin and severs actin filaments, therefore new F-actin polymerization could be induced. This might account for mitochondrial enlargement as it was shown that increased levels of F-actin led to bigger mitochondria (see chapter 3.2.1). However, one cannot rule out that cofilin has a direct effect on mitochondria, e.g. by binding to mitochondria directly or translocating to mitochondria as reported for mitochondria associated apoptosis (Chua et al., 2003).

On the other hand, SRF deficiency resulted in hyperphosphorylation of cofilin as the inhibition of LIMK is abrogated. Thus, phosphorylated cofilin cannot bind to F-actin and exert its severing function. It is unclear whether this reduced F-actin turnover observed upon SRF

deficiency accounts for mitochondrial fragmentation alone or whether phosphorylated cofilin has a direct effect on mitochondria (see Figure 4.2).

However, this SRF-cofilin-actin axis seems to be an interesting model to explain the observed phenotypes in this study. Here, for the first time a possible albeit indirect effect of SRF on a cellular organelle is proposed: Normally, SRF inhibits cofilin phosphorylation. Thus, active cofilin leads to F-actin turnover, thereby controlling mitochondrial size. Overactivation of SRF increases cofilin activity that could possibly increase the F-actin pool and lead to mitochondrial enlargement. SRF ablation in turn would decrease cofilin activity, therefore F-actin turnover and the formation of new F-actin is reduced. Consequently, mitochondrial fragmentation could take place.

However, this model is still highly speculative as one cannot rule out direct effects of cofilin

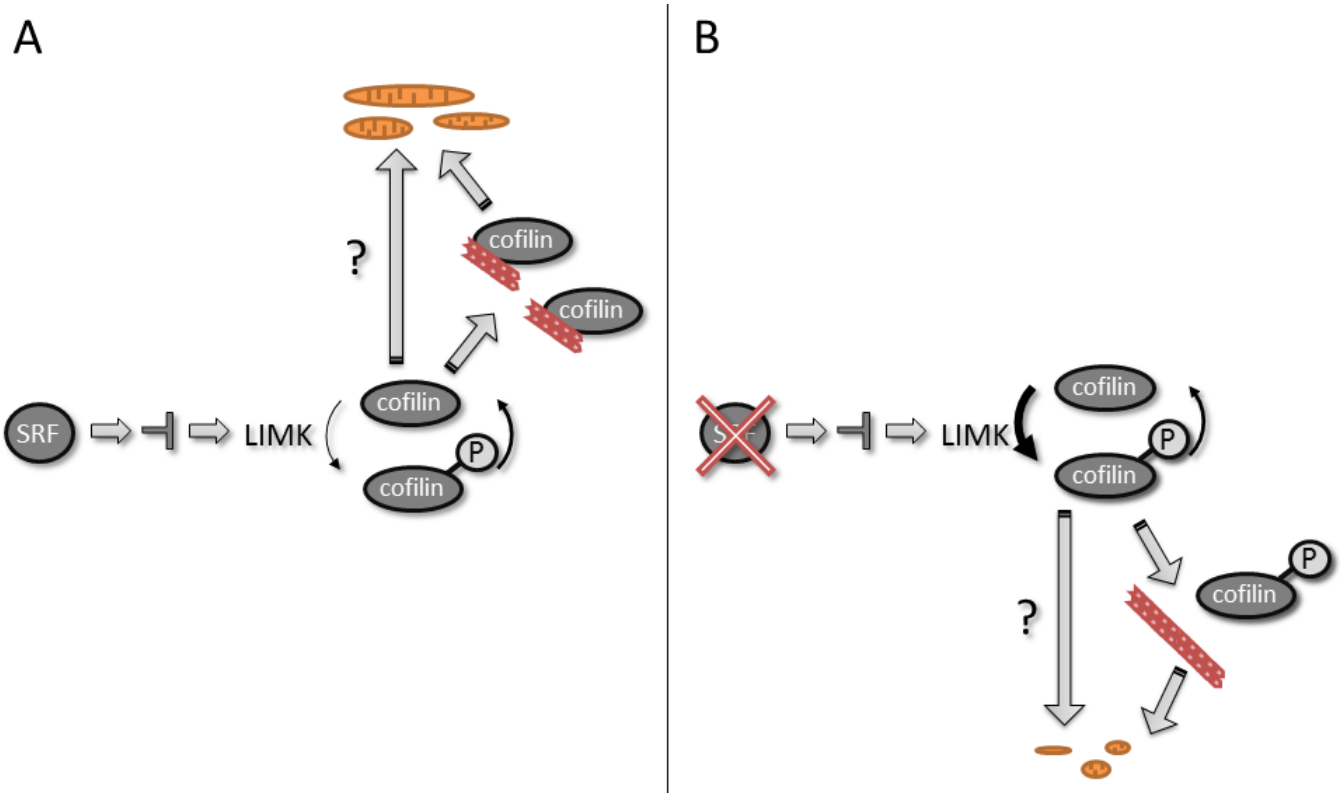

Figure 4.2 Possible regulation of mitochondrial size via the SRF-cofilin-actin axis

(A) Under normal conditions SRF inhibits LIMK activity (Mokalled et al., 2010), therefore most of the cofilin is non-phosphorylated and can bind to actin filaments. Whether cofilin acts directly on mitochondria or indirectly via affecting the G/F-actin treadmilling is unclear (see question mark).

(B) Upon SRF deficiency LIMK gets overactivated resulting in hyperphosphorylated cofilin levels. Again, it is not clear whether phosphorylated cofilin acts directly on mitochondria (see question mark), thereby decreasing their size, or indirectly by diminishing F-actin turnover.

on mitochondria as well as SRF mediating the expression of mitochondria related target genes. Furthermore, it is currently not understood how F-actin formation could lead to mitochondrial enlargement and still actin-specific adaptor molecules have not been identified. Thus, additional research is required to enlighten the picture of the SRF-cofilin-actin axis mediating the control of mitochondrial size and additionally distribution and trafficking.

4.4 Neuropathological implications of SRF mediated regulation of mitochondrial function

Many neurodegenerative diseases rely on impaired mitochondrial dynamics as neurons are totally dependent on functioning mitochondria (detailed introduction into mitochondria and neurodegenerative diseases see chapter 1.3.5). Many of the mitochondrial phenotypes observed upon SRF deficiency are reminiscent of different neuropathological diseases; thus, it is likely that SRF itself exerts a neuroprotective function.

It is worth mentioning, that changes in mitochondrial ultrastructure initially observed in corpus callosal cross sections by electron microscopy resembled mitochondrial vacuolization in an Amyotrophic Lateral Sclerosis disease model mouse (Martin et al., 2009). In this research a mouse transgenic for a mutant SOD1 (superoxide dismutase) was investigated and reported to display megamitochondria and vacuolization *in vivo* (see Figure 1.13). However, the expression of SOD1 was unchanged in *Srf* mutant tissue (investigated by qPCR, data not shown) indicating that this might be an unrelated but phenotypically similar effect.

SRF deficiency *in vitro* resulted in mitochondrial fragmentation, perinuclear clustering, impaired trafficking and altered ultrastructure. Interestingly, *in vitro* models of Huntington's disease display similar mitochondrial phenotypes (Orr et al., 2008). In line with this published data, an aggregation-competent huntingtin protein overexpressed in wild-type neurons resulted in mitochondrial fragmentation and neurite clearance (see chapter 3.4.1). Interestingly, overexpression of constitutively active SRF-VP16 alleviated the effect of mutant huntingtin *in vitro*. Thereupon, mitochondrial size as well as distribution and trafficking were restored in huntingtin positive neurons (see Figure 3.23 I, J and Figure 3.24). This effect could be accomplished by just simply "overwriting" the huntingtin effect or by direct interference with mutant huntingtin. Interestingly, an *in vivo* Huntington's disease

mouse model showed reduced levels of SRF expression in brain regions positive for huntingtin aggregates (see Figure 3.25) as investigated by immunohistochemistry as well as immunoblotting of brain tissue lysates.

This draws to the conclusion that SRF is directly integrated into mutant huntingtin's action on mitochondria in neurons. In such a model huntingtin could down-regulate SRF as huntingtin has been reported to influence gene expression negatively (Cui et al., 2006). Thus, huntingtin mediated impairment of SRF expression would thereby influence mitochondrial dynamics. Consequently, mutant huntingtin's effects on mitochondria would be averted by additional expression of active SRF-VP16 as observed in Figure 3.24.

The latter experiment shows for the first time a direct implication of SRF activity in a neurodegenerative model. In this context, SRF seems to exert a neuroprotective function by maintaining mitochondrial dynamics.

Additionally, in a more artificial model SRF protected mitochondria against the toxic agent FCCP. This substance directly uncouples the mitochondrial membrane potential and has been shown to induce mitochondrial fragmentation (Cereghetti et al., 2010). Again, SRF-VP16 was able to protect neuronal mitochondria against FCCP-induced mitochondrial fragmentation (see Figure 3.26). Thus, SRF seems to have a general protective effect on mitochondria even under toxic stress unrelated to a neurodegenerative disease. To date, it is not clear how SRF influences mitochondria and protects them against e.g. uncoupling agents. However, it seems likely that SRF does not only affect mitochondria indirectly (e.g. via the actin cytoskeleton) but in a more direct way to circumvent a toxic depolarization of the mitochondrial membrane potential.

Although SRF's protective function is not fully understood, at least in case of protection against mitochondrial uncoupling, this is still the first experiment showing that SRF might have a mitochondria- and thereby neuroprotective function *in vitro*. Additionally, for the first time a possible involvement of SRF in a neurodegenerative disease is shown in case of Huntington's disease. These findings might provide a new understanding for mitochondrial related neurodegenerative diseases as in this study SRF is shown to be a novel transcription factor regulating and protecting mitochondrial dynamics. Hopefully, further research will enlighten the detailed impact of SRF on mitochondrial biology and offer new perspectives to cure neurodegenerative diseases.

5. Summary

This work addresses the influences of the transcription factor SRF, actin treadmilling and cofilin activity on mitochondrial dynamics with regard to size, (ultra)structure and trafficking.

In vivo experiments showed that SRF loss-of-function (LOF) resulted in multi-vesiculated mitochondria in corpus-callosal cross-sections and impairment of mitochondrial distribution in cortical neurons. Furthermore, ATP-content of *Srf* mutant brain was reduced as well as ATP-production capacity.

In vitro Srf mutant neurons displayed mitochondrial fragmentation, impaired mitochondrial occupancy and ultrastructural membrane disorganization. Furthermore, fewer mitochondria moved at slower velocities as compared to wild-type neurons. Of note, all parameters could be rescued upon overexpression of constitutively active SRF-VP16 in an *Srf* mutant background. Furthermore, in wild-type neurons SRF-VP16 overexpression resulted in the formation of large mitochondrial networks and increased movement velocity. These effects were SRF- as well as mitochondria-specific.

As SRF is a major regulator of actin treadmilling, the contribution of actin microfilament dynamics to mitochondria was investigated. It turned out that shifting the G/F-actin ratio towards monomeric G-actin led to mitochondrial fragmentation (similar to SRF LOF), whereas increasing the F-actin amount enlarged mitochondria and directed them to F-actin rich growth cone areas.

Furthermore, it was shown that cofilin activity regulates mitochondrial size and distribution. A constitutively active cofilin mutant as well as increasing the cofilin activity by overexpression of slingshot phosphatase rescued mitochondria as well as neurite outgrowth in *Srf* mutant neurons. Furthermore, a permanently inactive cofilin mutant decreased mitochondrial size and circumvented the SRF-VP16-effect on mitochondria.

This speaks in favor of an **SRF-cofilin-actin axis** controlling mitochondrial dynamics: SRF normally activates cofilin indirectly, leading to actin severing, formation of new F-actin filaments and subsequent positive effects on mitochondrial size as well as distribution.

Additionally, it was shown that SRF exerts a mitochondria-protective function by saving mitochondria against toxic stress or protecting them against the effects of mutant huntingtin protein. In this context SRF expression was reduced in mutant huntingtin brains which might provide a new understanding of this neurodegenerative disease.

6. Abbreviations

µF	microfarad
µg	microgramm
µm	micrometer
A.U.	arbitrary units
aa	amino acid
ABP	actin binding protein
ADF	actin depolymerizing factor
ADP	adenosinediphosphate
ANOVA	analysis of variance
APAF-1	apoptotic protease activating factor
APS	ammonium persulfate
Arp 2/3	actin related protein 2/3
ATP	adenosinetriphosphate
A.U.	arbitrary units
BDNF	brain derived neurotrophic factor
bp	base pair
BSA	bovine serum albumin
CaM	calmodulin
CamK	calcium/calmodulin dependent kinase
CdC42	cell division cycle 42
Cdk5	cyclin dependent kinase 5
c-fos	cellular FBJ (Finkel Biskis Jinkins) osteosarcoma oncogene
CNS	central nervous system
Cre	cyclization / recombination
CTGF	connective tissue growth factor
DAPI	4‘,6-diamidin-2-phenylindol
DMEM	Dulbecco’s Modified Eagle Medium
DMSO	dimethyl sulfoxide
DNA	desoxyribonucleic acid

dNTP	desoxy nucleotide triphosphate
DRG	dorsal root ganglion
Drp1	dynamin related protein 1
e.g.	*exempli gratia* (for example)
ECL	enhanced chemoluminescence
EDTA	ethylenediaminetetraacetic acid
Egr-1	early growth response
ELK	Ets-like transcription factor
ERK	extracellular signal-regulated kinase
ETS	E-twenty-six
F-actin	filamentous actin
FADH2	flavin adenine dinucleotide – associated with 2 hydrogens
FCCP	carbonyl cyanide-*p*-trifluoro-methoxyphenylhydrazone
FCS	fetal calf serum
Figs	figures
Fis1	fission protein 1
g	gravitation constant
GABA	gamma-aminobutyric acid
G-actin	globular actin
GAPDH	glycerinealdehyde 3-phoshphate dehydrogenase
GED	GTPase (guanosintriphosphatase) effector domain
GFP	green fluorescent protein
GM130	golgi matrix protein 130
GOF	gain-of-function
h	hour
HAP-1	huntingtin associated protein 1
HBSS	Hank's Buffered Salt Solution
HD	Huntington's disease
HEK	humen embryonic kidney
HRP	horseradish peroxidase
Htr	high temperature requirement
HTT	huntingtin

i.e.	*id est* (that is)
IC	immunocytochemistry
IEG	immediate early gene
IgG	immunoglobulin G
IHC	immunohistochemistry
IMM	inner mitochondrial membrane
kDa	kilodalton
KIF	kinesin family
LAMP1	lysosome associated membrane protein 1
LB-medium	Luria-Bertani-medium
LC8	light chain 8
LIMK	LIM (Lin11, Isl-1, Mec-3) kinase
LOF	loss-of-function
LPA	lysophosphatidic acid
LTP	long term potentiation
M	molar
mA	milliampere
MADS	MCM1, Agamous, Deficiens, serum response factor
MAL	megakaryoblastic leukemia
MAPK	mitogen activated protein kinase
MEK	MAP / ERK kinase
MEM	minimal essential medium
MFN	mitofusin
min	minute
Miro	mitochondrial rho
ml	milliliter
mm	millimeter
mM	millimolar
MRTF	myocardin related transcription factor
ms	millisecond
mV	millivolt
NADH	nicotinamide dinucleotide – assiciated with 1 hydrogen

NET	new ETS transcription factor
NGF	nerve growth factor
NGS	normal goat serum
NLS	nuclear localization signal
NMDA	N-Methyl-D-aspartate
NMEM	neuronal minimal essential medium
o/N	over night
OD	optic density
OMM	outer mitochondrial membrane
OPA	optic atrophy
PAA	poly-acrylamide
PAGE	polyacrylamide gel electrophoresis
PAK1	p21 activated kinase
PBS	phosphate buffered saline
PBST	phosphate buffered saline with tween
PCR	polymerase chain reaction
PEG	polyethylene glycol
PFA	para-formaldehyde
PFKBP3	6-phosphofructo-2-kinase/fructose-2,6-bisphosphatase 3
PGC-1α	peroxisome proliferator-activated receptor-gamma coactivator 1 alpha
pH	potentia hydrogenii
Pi	anorganic phosphate
PINK1	PTEN-induced putative kinase 1
PLL	poly-L-lysine
PVDF	polyvinylidene fluoride
qPCR	quantitative polymerase chain reaction
Rac	Ras-related C3 botulinum toxin substrate
Raf	rapidly accelerated fibrosacroma
Ras	rat sarcoma
RelA	v-Rel (reticuloendotheliosis viral oncogene homolog) A
RFP	red fluorescent protein
RMS	rostral migratory stream

ROCK	Rho kinase
rpm	rounds per minute
s	second
SAP	SRF accessory protein
SDS	sodium dodecyl sulfate
SEM	standard error of the mean
SOD1	superoxide dismutase 1
SRE	serum response element
SRF	serum response factor
Ssh	slingshot
SVZ	subventricular zone
TBS	Tris buffered saline
TBST	Tris buffered saline with tween
TCF	ternary complex factor
TEMED	tetramethylethylenediamin
TNF	tumor necrosis factor
TOM20	translocator of outer membrane 20
TRAK1	trafficking kinesin protein 1
UV	ultraviolet
V	volt
v/v	volume per volume
VDAC	voltage dependent anion channel
VSCC	voltage sensitive calcium channel
w/v	weight per volume
WAVE1	WASP-family verprolin-homologous protein
WB	western blot

7. Literature

Agnew BJ, Minamide LS, Bamburg JR. 1995. Reactivation of phosphorylated actin depolymerizing factor and identification of the regulatory site. J Biol Chem 270:17582-17587.

Alberti S, Krause SM, Kretz O, Philippar U, Lemberger T, Casanova E, Wiebel FF, Schwarz H, Frotscher M, Schutz G, Nordheim A. 2005. Neuronal migration in the murine rostral migratory stream requires serum response factor. Proc Natl Acad Sci U S A 102:6148-6153.

Alexander C, Votruba M, Pesch UE, Thiselton DL, Mayer S, Moore A, Rodriguez M, Kellner U, Leo-Kottler B, Auburger G, Bhattacharya SS, Wissinger B. 2000. OPA1, encoding a dynamin-related GTPase, is mutated in autosomal dominant optic atrophy linked to chromosome 3q28. Nat Genet 26:211-215.

Almeida A, Almeida J, Bolanos JP, Moncada S. 2001. Different responses of astrocytes and neurons to nitric oxide: the role of glycolytically generated ATP in astrocyte protection. Proc Natl Acad Sci U S A 98:15294-15299.

Andrianantoandro E, Pollard TD. 2006. Mechanism of actin filament turnover by severing and nucleation at different concentrations of ADF/cofilin. Mol Cell 24:13-23.

Arsenian S, Weinhold B, Oelgeschlager M, Ruther U, Nordheim A. 1998. Serum response factor is essential for mesoderm formation during mouse embryogenesis. Embo J 17:6289-6299.

Azari NP, Pettigrew KD, Schapiro MB, Haxby JV, Grady CL, Pietrini P, Salerno JA, Heston LL, Rapoport SI, Horwitz B. 1993. Early detection of Alzheimer's disease: a statistical approach using positron emission tomographic data. J Cereb Blood Flow Metab 13:438-447.

Baas PW. 2002. Neuronal polarity: microtubules strike back. Nat Cell Biol 4:E194-195.

Bamburg JR. 1999. Proteins of the ADF/cofilin family: essential regulators of actin dynamics. Annu Rev Cell Dev Biol 15:185-230.

Bamburg JR, Bernstein BW. 2008. ADF/cofilin. Curr Biol 18:R273-275.

Bamburg JR, Bernstein BW, Davis RC, Flynn KC, Goldsbury C, Jensen JR, Maloney MT, Marsden IT, Minamide LS, Pak CW, Shaw AE, Whiteman I, Wiggan O. 2010. ADF/Cofilin-actin rods in neurodegenerative diseases. Curr Alzheimer Res 7:241-250.

Bereiter-Hahn J. 1990. Behavior of mitochondria in the living cell. Int Rev Cytol 122:1-63.

Bernard O. 2007. Lim kinases, regulators of actin dynamics. Int J Biochem Cell Biol 39:1071-1076.

Bernstein BW, Bamburg JR. 2003. Actin-ATP hydrolysis is a major energy drain for neurons. J Neurosci 23:1-6.

Bernstein BW, Painter WB, Chen H, Minamide LS, Abe H, Bamburg JR. 2000. Intracellular pH modulation of ADF/cofilin proteins. Cell Motil Cytoskeleton 47:319-336.

Berridge MJ, Lipp P, Bootman MD. 2000. The versatility and universality of calcium signalling. Nat Rev Mol Cell Biol 1:11-21.

Besnard A, Galan-Rodriguez B, Vanhoutte P, Caboche J. 2011. Elk-1 a transcription factor with multiple facets in the brain. Front Neurosci 5:35.

Birkenfeld J, Betz H, Roth D. 2001. Inhibition of neurite extension by overexpression of individual domains of LIM kinase 1. J Neurochem 78:924-927.

Bolanos JP, Almeida A, Moncada S. 2009. Glycolysis: a bioenergetic or a survival pathway? Trends Biochem Sci 35:145-149.

Bolanos JP, Peuchen S, Heales SJ, Land JM, Clark JB. 1994. Nitric oxide-mediated inhibition of the mitochondrial respiratory chain in cultured astrocytes. J Neurochem 63:910-916.

Bossy-Wetzel E, Petrilli A, Knott AB. 2008. Mutant huntingtin and mitochondrial dysfunction. Trends Neurosci 31:609-616.

Brickley K, Smith MJ, Beck M, Stephenson FA. 2005. GRIF-1 and OIP106, members of a novel gene family of coiled-coil domain proteins: association in vivo and in vitro with kinesin. J Biol Chem 280:14723-14732.

Buchwalter G, Gross C, Wasylyk B. 2004. Ets ternary complex transcription factors. Gene 324:1-14.

Burbulla LF, Kruger R. 2011. Converging environmental and genetic pathways in the pathogenesis of Parkinson's disease. J Neurol Sci 306:1-8.

Burbulla LF, Schelling C, Kato H, Rapaport D, Woitalla D, Schiesling C, Schulte C, Sharma M, Illig T, Bauer P, Jung S, Nordheim A, Schols L, Riess O, Kruger R. 2010. Dissecting the role of the mitochondrial chaperone mortalin in Parkinson's disease: functional impact of disease-related variants on mitochondrial homeostasis. Hum Mol Genet 19:4437-4452.

Cai Q, Gerwin C, Sheng ZH. 2005. Syntabulin-mediated anterograde transport of mitochondria along neuronal processes. J Cell Biol 170:959-969.

Carlier MF, Laurent V, Santolini J, Melki R, Didry D, Xia GX, Hong Y, Chua NH, Pantaloni D. 1997. Actin depolymerizing factor (ADF/cofilin) enhances the rate of filament turnover: implication in actin-based motility. J Cell Biol 136:1307-1322.

Casanova E, Fehsenfeld S, Mantamadiotis T, Lemberger T, Greiner E, Stewart AF, Schutz G. 2001. A CamKIIalpha iCre BAC allows brain-specific gene inactivation. Genesis 31:37-42.

Cattaneo E, Zuccato C, Tartari M. 2005. Normal huntingtin function: an alternative approach to Huntington's disease. Nat Rev Neurosci 6:919-930.

Caviston JP, Ross JL, Antony SM, Tokito M, Holzbaur EL. 2007. Huntingtin facilitates dynein/dynactin-mediated vesicle transport. Proc Natl Acad Sci U S A 104:10045-10050.

Cereghetti GM, Costa V, Scorrano L. 2010. Inhibition of Drp1-dependent mitochondrial fragmentation and apoptosis by a polypeptide antagonist of calcineurin. Cell Death Differ 17:1785-1794.

Chada SR, Hollenbeck PJ. 2003. Mitochondrial movement and positioning in axons: the role of growth factor signaling. J Exp Biol 206:1985-1992.

Chada SR, Hollenbeck PJ. 2004. Nerve growth factor signaling regulates motility and docking of axonal mitochondria. Curr Biol 14:1272-1276.

Chai J, Tarnawski AS. 2002. Serum response factor: discovery, biochemistry, biological roles and implications for tissue injury healing. J Physiol Pharmacol 53:147-157.

Chan C, Beltzner CC, Pollard TD. 2009. Cofilin dissociates Arp2/3 complex and branches from actin filaments. Curr Biol 19:537-545.

Chang CR, Blackstone C. 2007. Cyclic AMP-dependent protein kinase phosphorylation of Drp1 regulates its GTPase activity and mitochondrial morphology. J Biol Chem 282:21583-21587.

Chang DT, Rintoul GL, Pandipati S, Reynolds IJ. 2006. Mutant huntingtin aggregates impair mitochondrial movement and trafficking in cortical neurons. Neurobiol Dis 22:388-400.

Chen H, Detmer SA, Ewald AJ, Griffin EE, Fraser SE, Chan DC. 2003. Mitofusins Mfn1 and Mfn2 coordinately regulate mitochondrial fusion and are essential for embryonic development. J Cell Biol 160:189-200.

Chen TJ, Gehler S, Shaw AE, Bamburg JR, Letourneau PC. 2006. Cdc42 participates in the regulation of ADF/cofilin and retinal growth cone filopodia by brain derived neurotrophic factor. J Neurobiol 66:103-114.

Chen YM, Gerwin C, Sheng ZH. 2009. Dynein light chain LC8 regulates syntaphilin-mediated mitochondrial docking in axons. J Neurosci 29:9429-9438.

Chua BT, Volbracht C, Tan KO, Li R, Yu VC, Li P. 2003. Mitochondrial translocation of cofilin is an early step in apoptosis induction. Nat Cell Biol 5:1083-1089.

Cichon J, Sun C, Chen B, Jiang M, Chen XA, Sun Y, Wang Y, Chen G. 2011. Cofilin aggregation blocks intracellular trafficking and induces synaptic loss in hippocampal neurons. J Biol Chem 287:3919-3929.

Colin E, Zala D, Liot G, Rangone H, Borrell-Pages M, Li XJ, Saudou F, Humbert S. 2008. Huntingtin phosphorylation acts as a molecular switch for anterograde/retrograde transport in neurons. EMBO J 27:2124-2134.

Condeelis J. 2001. How is actin polymerization nucleated in vivo? Trends Cell Biol 11:288-293.

Costa V, Giacomello M, Hudec R, Lopreiato R, Ermak G, Lim D, Malorni W, Davies KJ, Carafoli E, Scorrano L. 2010. Mitochondrial fission and cristae disruption increase the response of cell models of Huntington's disease to apoptotic stimuli. EMBO Mol Med 2:490-503.

Cui L, Jeong H, Borovecki F, Parkhurst CN, Tanese N, Krainc D. 2006. Transcriptional repression of PGC-1alpha by mutant huntingtin leads to mitochondrial dysfunction and neurodegeneration. Cell 127:59-69.

Danial NN, Korsmeyer SJ. 2004. Cell death: critical control points. Cell 116:205-219.

Darios F, Corti O, Lucking CB, Hampe C, Muriel MP, Abbas N, Gu WJ, Hirsch EC, Rooney T, Ruberg M, Brice A. 2003. Parkin prevents mitochondrial swelling and cytochrome c release in mitochondria-dependent cell death. Hum Mol Genet 12:517-526.

Davis RC, Maloney MT, Minamide LS, Flynn KC, Stonebraker MA, Bamburg JR. 2009. Mapping cofilin-actin rods in stressed hippocampal slices and the role of cdc42 in amyloid-beta-induced rods. J Alzheimers Dis 18:35-50.

De Vos KJ, Allan VJ, Grierson AJ, Sheetz MP. 2005. Mitochondrial function and actin regulate dynamin-related protein 1-dependent mitochondrial fission. Curr Biol 15:678-683.

Descot A, Hoffmann R, Shaposhnikov D, Reschke M, Ullrich A, Posern G. 2009. Negative regulation of the EGFR-MAPK cascade by actin-MAL-mediated Mig6/Errfi-1 induction. Mol Cell 35:291-304.

Detmer SA, Chan DC. 2007. Functions and dysfunctions of mitochondrial dynamics. Nat Rev Mol Cell Biol 8:870-879.

DiFiglia M, Sapp E, Chase KO, Davies SW, Bates GP, Vonsattel JP, Aronin N. 1997. Aggregation of huntingtin in neuronal intranuclear inclusions and dystrophic neurites in brain. Science 277:1990-1993.

DiMauro S, Schon EA. 2008. Mitochondrial disorders in the nervous system. Annu Rev Neurosci 31:91-123.

Dominguez R, Holmes KC. 2011. Actin structure and function. Annu Rev Biophys 40:169-186.

Duchen MR. 2004. Mitochondria in health and disease: perspectives on a new mitochondrial biology. Mol Aspects Med 25:365-451.

Endo M, Ohashi K, Mizuno K. 2007. LIM kinase and slingshot are critical for neurite extension. J Biol Chem 282:13692-13702.

Etkin A, Alarcon JM, Weisberg SP, Touzani K, Huang YY, Nordheim A, Kandel ER. 2006. A role in learning for SRF: deletion in the adult forebrain disrupts LTD and the formation of an immediate memory of a novel context. Neuron 50:127-143.

Faix J, Grosse R. 2006. Staying in shape with formins. Dev Cell 10:693-706.

Fichera M, Lo Giudice M, Falco M, Sturnio M, Amata S, Calabrese O, Bigoni S, Calzolari E, Neri M. 2004. Evidence of kinesin heavy chain (KIF5A) involvement in pure hereditary spastic paraplegia. Neurology 63:1108-1110.

Figge C, Loers G, Schachner M, Tilling T. 2012. Neurite outgrowth triggered by the cell adhesion molecule L1 requires activation and inactivation of the cytoskeletal protein cofilin. Mol Cell Neurosci 49:196-204.

Foth BJ, Goedecke MC, Soldati D. 2006. New insights into myosin evolution and classification. Proc Natl Acad Sci U S A 103:3681-3686.

Frank J, Wagenknecht T, McEwen BF, Marko M, Hsieh CE, Mannella CA. 2002. Three-dimensional imaging of biological complexity. J Struct Biol 138:85-91.

Fransson S, Ruusala A, Aspenstrom P. 2006. The atypical Rho GTPases Miro-1 and Miro-2 have essential roles in mitochondrial trafficking. Biochem Biophys Res Commun 344:500-510.

Frederick RL, Shaw JM. 2007. Moving mitochondria: establishing distribution of an essential organelle. Traffic 8:1668-1675.

Fujii T, Iwane AH, Yanagida T, Namba K. 2010. Direct visualization of secondary structures of F-actin by electron cryomicroscopy. Nature 467:724-728.

Fulga TA, Elson-Schwab I, Khurana V, Steinhilb ML, Spires TL, Hyman BT, Feany MB. 2007. Abnormal bundling and accumulation of F-actin mediates tau-induced neuronal degeneration in vivo. Nat Cell Biol 9:139-148.

Galkin VE, Orlova A, Lukoyanova N, Wriggers W, Egelman EH. 2001. Actin depolymerizing factor stabilizes an existing state of F-actin and can change the tilt of F-actin subunits. J Cell Biol 153:75-86.

Gallo G, Letourneau PC. 2004. Regulation of growth cone actin filaments by guidance cues. J Neurobiol 58:92-102.

Garvalov BK, Flynn KC, Neukirchen D, Meyn L, Teusch N, Wu X, Brakebusch C, Bamburg JR, Bradke F. 2007. Cdc42 regulates cofilin during the establishment of neuronal polarity. J Neurosci 27:13117-13129.

Gauthier LR, Charrin BC, Borrell-Pages M, Dompierre JP, Rangone H, Cordelieres FP, De Mey J, MacDonald ME, Lessmann V, Humbert S, Saudou F. 2004. Huntingtin controls neurotrophic support and survival of neurons by enhancing BDNF vesicular transport along microtubules. Cell 118:127-138.

Gineitis D, Treisman R. 2001. Differential usage of signal transduction pathways defines two types of serum response factor target gene. J Biol Chem 276:24531-24539.

Giovane A, Pintzas A, Maira SM, Sobieszczuk P, Wasylyk B. 1994. Net, a new ets transcription factor that is activated by Ras. Genes Dev 8:1502-1513.

Glater EE, Megeath LJ, Stowers RS, Schwarz TL. 2006. Axonal transport of mitochondria requires milton to recruit kinesin heavy chain and is light chain independent. J Cell Biol 173:545-557.

Goldberg DJ, Foley MS, Tang D, Grabham PW. 2000. Recruitment of the Arp2/3 complex and mena for the stimulation of actin polymerization in growth cones by nerve growth factor. J Neurosci Res 60:458-467.

Goldstein JC, Waterhouse NJ, Juin P, Evan GI, Green DR. 2000. The coordinate release of cytochrome c during apoptosis is rapid, complete and kinetically invariant. Nat Cell Biol 2:156-162.

Graceffa P, Dominguez R. 2003. Crystal structure of monomeric actin in the ATP state. Structural basis of nucleotide-dependent actin dynamics. J Biol Chem 278:34172-34180.

Greenberg ME, Ziff EB. 1984. Stimulation of 3T3 cells induces transcription of the c-fos proto-oncogene. Nature 311:433-438.

Harder Z, Zunino R, McBride H. 2004. Sumo1 conjugates mitochondrial substrates and participates in mitochondrial fission. Curr Biol 14:340-345.

Hassler M, Richmond TJ. 2001. The B-box dominates SAP-1-SRF interactions in the structure of the ternary complex. Embo J 20:3018-3028.

Hayden SM, Miller PS, Brauweiler A, Bamburg JR. 1993. Analysis of the interactions of actin depolymerizing factor with G- and F-actin. Biochemistry 32:9994-10004.

Heidemann SR, Landers JM, Hamborg MA. 1981. Polarity orientation of axonal microtubules. J Cell Biol 91:661-665.

Heidenreich O, Neininger A, Schratt G, Zinck R, Cahill MA, Engel K, Kotlyarov A, Kraft R, Kostka S, Gaestel M, Nordheim A. 1999. MAPKAP kinase 2 phosphorylates serum response factor in vitro and in vivo. J Biol Chem 274:14434-14443.

Herdegen T, Blume A, Buschmann T, Georgakopoulos E, Winter C, Schmid W, Hsieh TF, Zimmermann M, Gass P. 1997. Expression of activating transcription factor-2, serum response factor and cAMP/Ca response element binding protein in the adult rat brain following generalized seizures, nerve fibre lesion and ultraviolet irradiation. Neuroscience 81:199-212.

Hipskind RA, Baccarini M, Nordheim A. 1994. Transient activation of RAF-1, MEK, and ERK2 coincides kinetically with ternary complex factor phosphorylation and immediate-early gene promoter activity in vivo. Mol Cell Biol 14:6219-6231.

Hipskind RA, Buscher D, Nordheim A, Baccarini M. 1994. Ras/MAP kinase-dependent and -independent signaling pathways target distinct ternary complex factors. Genes Dev 8:1803-1816.

Hirokawa N, Niwa S, Tanaka Y. 2010. Molecular motors in neurons: transport mechanisms and roles in brain function, development, and disease. Neuron 68:610-638.

Hirokawa N, Sato-Yoshitake R, Yoshida T, Kawashima T. 1990. Brain dynein (MAP1C) localizes on both anterogradely and retrogradely transported membranous organelles in vivo. J Cell Biol 111:1027-1037.

Hollenbeck PJ, Saxton WM. 2005. The axonal transport of mitochondria. J Cell Sci 118:5411-5419.

Huang TY, DerMardirossian C, Bokoch GM. 2006. Cofilin phosphatases and regulation of actin dynamics. Curr Opin Cell Biol 18:26-31.

Hubley MJ, Locke BR, Moerland TS. 1996. The effects of temperature, pH, and magnesium on the diffusion coefficient of ATP in solutions of physiological ionic strength. Biochim Biophys Acta 1291:115-121.

Iida K, Matsumoto S, Yahara I. 1992. The KKRKK sequence is involved in heat shock-induced nuclear translocation of the 18-kDa actin-binding protein, cofilin. Cell Struct Funct 17:39-46.

Ingerman E, Perkins EM, Marino M, Mears JA, McCaffery JM, Hinshaw JE, Nunnari J. 2005. Dnm1 forms spirals that are structurally tailored to fit mitochondria. J Cell Biol 170:1021-1027.

Iyer D, Chang D, Marx J, Wei L, Olson EN, Parmacek MS, Balasubramanyam A, Schwartz RJ. 2006. Serum response factor MADS box serine-162 phosphorylation switches proliferation and myogenic gene programs. Proc Natl Acad Sci U S A 103:4516-4521.

Janknecht R, Ernst WH, Houthaeve T, Nordheim A. 1993. C-terminal phosphorylation of the serum-response factor. Eur J Biochem 216:469-475.

Johansen FE, Prywes R. 1993. Identification of transcriptional activation and inhibitory domains in serum response factor (SRF) by using GAL4-SRF constructs. Mol Cell Biol 13:4640-4647.

Johnson AW, Crombag HS, Smith DR, Ramanan N. 2011. Effects of serum response factor (SRF) deletion on conditioned reinforcement. Behav Brain Res 220:312-318.

Johnson CM, Hill CS, Chawla S, Treisman R, Bading H. 1997. Calcium controls gene expression via three distinct pathways that can function independently of the Ras/mitogen-activated protein kinases (ERKs) signaling cascade. J Neurosci 17:6189-6202.

Jucker M, Walker LC. 2011. Pathogenic protein seeding in Alzheimer disease and other neurodegenerative disorders. Ann Neurol 70:532-540.

Kabsch W, Mannherz HG, Suck D, Pai EF, Holmes KC. 1990. Atomic structure of the actin:DNase I complex. Nature 347:37-44.

Kalil K, Dent EW. 2005. Touch and go: guidance cues signal to the growth cone cytoskeleton. Curr Opin Neurobiol 15:521-526.

Kalita K, Kharebava G, Zheng JJ, Hetman M. 2006. Role of megakaryoblastic acute leukemia-1 in ERK1/2-dependent stimulation of serum response factor-driven transcription by BDNF or increased synaptic activity. J Neurosci 26:10020-10032.

Kang JS, Tian JH, Pan PY, Zald P, Li C, Deng C, Sheng ZH. 2008. Docking of axonal mitochondria by syntaphilin controls their mobility and affects short-term facilitation. Cell 132:137-148.

Karbowski M, Neutzner A, Youle RJ. 2007. The mitochondrial E3 ubiquitin ligase MARCH5 is required for Drp1 dependent mitochondrial division. J Cell Biol 178:71-84.

Karki S, Holzbaur EL. 1999. Cytoplasmic dynein and dynactin in cell division and intracellular transport. Curr Opin Cell Biol 11:45-53.

Kasischke KA, Vishwasrao HD, Fisher PJ, Zipfel WR, Webb WW. 2004. Neural activity triggers neuronal oxidative metabolism followed by astrocytic glycolysis. Science 305:99-103.

Kegel KB, Meloni AR, Yi Y, Kim YJ, Doyle E, Cuiffo BG, Sapp E, Wang Y, Qin ZH, Chen JD, Nevins JR, Aronin N, DiFiglia M. 2002. Huntingtin is present in the nucleus, interacts with the transcriptional corepressor C-terminal binding protein, and represses transcription. J Biol Chem 277:7466-7476.

Kemp PR, Metcalfe JC. 2000. Four isoforms of serum response factor that increase or inhibit smooth-muscle-specific promoter activity. Biochem J 345 Pt 3:445-451.

Kerkhoff E. 2006. Cellular functions of the Spir actin-nucleation factors. Trends Cell Biol 16:477-483.

King SJ, Schroer TA. 2000. Dynactin increases the processivity of the cytoplasmic dynein motor. Nat Cell Biol 2:20-24.

Klamt F, Zdanov S, Levine RL, Pariser A, Zhang Y, Zhang B, Yu LR, Veenstra TD, Shacter E. 2009. Oxidant-induced apoptosis is mediated by oxidation of the actin-regulatory protein cofilin. Nat Cell Biol 11:1241-1246.

Klemke M, Wabnitz GH, Funke F, Funk B, Kirchgessner H, Samstag Y. 2008. Oxidation of cofilin mediates T cell hyporesponsiveness under oxidative stress conditions. Immunity 29:404-413.

Knöll B, Kretz O, Fiedler C, Alberti S, Schutz G, Frotscher M, Nordheim A. 2006. Serum response factor controls neuronal circuit assembly in the hippocampus. Nat Neurosci 9:195-204.

Knöll B, Nordheim A. 2009. Functional versatility of transcription factors in the nervous system: the SRF paradigm. Trends Neurosci 32:432-442.

Knott AB, Perkins G, Schwarzenbacher R, Bossy-Wetzel E. 2008. Mitochondrial fragmentation in neurodegeneration. Nat Rev Neurosci 9:505-518.

Koshiba T, Detmer SA, Kaiser JT, Chen H, McCaffery JM, Chan DC. 2004. Structural basis of mitochondrial tethering by mitofusin complexes. Science 305:858-862.

Li P, Nijhawan D, Budihardjo I, Srinivasula SM, Ahmad M, Alnemri ES, Wang X. 1997. Cytochrome c and dATP-dependent formation of Apaf-1/caspase-9 complex initiates an apoptotic protease cascade. Cell 91:479-489.

Li Z, Okamoto K, Hayashi Y, Sheng M. 2004. The importance of dendritic mitochondria in the morphogenesis and plasticity of spines and synapses. Cell 119:873-887.

Ligon LA, Steward O. 2000. Role of microtubules and actin filaments in the movement of mitochondria in the axons and dendrites of cultured hippocampal neurons. J Comp Neurol 427:351-361.

Ligon LA, Tokito M, Finklestein JM, Grossman FE, Holzbaur EL. 2004. A direct interaction between cytoplasmic dynein and kinesin I may coordinate motor activity. J Biol Chem 279:19201-19208.

Liu J, Lillo C, Jonsson PA, Vande Velde C, Ward CM, Miller TM, Subramaniam JR, Rothstein JD, Marklund S, Andersen PM, Brannstrom T, Gredal O, Wong PC, Williams DS, Cleveland DW. 2004. Toxicity of familial ALS-linked SOD1 mutants from selective recruitment to spinal mitochondria. Neuron 43:5-17.

Lu M, Witke W, Kwiatkowski DJ, Kosik KS. 1997. Delayed retraction of filopodia in gelsolin null mice. J Cell Biol 138:1279-1287.

Lu PP, Ramanan N. 2011. Serum response factor is required for cortical axon growth but is dispensable for neurogenesis and neocortical lamination. J Neurosci 31:16651-16664.

Lu PP, Ramanan N. 2012. A critical cell-intrinsic role for serum response factor in glial specification in the CNS. J Neurosci 32:8012-8023.

MacAskill AF, Kittler JT. 2009. Control of mitochondrial transport and localization in neurons. Trends Cell Biol 20:102-112.

MacAskill AF, Rinholm JE, Twelvetrees AE, Arancibia-Carcamo IL, Muir J, Fransson A, Aspenstrom P, Attwell D, Kittler JT. 2009. Miro1 is a calcium sensor for glutamate receptor-dependent localization of mitochondria at synapses. Neuron 61:541-555.

Maciver SK, Weeds AG. 1994. Actophorin preferentially binds monomeric ADP-actin over ATP-bound actin: consequences for cell locomotion. FEBS Lett 347:251-256.

Mahad D, Lassmann H, Turnbull D. 2008. Review: Mitochondria and disease progression in multiple sclerosis. Neuropathol Appl Neurobiol 34:577-589.

Manak JR, Prywes R. 1991. Mutation of serum response factor phosphorylation sites and the mechanism by which its DNA-binding activity is increased by casein kinase II. Mol Cell Biol 11:3652-3659.

Mangiarini L, Sathasivam K, Seller M, Cozens B, Harper A, Hetherington C, Lawton M, Trottier Y, Lehrach H, Davies SW, Bates GP. 1996. Exon 1 of the HD gene with an expanded CAG repeat is sufficient to cause a progressive neurological phenotype in transgenic mice. Cell 87:493-506.

Mannella CA. 1992. The 'ins' and 'outs' of mitochondrial membrane channels. Trends Biochem Sci 17:315-320.

Marais RM, Hsuan JJ, McGuigan C, Wynne J, Treisman R. 1992. Casein kinase II phosphorylation increases the rate of serum response factor-binding site exchange. Embo J 11:97-105.

Marsick BM, Roche FK, Letourneau PC. 2012. Repulsive axon guidance cues ephrin-A2 and slit3 stop protrusion of the growth cone leading margin concurrently with inhibition of ADF/cofilin and ERM proteins. Cytoskeleton (Hoboken).

Martin LJ, Gertz B, Pan Y, Price AC, Molkentin JD, Chang Q. 2009. The mitochondrial permeability transition pore in motor neurons: involvement in the pathobiology of ALS mice. Exp Neurol 218:333-346.

Martin M, Iyadurai SJ, Gassman A, Gindhart JG, Jr., Hays TS, Saxton WM. 1999. Cytoplasmic dynein, the dynactin complex, and kinesin are interdependent and essential for fast axonal transport. Mol Biol Cell 10:3717-3728.

Mastrogiacomo F, Bergeron C, Kish SJ. 1993. Brain alpha-ketoglutarate dehydrogenase complex activity in Alzheimer's disease. J Neurochem 61:2007-2014.

Mattson MP. 2004. Pathways towards and away from Alzheimer's disease. Nature 430:631-639.

McGough A, Pope B, Chiu W, Weeds A. 1997. Cofilin changes the twist of F-actin: implications for actin filament dynamics and cellular function. J Cell Biol 138:771-781.

McGuire JR, Rong J, Li SH, Li XJ. 2006. Interaction of Huntingtin-associated protein-1 with kinesin light chain: implications in intracellular trafficking in neurons. J Biol Chem 281:3552-3559.

Meberg PJ, Bamburg JR. 2000. Increase in neurite outgrowth mediated by overexpression of actin depolymerizing factor. J Neurosci 20:2459-2469.

Meeusen S, DeVay R, Block J, Cassidy-Stone A, Wayson S, McCaffery JM, Nunnari J. 2006. Mitochondrial inner-membrane fusion and crista maintenance requires the dynamin-related GTPase Mgm1. Cell 127:383-395.

Meier C, Anastasiadou S, Knöll B. 2011. Ephrin-A5 suppresses neurotrophin evoked neuronal motility, ERK activation and gene expression. PLoS One 6:e26089.

Metzger D, Feil R. 1999. Engineering the mouse genome by site-specific recombination. Curr Opin Biotechnol 10:470-476.

Minamide LS, Striegl AM, Boyle JA, Meberg PJ, Bamburg JR. 2000. Neurodegenerative stimuli induce persistent ADF/cofilin-actin rods that disrupt distal neurite function. Nat Cell Biol 2:628-636.

Minin AA, Kulik AV, Gyoeva FK, Li Y, Goshima G, Gelfand VI. 2006. Regulation of mitochondria distribution by RhoA and formins. J Cell Sci 119:659-670.

Minty A, Kedes L. 1986. Upstream regions of the human cardiac actin gene that modulate its transcription in muscle cells: presence of an evolutionarily conserved repeated motif. Mol Cell Biol 6:2125-2136.

Miralles F, Posern G, Zaromytidou AI, Treisman R. 2003. Actin dynamics control SRF activity by regulation of its coactivator MAL. Cell 113:329-342.

Mironov SL. 2007. ADP regulates movements of mitochondria in neurons. Biophys J 92:2944-2952.

Misgeld T, Kerschensteiner M, Bareyre FM, Burgess RW, Lichtman JW. 2007. Imaging axonal transport of mitochondria in vivo. Nat Methods 4:559-561.

Misra RP, Bonni A, Miranti CK, Rivera VM, Sheng M, Greenberg ME. 1994. L-type voltage-sensitive calcium channel activation stimulates gene expression by a serum response factor-dependent pathway. J Biol Chem 269:25483-25493.

Mokalled MH, Johnson A, Kim Y, Oh J, Olson EN. 2010. Myocardin-related transcription factors regulate the Cdk5/Pctaire1 kinase cascade to control neurite outgrowth, neuronal migration and brain development. Development 137:2365-2374.

Moraczewska J, Wawro B, Seguro K, Strzelecka-Golaszewska H. 1999. Divalent cation-, nucleotide-, and polymerization-dependent changes in the conformation of subdomain 2 of actin. Biophys J 77:373-385.

Morris RL, Hollenbeck PJ. 1995. Axonal transport of mitochondria along microtubules and F-actin in living vertebrate neurons. J Cell Biol 131:1315-1326.

Mouilleron S, Guettler S, Langer CA, Treisman R, McDonald NQ. 2008. Molecular basis for G-actin binding to RPEL motifs from the serum response factor coactivator MAL. EMBO J 27:3198-3208.

Mozdy AD, McCaffery JM, Shaw JM. 2000. Dnm1p GTPase-mediated mitochondrial fission is a multi-step process requiring the novel integral membrane component Fis1p. J Cell Biol 151:367-380.

Muehlich S, Wang R, Lee SM, Lewis TC, Dai C, Prywes R. 2008. Serum-induced phosphorylation of the serum response factor coactivator MKL1 by the extracellular signal-regulated kinase 1/2 pathway inhibits its nuclear localization. Mol Cell Biol 28:6302-6313.

Munsie L, Caron N, Atwal RS, Marsden I, Wild EJ, Bamburg JR, Tabrizi SJ, Truant R. 2011. Mutant huntingtin causes defective actin remodeling during stress: defining a new role for transglutaminase 2 in neurodegenerative disease. Hum Mol Genet 20:1937-1951.

Myers RH. 2004. Huntington's disease genetics. NeuroRx 1:255-262.

Naisbitt S, Valtschanoff J, Allison DW, Sala C, Kim E, Craig AM, Weinberg RJ, Sheng M. 2000. Interaction of the postsynaptic density-95/guanylate kinase domain-associated protein complex with a light chain of myosin-V and dynein. J Neurosci 20:4524-4534.

Nakanishi-Matsui M, Sekiya M, Nakamoto RK, Futai M. 2010. The mechanism of rotating proton pumping ATPases. Biochim Biophys Acta 1797:1343-1352.

Norman C, Runswick M, Pollock R, Treisman R. 1988. Isolation and properties of cDNA clones encoding SRF, a transcription factor that binds to the c-fos serum response element. Cell 55:989-1003.

Oda T, Iwasa M, Aihara T, Maeda Y, Narita A. 2009. The nature of the globular- to fibrous-actin transition. Nature 457:441-445.

Olson EN, Nordheim A. 2010. Linking actin dynamics and gene transcription to drive cellular motile functions. Nat Rev Mol Cell Biol 11:353-365.

Orr AL, Li S, Wang CE, Li H, Wang J, Rong J, Xu X, Mastroberardino PG, Greenamyre JT, Li XJ. 2008. N-terminal mutant huntingtin associates with mitochondria and impairs mitochondrial trafficking. J Neurosci 28:2783-2792.

Pak CW, Flynn KC, Bamburg JR. 2008. Actin-binding proteins take the reins in growth cones. Nat Rev Neurosci 9:136-147.

Palade GE. 1953. An electron microscope study of the mitochondrial structure. J Histochem Cytochem 1:188-211.

Panov AV, Gutekunst CA, Leavitt BR, Hayden MR, Burke JR, Strittmatter WJ, Greenamyre JT. 2002. Early mitochondrial calcium defects in Huntington's disease are a direct effect of polyglutamines. Nat Neurosci 5:731-736.

Pathak D, Sepp KJ, Hollenbeck PJ. 2010. Evidence that myosin activity opposes microtubule-based axonal transport of mitochondria. J Neurosci 30:8984-8992.

Pavlov D, Muhlrad A, Cooper J, Wear M, Reisler E. 2006. Severing of F-actin by yeast cofilin is pH-independent. Cell Motil Cytoskeleton 63:533-542.

Pendleton A, Pope B, Weeds A, Koffer A. 2003. Latrunculin B or ATP depletion induces cofilin-dependent translocation of actin into nuclei of mast cells. J Biol Chem 278:14394-14400.

Petit A, Kawarai T, Paitel E, Sanjo N, Maj M, Scheid M, Chen F, Gu Y, Hasegawa H, Salehi-Rad S, Wang L, Rogaeva E, Fraser P, Robinson B, St George-Hyslop P, Tandon A. 2005. Wild-type PINK1 prevents basal and induced neuronal apoptosis, a protective effect abrogated by Parkinson disease-related mutations. J Biol Chem 280:34025-34032.

Pigino G, Morfini G, Pelsman A, Mattson MP, Brady ST, Busciglio J. 2003. Alzheimer's presenilin 1 mutations impair kinesin-based axonal transport. J Neurosci 23:4499-4508.

Pilling AD, Horiuchi D, Lively CM, Saxton WM. 2006. Kinesin-1 and Dynein are the primary motors for fast transport of mitochondria in Drosophila motor axons. Mol Biol Cell 17:2057-2068.

Pipes GC, Creemers EE, Olson EN. 2006. The myocardin family of transcriptional coactivators: versatile regulators of cell growth, migration, and myogenesis. Genes Dev 20:1545-1556.

Platenik J, Kuramoto N, Yoneda Y. 2000. Molecular mechanisms associated with long-term consolidation of the NMDA signals. Life Sci 67:335-364.

Pollard TD, Borisy GG. 2003. Cellular motility driven by assembly and disassembly of actin filaments. Cell 112:453-465.

Pollitt AY, Insall RH. 2009. WASP and SCAR/WAVE proteins: the drivers of actin assembly. J Cell Sci 122:2575-2578.

Polymeropoulos MH, Lavedan C, Leroy E, Ide SE, Dehejia A, Dutra A, Pike B, Root H, Rubenstein J, Boyer R, Stenroos ES, Chandrasekharappa S, Athanassiadou A, Papapetropoulos T, Johnson WG, Lazzarini AM, Duvoisin RC, Di Iorio G, Golbe LI, Nussbaum RL. 1997. Mutation in the alpha-synuclein gene identified in families with Parkinson's disease. Science 276:2045-2047.

Posern G, Miralles F, Guettler S, Treisman R. 2004. Mutant actins that stabilise F-actin use distinct mechanisms to activate the SRF coactivator MAL. EMBO J 23:3973-3983.

Posern G, Sotiropoulos A, Treisman R. 2002. Mutant actins demonstrate a role for unpolymerized actin in control of transcription by serum response factor. Mol Biol Cell 13:4167-4178.

Posern G, Treisman R. 2006. Actin' together: serum response factor, its cofactors and the link to signal transduction. Trends Cell Biol 16:588-596.

Puigserver P, Spiegelman BM. 2003. Peroxisome proliferator-activated receptor-gamma coactivator 1 alpha (PGC-1 alpha): transcriptional coactivator and metabolic regulator. Endocr Rev 24:78-90.

Quintero OA, DiVito MM, Adikes RC, Kortan MB, Case LB, Lier AJ, Panaretos NS, Slater SQ, Rengarajan M, Feliu M, Cheney RE. 2009. Human Myo19 is a novel myosin that associates with mitochondria. Curr Biol 19:2008-2013.

Ramanan N, Shen Y, Sarsfield S, Lemberger T, Schutz G, Linden DJ, Ginty DD. 2005. SRF mediates activity-induced gene expression and synaptic plasticity but not neuronal viability. Nat Neurosci 8:759-767.

Rehklau K, Gurniak CB, Conrad M, Friauf E, Ott M, Rust MB. 2011. ADF/cofilin proteins translocate to mitochondria during apoptosis but are not generally required for cell death signaling. Cell Death Differ.

Rintoul GL, Filiano AJ, Brocard JB, Kress GJ, Reynolds IJ. 2003. Glutamate decreases mitochondrial size and movement in primary forebrain neurons. J Neurosci 23:7881-7888.

Riva A, Tandler B, Ushiki T, Usai P, Isola R, Conti G, Loy F, C LH. 2010. Mitochondria of human Leydig cells as seen by high resolution scanning electron microscopy. Arch Histol Cytol 73:37-44.

Rivera VM, Miranti CK, Misra RP, Ginty DD, Chen RH, Blenis J, Greenberg ME. 1993. A growth factor-induced kinase phosphorylates the serum response factor at a site that regulates its DNA-binding activity. Mol Cell Biol 13:6260-6273.

Robinson RC, Turbedsky K, Kaiser DA, Marchand JB, Higgs HN, Choe S, Pollard TD. 2001. Crystal structure of Arp2/3 complex. Science 294:1679-1684.

Roesch K, Curran SP, Tranebjaerg L, Koehler CM. 2002. Human deafness dystonia syndrome is caused by a defect in assembly of the DDP1/TIMM8a-TIMM13 complex. Hum Mol Genet 11:477-486.

Rosas HD, Liu AK, Hersch S, Glessner M, Ferrante RJ, Salat DH, van der Kouwe A, Jenkins BG, Dale AM, Fischl B. 2002. Regional and progressive thinning of the cortical ribbon in Huntington's disease. Neurology 58:695-701.

Russo GJ, Louie K, Wellington A, Macleod GT, Hu F, Panchumarthi S, Zinsmaier KE. 2009. Drosophila Miro is required for both anterograde and retrograde axonal mitochondrial transport. J Neurosci 29:5443-5455.

Saotome M, Safiulina D, Szabadkai G, Das S, Fransson A, Aspenstrom P, Rizzuto R, Hajnoczky G. 2008. Bidirectional Ca2+-dependent control of mitochondrial dynamics by the Miro GTPase. Proc Natl Acad Sci U S A 105:20728-20733.

Schratt G, Philippar U, Berger J, Schwarz H, Heidenreich O, Nordheim A. 2002. Serum response factor is crucial for actin cytoskeletal organization and focal adhesion assembly in embryonic stem cells. J Cell Biol 156:737-750.

Schratt G, Weinhold B, Lundberg AS, Schuck S, Berger J, Schwarz H, Weinberg RA, Ruther U, Nordheim A. 2001. Serum response factor is required for immediate-early gene activation yet is dispensable for proliferation of embryonic stem cells. Mol Cell Biol 21:2933-2943.

Schwarzer C, Barnikol-Watanabe S, Thinnes FP, Hilschmann N. 2002. Voltage-dependent anion-selective channel (VDAC) interacts with the dynein light chain Tctex1 and the heat-shock protein PBP74. Int J Biochem Cell Biol 34:1059-1070.

Sheng ZH, Cai Q. 2012. Mitochondrial transport in neurons: impact on synaptic homeostasis and neurodegeneration. Nat Rev Neurosci 13:77-93.

Shore P, Sharrocks AD. 1995. The ETS-domain transcription factors Elk-1 and SAP-1 exhibit differential DNA binding specificities. Nucleic Acids Res 23:4698-4706.

Smirnova E, Shurland DL, Ryazantsev SN, van der Bliek AM. 1998. A human dynamin-related protein controls the distribution of mitochondria. J Cell Biol 143:351-358.

Sommer H, Beltran JP, Huijser P, Pape H, Lonnig WE, Saedler H, Schwarz-Sommer Z. 1990. Deficiens, a homeotic gene involved in the control of flower morphogenesis in Antirrhinum majus: the protein shows homology to transcription factors. Embo J 9:605-613.

Sotiropoulos A, Gineitis D, Copeland J, Treisman R. 1999. Signal-regulated activation of serum response factor is mediated by changes in actin dynamics. Cell 98:159-169.

Steketee MB, Tosney KW. 2002. Three functionally distinct adhesions in filopodia: shaft adhesions control lamellar extension. J Neurosci 22:8071-8083.

Stern S, Debre E, Stritt C, Berger J, Posern G, Knöll B. 2009. A nuclear actin function regulates neuronal motility by serum response factor-dependent gene transcription. J Neurosci 29:4512-4518.

Stern S, Sinske D, Knöll B. 2012. SERUM response factor modulates neuron survival during peripheral axon injury. J Neuroinflammation 9:78.

Stokin GB, Lillo C, Falzone TL, Brusch RG, Rockenstein E, Mount SL, Raman R, Davies P, Masliah E, Williams DS, Goldstein LS. 2005. Axonopathy and transport deficits early in the pathogenesis of Alzheimer's disease. Science 307:1282-1288.

Strauss KM, Martins LM, Plun-Favreau H, Marx FP, Kautzmann S, Berg D, Gasser T, Wszolek Z, Muller T, Bornemann A, Wolburg H, Downward J, Riess O, Schulz JB, Kruger R. 2005. Loss of function mutations in the gene encoding Omi/HtrA2 in Parkinson's disease. Hum Mol Genet 14:2099-2111.

Strehlow AN, Li JZ, Myers RM. 2007. Wild-type huntingtin participates in protein trafficking between the Golgi and the extracellular space. Hum Mol Genet 16:391-409.

Stringer JL, Belaguli NS, Iyer D, Schwartz RJ, Balasubramanyam A. 2002. Developmental expression of serum response factor in the rat central nervous system. Brain Res Dev Brain Res 138:81-86.

Stritt C, Knöll B. 2010. Serum response factor regulates hippocampal lamination and dendrite development and is connected with reelin signaling. Mol Cell Biol 30:1828-1837.

Stritt C, Stern S, Harting K, Manke T, Sinske D, Schwarz H, Vingron M, Nordheim A, Knöll B. 2009. Paracrine control of oligodendrocyte differentiation by SRF-directed neuronal gene expression. Nat Neurosci 12:418-427.

Sturtz LA, Diekert K, Jensen LT, Lill R, Culotta VC. 2001. A fraction of yeast Cu,Zn-superoxide dismutase and its metallochaperone, CCS, localize to the intermembrane space of mitochondria. A physiological role for SOD1 in guarding against mitochondrial oxidative damage. J Biol Chem 276:38084-38089.

Sun Q, Chen G, Streb JW, Long X, Yang Y, Stoeckert CJ, Jr., Miano JM. 2006. Defining the mammalian CArGome. Genome Res 16:197-207.

Sung JY, Engmann O, Teylan MA, Nairn AC, Greengard P, Kim Y. 2008. WAVE1 controls neuronal activity-induced mitochondrial distribution in dendritic spines. Proc Natl Acad Sci U S A 105:3112-3116.

Szabadkai G, Duchen MR. 2008. Mitochondria: the hub of cellular Ca2+ signaling. Physiology (Bethesda) 23:84-94.

Tabuchi A, Estevez M, Henderson JA, Marx R, Shiota J, Nakano H, Baraban JM. 2005. Nuclear translocation of the SRF co-activator MAL in cortical neurons: role of RhoA signalling. J Neurochem 94:169-180.

Tanaka Y, Kanai Y, Okada Y, Nonaka S, Takeda S, Harada A, Hirokawa N. 1998. Targeted disruption of mouse conventional kinesin heavy chain, kif5B, results in abnormal perinuclear clustering of mitochondria. Cell 93:1147-1158.

Tatuch Y, Christodoulou J, Feigenbaum A, Clarke JT, Wherret J, Smith C, Rudd N, Petrova-Benedict R, Robinson BH. 1992. Heteroplasmic mtDNA mutation (T----G) at 8993 can cause Leigh disease when the percentage of abnormal mtDNA is high. Am J Hum Genet 50:852-858.

Tondeleir D, Vandamme D, Vandekerckhove J, Ampe C, Lambrechts A. 2009. Actin isoform expression patterns during mammalian development and in pathology: insights from mouse models. Cell Motil Cytoskeleton 66:798-815.

Treisman R. 1986. Identification of a protein-binding site that mediates transcriptional response of the c-fos gene to serum factors. Cell 46:567-574.

Turjanski AG, Vaque JP, Gutkind JS. 2007. MAP kinases and the control of nuclear events. Oncogene 26:3240-3253.

Van Troys M, Huyck L, Leyman S, Dhaese S, Vandekerkhove J, Ampe C. 2008. Ins and outs of ADF/cofilin activity and regulation. Eur J Cell Biol 87:649-667.

Vartiainen MK. 2008. Nuclear actin dynamics--from form to function. FEBS Lett 582:2033-2040.

Vartiainen MK, Guettler S, Larijani B, Treisman R. 2007. Nuclear actin regulates dynamic subcellular localization and activity of the SRF cofactor MAL. Science 316:1749-1752.

Vartiainen MK, Mustonen T, Mattila PK, Ojala PJ, Thesleff I, Partanen J, Lappalainen P. 2002. The three mouse actin-depolymerizing factor/cofilins evolved to fulfill cell-type-specific requirements for actin dynamics. Mol Biol Cell 13:183-194.

Wang DZ, Li S, Hockemeyer D, Sutherland L, Wang Z, Schratt G, Richardson JA, Nordheim A, Olson EN. 2002. Potentiation of serum response factor activity by a family of myocardin-related transcription factors. Proc Natl Acad Sci U S A 99:14855-14860.

Wang H, Lim PJ, Karbowski M, Monteiro MJ. 2009. Effects of overexpression of huntingtin proteins on mitochondrial integrity. Hum Mol Genet 18:737-752.

Wang X, Schwarz TL. 2009. The mechanism of Ca2+ -dependent regulation of kinesin-mediated mitochondrial motility. Cell 136:163-174.

Wang Z, Wang DZ, Hockemeyer D, McAnally J, Nordheim A, Olson EN. 2004. Myocardin and ternary complex factors compete for SRF to control smooth muscle gene expression. Nature 428:185-189.

Weaver AM, Young ME, Lee WL, Cooper JA. 2003. Integration of signals to the Arp2/3 complex. Curr Opin Cell Biol 15:23-30.

Wegner A. 1976. Head to tail polymerization of actin. J Mol Biol 108:139-150.

Welte MA. 2004. Bidirectional transport along microtubules. Curr Biol 14:R525-537.

Westermann B. 2010. Mitochondrial fusion and fission in cell life and death. Nat Rev Mol Cell Biol 11:872-884.

Weydt P, Pineda VV, Torrence AE, Libby RT, Satterfield TF, Lazarowski ER, Gilbert ML, Morton GJ, Bammler TK, Strand AD, Cui L, Beyer RP, Easley CN, Smith AC, Krainc D, Luquet S, Sweet IR, Schwartz MW, La Spada AR. 2006. Thermoregulatory and metabolic defects in Huntington's disease transgenic mice implicate PGC-1alpha in Huntington's disease neurodegeneration. Cell Metab 4:349-362.

Whiteman IT, Gervasio OL, Cullen KM, Guillemin GJ, Jeong EV, Witting PK, Antao ST, Minamide LS, Bamburg JR, Goldsbury C. 2009. Activated actin-depolymerizing factor/cofilin sequesters phosphorylated microtubule-associated protein during the assembly of alzheimer-like neuritic cytoskeletal striations. J Neurosci 29:12994-13005.

Whitmarsh AJ, Shore P, Sharrocks AD, Davis RJ. 1995. Integration of MAP kinase signal transduction pathways at the serum response element. Science 269:403-407.

Wickramasinghe SR, Alvania RS, Ramanan N, Wood JN, Mandai K, Ginty DD. 2008. Serum response factor mediates NGF-dependent target innervation by embryonic DRG sensory neurons. Neuron 58:532-545.

Wiebel FF, Rennekampff V, Vintersten K, Nordheim A. 2002. Generation of mice carrying conditional knockout alleles for the transcription factor SRF. Genesis 32:124-126.

Wysocka J, Herr W. 2003. The herpes simplex virus VP16-induced complex: the makings of a regulatory switch. Trends Biochem Sci 28:294-304.

Xia Z, Dudek H, Miranti CK, Greenberg ME. 1996. Calcium influx via the NMDA receptor induces immediate early gene transcription by a MAP kinase/ERK-dependent mechanism. J Neurosci 16:5425-5436.

Yoo Y, Ho HJ, Wang C, Guan JL. 2009. Tyrosine phosphorylation of cofilin at Y68 by v-Src leads to its degradation through ubiquitin-proteasome pathway. Oncogene 29:263-272.

Yordy JS, Muise-Helmericks RC. 2000. Signal transduction and the Ets family of transcription factors. Oncogene 19:6503-6513.

Zanelli SA, Trimmer PA, Solenski NJ. 2006. Nitric oxide impairs mitochondrial movement in cortical neurons during hypoxia. J Neurochem 97:724-736.

Zhang L, Shimoji M, Thomas B, Moore DJ, Yu SW, Marupudi NI, Torp R, Torgner IA, Ottersen OP, Dawson TM, Dawson VL. 2005. Mitochondrial localization of the Parkinson's disease related protein DJ-1: implications for pathogenesis. Hum Mol Genet 14:2063-2073.

Zhao L, Ma QL, Calon F, Harris-White ME, Yang F, Lim GP, Morihara T, Ubeda OJ, Ambegaokar S, Hansen JE, Weisbart RH, Teter B, Frautschy SA, Cole GM. 2006. Role of p21-activated kinase pathway defects in the cognitive deficits of Alzheimer disease. Nat Neurosci 9:234-242.

Zinck R, Hipskind RA, Pingoud V, Nordheim A. 1993. c-fos transcriptional activation and repression correlate temporally with the phosphorylation status of TCF. Embo J 12:2377-2387.

Zuchner S, Mersiyanova IV, Muglia M, Bissar-Tadmouri N, Rochelle J, Dadali EL, Zappia M, Nelis E, Patitucci A, Senderek J, Parman Y, Evgrafov O, Jonghe PD, Takahashi Y, Tsuji S, Pericak-Vance MA, Quattrone A, Battaloglu E, Polyakov AV, Timmerman V, Schroder JM, Vance JM. 2004. Mutations in the mitochondrial GTPase mitofusin 2 cause Charcot-Marie-Tooth neuropathy type 2A. Nat Genet 36:449-451.

Acknowledgment

Special thanks to my supervisor Bernd Knöll for giving me the chance to perform this doctoral project in his lab, for his cooperative way of supporting me and his helpful scientific advice.

Thanks to my co-supervisors Mathias Jucker and Simone Di Giovanni for their professional way of reviewing my work.

I thank all the members of the Knöll-lab (namely Tine, Christin, Sina, Cveta, Daniela, Uli, Stephi and Manuel) for the positive working attitude and the joyful atmosphere.
Especially I would like to thank Blotmanager 10 aka Kai V. for maintaining a “healthy level of insanity” even during tough times.
Further thanks to Sofia and Blotmanager 12 aka Christopher for providing an awesome working spirit.

Of course, thanks to my parents who always educated, encouraged and enabled me to do what I want.

Thanks to my sister is far too less. I am proud of being her brother and deeply grateful for her commitment. For scraping me off the tarmac whenever I crashed. For giving me the most impressive advice. For being the ultimate support – right on cue.